A STUDY OF HELICOPTER STABILITY AND CONTROL INCLUDING BLADE DYNAMICS

Xin Zhao
H. C. Curtiss, Jr.

Department of Mechanical and Aerospace
Engineering
Princeton University
Princeton, NJ 08544-5263

Principal Investigator: H. C. Curtiss, Jr.

Technical Report No. 1823T

NASA Ames Research Center Grant No. NAG 2-244
Studies in Helicopter Aerodynamics and Control

NASA Technical Officer for this Grant: W. A. Decker

FINAL REPORT
Covering the period July 1983-- September 1987

October 1988

ABSTRACT

A linearized model of rotorcraft dynamics has been developed through the use of symbolic automatic equation generating techniques. The dynamic model has been formulated in a unique way such that it can be used to analyze a variety of rotor/body coupling problems including a rotor mounted on a flexible shaft with a number of modes as well as free-flight stability and control characteristics. Direct comparison of the time response to longitudinal, lateral and directional control inputs at various trim conditions shows that the linear model yields good to very good correlation with flight test. In particular it is shown that a dynamic inflow model is essential to obtain good time response correlation, especially for the hover trim condition. It also is shown that the main rotor wake interaction with the tail rotor and fixed tail surfaces is a significant contributor to the response at translational flight trim conditions. A relatively simple model for the downwash and sidewash at the tail surfaces based on flat vortex wake theory is shown to produce good agreement.

Then, the influence of rotor flap and lag dynamics on automatic control systems feedback gain limitations is investigated with the model. It is shown that the blade dynamics, especially lagging dynamics, can severely limit the useable values of the feedback gain for simple feedback control and that multivariable optimal control theory is a powerful tool to design high gain augmentation control system. The frequency-shaped optimal control design can offer much better flight dynamic characteristics and a stable margin for the feedback system without need to model the lagging dynamics.

BIBLIOGRAPHY

The following papers were presented as part of this grant:-

Curtiss, H. C., Jr., Stability and Control Modelling, paper No. 41, Twelfth European Rotorcraft Forum, Garmisch-Partenkirchen, Federal Republic of Germany, September 22-24, 1986.

Zhao, X., Curtiss, H. C., Jr., A Linearized Model of Helicopter Dynamics Including Correlation with Flight Test, 2nd International Conference on Rotorcraft Basic Research, College Park, MD, February 1988.

In addition two presentations consisting of figures only were made:

Curtiss, H. C., Jr., McKillip, R. M., Stability and Control Modelling, Workshop on Dynamics and Aeroelastic Stability Modeling of Rotor Systems, Atlanta, GA, December 4-5, 1985.

Curtiss, H. C., Jr., The Influence of Blade Degrees of Freedom and Dynamic Inflow on Helicopter Stability and Control. Second Technical Workshop on Dynamics and Aeroelastic Modeling of Rotorcraft Systems, Florida Atlantic University, November 18-20, 1987.

CONTENTS

ORIGINAL PAGE IS
OF POOR QUALITY

ORIGINAL PAGE IS OF POOR QUALITY

LIST OF TABLES

LIST OF FIGURES

Chapter I

INTRODUCTION AND BACKGROUND

1.1 Introduction

Aeroelastic and aeromechanical stability, control and response problems associated with rotary-wing aircraft represent some of the most challenging problems in the area of dynamic systems. Due to the complicated nature of the problem, stability and control analysis is usually treated separately from aeroelastic and aeromechanical stability. Aeroelastic analyses usually concentrate on the character of the system eigenvalues and do not concern themselves with system response characteristics. In many instances, stability and control analyses are based on a quasi-static, rigid-body stablity-and-control-derivative model in which the blade dynamics are neglected and the rotor lag and flap angles are determined from the instantaneous value of the body angular and translational displacements, rates, and accelerations.

Although use of the conventional quasi-static stability derivative model is adequate for many applications associated with low-frequency and steady-state flight behavior and promotes physical insight, the true physical behavior of the highly coupled rotor/fuselage dynamical system can only be captured by developing a mathematical model based upon a consistent formulation in which the influence of the coupled body blade motion is properly incorporated. Many years ago, C.W.Ellis[1] found that the conventional quasi-static stability-derivative model was not representative of the higher frequency short-period dynamics, owing to the strong influence of the unmodeled rotor modes. R.E.Donham and S.V.Cardinale[2] concluded that the oscillating rotor could excite the body's natural modes, and showed that a body attitude feedback system had an important influence on the total system stability. Hansen[3] has noted the importance of the flapping dynamics in parameter identification studies.

Along with the development of feedback control systems, especially with an increasing emphasis on superaugmented, high-gain flight control systems for military rotorcraft in order to meet the requirements for demanding misson tasks such as nap-of-the-Earth(NOE) flight, blade dynamics are increasingly important in the flight dynamic analysis of helicopters. In the design and analysis of such high gain control systems, it is essential that high-order dynamics of the system components be adequately modeled. In theoretical analyses, K.Miyajima[4] has found that the blade-flapping regressing mode should be included in a stability and control augmentation system design, otherwise a very important oscillatory mode with short period frequencies would not be included. H.C.Curtiss[5] has found that for helicopter control systems attitude feedback gain is limited primarily by body-flap coupling, and rate gain is limited by the lag degrees of freedom. It is also shown that dynamic inflow produces significant changes in the modes of motion and response of the system. W.E.Hall[6] has shown that, for tight control, neglecting the rotor dynamics in designing a high gain feedback system results in unstable closed-loop responses when the rotor flap dynamics are included. In practice, the operators of variable-stability research helicopters have long been aware of severe limitations in feedback gain settings when attempting to increase the bandwidth of flight control systems. These same limitations have also been encountered in the helicopter industry, where achievable stability augmentation system gains obtained from flight tests have often been far below predicted values[7]. Even for the vibration analysis of helicopters it has been concluded that the method of rotor induced vibration prediction by applying the rotor forces and moments acting on a rigid support to the flexible airframe can lead to large errors of either over or under prediction of vibrations[8].

In addition, with the shift of emphasis in hingeless and bearingless rotor design to soft-inplane configurations, coupled rotor/fuselage mechanical instability becomes one of the main concerns of designers and researchers. This is not only because there is strong coupling between the rotor and fuselage and therefore the aeromechanical stability characteristics are highly sensitive to aerodynamic and structural feedback, but also because the influences of the aeroelastic coupling, which can play a key role in alleviating aeromechanical instability, often are different on the coupled rotor/fuselage system than on the isolated blade[9].

Hence, there is a widespread need for analyses capable of modeling coupled rotor/fuselage aeroelastic or aeromechanical systems.

1.2 Approaches For Analysis of Coupled Rotor/Fuselage System

For a subject as complex as coupled rotor/fuselage systems, an adequate understanding of physical phenomena can not be attained unless a reasonably accurate analytical representation of the system has been developed and verified. Such a representation is necessary to provide a usable design tool, to develop an understanding of configuration behavior through systematic parametric studies, and to search for and evaluate the feasibility of particular advanced configuration concepts. Because of the complexity of the description of the coupled rotor/fuselage system, an important element of the development of practical analytical tools is to determine what is an acceptable level of approximation for the various parts of the analysis. It is important to avoid making a design tool impractically large for efficient computation.

Several mathematical approaches are available for helicopter analysts to perform a coupled rotor/fuselage analysis. The most popular ones are mode displacement, force integration, and matrix displacement methods.

The mode displacement method allows a completely coupled rotor/fuselage system to be analyzed by replacing rotor inertia couplings in the fuselage equations with stiffness coupling; therefore the use of it enables a simplified sequential solution of the coupled rotor/fuselage dynamic equations. Most analysis methods result in inertial coupling between the rotor and the fuselage in both sets of equations. However, the mode displacement approach allows a simpler stiffness type coupling of the rotor degrees of freedom in the fuselage equations. This is possible since modal coefficients are used to calculate hub shears and hub moments, eliminating the acceleration terms in the fuselage/pylon equations that are due to the rotor degrees of freedom. The sequence of calculation begins with three independent computations for airframe and rotor aerodynamic forces, and hub shears and moments. The computation of the hub shears and moments is the process which actually uses the mode-displacement method. The aerodynamic forces acting on the airframe and the rotor are also calculated. These aerodynamic forces form the forcing function for the rigid-body fuselage accelerations. After the rigid body fuselage accelerations are calculated, they are used in conjunction with the hub shears and moments to calculate the acceleration of pylon coordinates at the following step. Additional inertia forces on the rotor which were not included in the calculation of the rotor modes are calculated from the fuselage and pylon accelerations. These inertia forces are then added to the rotor aerodynamic force calculated previously in order to calculate the accelerations of the rotor modal coordinates. Thus, accelerations are calculated for all of the degrees of freedom without having to solve a large set of simultaneous algebraic equations.

The force integration method is used to compute hub shears and moments by integrating dynamic and aerodynamic forces along each rotor blade. The analysis treats the rotor equations separately from those of the nonrotating system. In the rotor equations, inertial coupling terms due to pylon/fuselage motions are written explicitly and assumed to be known at a particular time point. To solve the rotor equations of motion at time t, the hub and pylon displacement, velocity, and acceleration vectors are obtained from the solution of the equations of motion for the nonrotating system at the previous time point. A predictor-corrector method is used for numerical integration of the rotor acceleration variables to obtain rotor velocity and displacement components. Equations of the pylon/fuselage system are derived with hub shears and hub moments appearing on the right side of the equations. The hub forces are calculated by integrating inertial and aerodynamic loading from blade tip to blade root for each blade and summing up for all the blades. The force integration is performed to a time point at which the predictor-corrector has converged the solution of the rotor equations. Given the hub shears and moments, the equations of motion for the pylon/fuselage are solved. The results define the hub motions which provide the fuselage inertial coupling terms in the rotor equations at the next time point.

These two approaches are widely used in the helicopter industry to calculate the rotor loads and the response of the coupled rotor/fuselage system. The disadvantage of these approaches is due to the fact that time histories are obtained by input integration so that quantitative stability analysis is not applicable, and they are not convenient for the systematic parametric studies as well. For most aeroelastic and aeromechanical stability and control problems, the matrix displacement method may be a good alternative.

The matrix displacement method uses a generalized coupling procedure which allows analysis of structural components in rotating and nonrotating reference frames. The method automates the dynamic couplings between the rotating and nonrotating systems and takes advantage of the high speed computer for the algebraic manipulation. Vector transformations are used in the method to generate position vectors for blade and fuselage points in fixed coordinates.

Then by using the Lagrangian approach, for example, the inertial contributions of the equations of motion for the coupled rotor/fuselage system are obtained. The same transformation also is used to generate air speeds and incidence angles relative to local blade sections, and through application of strip theory, for example, to obtain the aerodynamic generalized force contributions for the system. The disadvantage of the matrix displacement method is that some of the dynamic coupling terms carried in the component equation are cancelled if the equations are derived explicitly for the coupled system. This consumes more computer time and possibly degrades accuracy in the numerical solution.

Therefore, the matrix displacement method suggests a viable engineering tool for solving coupled rotor/fuselage problems. In this thesis, with the help of a symbolic computer processor, the matrix displacement method is used to obtain a coupled rotor-fuselage helicopter system description.

1.3 Outline of Previous Work

A number of powerful analyses which have been developed by industry and the government are developed or verified for only a particular technical problem that reflects the specific interest of the originating organization. A typical example is shown in Ref.10. The coupled rotor/fuselage system model is designed for the Black Hawk simulation. The model is a total system description and allows the simulation of any flight condition which can be experienced by a pilot. The mechanical and aerodynamic data used in the model are provided by wind tunnel tests for full angle of attack range.

Several researchers constructed mathematical models for the general coupled rotor/fuselage systems. W.Warmbrodt and P.Friedmann [11] have derived the governing equations of motion of a helicopter rotor coupled to a rigid body fuselage, which can be used to study coupled rotor/fuselage dynamics in forward flight. The final equations are presented in partial differential equations and the blade equations of motion are written in a rotating reference system whereas the matching conditions between the rotor and fuselage are written in a nonrotating reference frame. W.Johnson[12] has developed a comprehensive analysis for rotorcraft which is capable of modeling coupled rotor/fuselage problems by an integrated Newtonian approach. A modal representation is used to transform the partial differential equations to ordinary differential equations, which is equivalent to a Galerkin analysis based on the orthogonal modes of free vibration for the rotating blade. Its solution procedures for the transient, aeroelastic stability, and flight dynamics analyses begin from the harmonic balanced trim solution. Then the flight dynamics analysis calculates the rotor and airframe stability derivatives, and constructs linear differential equations for the aircraft rigid body motions; the poles, zeros, and eigenvectors of these equations define the aircraft flying qualities. The transient analysis numerically integrates the rigid body equations of motion for a prescribed control or gust input. The aeroelastic stability analysis constructs a set of linear differential equations describing the motion of the rotor and aircraft; the eigenvalues of these equations define the system stability.

Although their intention was to produce an analysis that is applicable to a wide range of problems and a wide class of vehicles, these nonlinear, periodic-coefficient, partial or ordinary differential equations are too complex to get physical insight for general understanding and the theoretical analysis. They are also not convenient for the systematic parametric studies. For analytical simplicity and an use as basis of the design of feedback control systems, a linear description of the system is highly desirable, especially if it can be shown to agree with experiment.

Owing to the complexity of including blade dynamics in forward flight, linearized models in the literature are limited to the hover case.

Hodges [13] has developed a system of linear, homogenous, ordinary differential equations which is suitable for modeling the aeromechanical stability of both bearingless and hingeless rotor in hover. The flexbeam equilibrium deflections are calculated through a nonlinear numerical iteration process, and the flexbeam structural loads for small perturbation of the equilibrium are determined through numerical perturbation of the equilibrium solution. By using the multiblade coordinate transformation, the terms with periodic coefficient are removed; Therefore, the resulting constant-coefficient equations can be solved as a conventional eigenvalue problem.

Another derivation of the air resonance problem in hover of an N-bladed hingeless rotor helicopter has been developed by Levin[14]. In his study the final equations of dynamic equilibrium are reduced to ordinary differential form by using Galerkin's method with a relatively small number of rotating blade modes. Provision for introducing active control of the rotor with the intent of eliminating the air resonance instability is included in the formulation.

A third model[15] by Lytwyn and Miao is obtained by means of the Lagrangian procedure. The virtual hinge representation has been used for the first in-plane (lead-lag) and the first vertical bending modes of each of the blades.

The most important assumptions upon which these formulations are based are: (1) the helicopter is in hover with low disc loading (low inflow ratio), (2) the rigid fuselage has only two translational degrees of freedom and two rotational degrees of freedom; vertical translation and rotation about the vertical axis (yawing) are eliminated, (3) the rotor consists of three or more hingeless blades, (4) each blade can bend in two mutually perpendicular direction normal to the elastic axis.

Several kinds of model mentioned above have been used in analyses of the aeroelastic and aeromechanical stability, response, and control problem. Hodges has conducted a theoretical study of aeromechanical stability of bearingless rotors in hover by comparing the hub-fixed motion, i.e. isolated blade stability, with the case when coupled rotor/ fuselage motion is considered. His studies dealt mostly with a soft-in-plane configuration using quasisteady aerodynamics. Straub and Warmbrodt[16] have studied the use of active blade control to increase helicopter rotor/fuselage damping. The chosen feedback parameters include cyclic rotor flap and lead-lag states, and the study focuses on ground resonance. Curtiss[5] has studied the influence of rotor dynamics and dynamic inflow on the stability and control characteristics of single rotor helicopter in hover, and discussed the body attitude and rate feedback limitations which arise due to rotor dynamics and dynamic inflow.

The restriction for obtaining a linearized model for forward flight is due partly to the complexity of the blade motion of the helicopter so that the algebra is increased substantially. This has led to attempts to share the algebra with computers through symbolic processors. Both general and special purpose programs have been developed and are available. Another difficulty faced for extending the linearized modeling to forward flight is that the multiblade transformation will not remove all periodic coefficients. Therefore the resulting linear dynamic system description will be time-varying. However, it has been found that the constant coefficient approximation for the remaining periodic coefficients is satisfactory for low-frequency modes under trimmed conditions[17]. Furthermore, all of the linearized models for hover assume that yaw motion and vertical motion of the helicopter are totally uncoupled; this is not the case for forward flight. In addition, the tail rotor and fixed tail surfaces, which operate in an extremely adverse aerodynamic and dynamic environment, must be taken into account. As a result, a relatively simple induced velocity model at tail position due to the influence of the main rotor wake is needed for a good overall system modelling.

With this background information established, the remainder of this thesis can be outlined. The first task undertaken will be to construct a linearized dynamic mathematical model for coupled rotor/fuselage helicopter system for both hover and forward flight by use of symbolic automatic equation generating techniques Also a relatively simple model for the downwash and sidewash at the tail surfaces based on flat vortex wake theory is employed to take the main rotor wake interaction with the tail rotor and fixed tails into account. The model will then be verified by comparing the response time histories for various prescribed control inputs at various trim conditions with the flight test results of Ref.18, which is obtained by a flight test program solely for the purpose of validating mathematical models of the Black Hawk helicopter. In addition, a study will be made of the influence of the blade flap and lag dynamics on automatic control system feedback gain limitations at hover and translational flight conditions.

Chapter II

A LINEAR DYNAMIC MATHEMATICAL MODEL FOR COUPLED ROTOR/FUSELAGE SYSTEM

2.1 Background and Introduction

One distinction of the coupled rotor/fuselage system is the fact that the analysis must accommodate both rotating and nonrotating coordinate systems. For the coupled rotor/fuselage system, the equations for each blade, which are usually written in a coordinate system rotating at a constant velocity, are transformed to a nonrotating coordinate system, to be combined with each other and with the fuselage system. Consequently, it is difficult to obtain the system description using a Newtonian approach because the required blade acceleration terms are very complex. The Lagrangian approach, which requires only velocity terms and position terms, is much more convenient for overall system modeling.

Another distinction of the coupled rotor/fuselage system is the increased number of degrees of freedom, which substantially increases the algebraic complexity in expressing the inertia and aerodynamic loads. In order to generate reasonably comprehensive aeroelastic equations of motion for a helicopter rotor, several axes of reference are usually required in the analysis. Thus, a material point on a rotor blade can most conveniently have its position coordinates defined by means of successive axis transformations. Although none of the transformations that change the coordinates of a point from one axis system to another may be particularly complicated, when equations of motion are derived through the use of Lagrange's equations, the exercise can prove quite arduous. The derivation of the equations involves a certain amount of differentiation, which, combined with the successive transformations, leads to an enormous amount of work on paper for the analyst. Furthermore, the possibility of errors creeping into the analysis is almost unavoidable.

Fortunately, there are serveral symbolic computer processors available for general computer systems so that it is possible to develop the system equations directly on the computer. The program generates the steady-state and linearized perturbation equations in symbolic form and then codes them into FORTRAN subroutines. Subsequently the coefficients for each equation and for each mode are identified through a numerical program. Through the use of symbolic automatic equation generating techniques, the final system equations are obtained in a systematic way. This also makes it relatively easy to rigorously investigate the effect of various ordering schemes on the calculated motion dynamics.

2.2 General Description of Model

The complete dynamic description of the multidimensional system is formulated by means of the Lagrangian procedure. The final set of linear second-order differential equations is obtained by a perturbation analysis performed on the set of original nonlinear equations.

The model has N degrees of freedom, each associated with a generalized coordinate and a corresponding mode shape. The model includes a number of rotor blades on one hub and a fuselage. Each rotor blade undergoes flap bending and lag bending; the torsional deflections are not included. Quasisteady strip theory is used to obtain the aerodynamic loads. Unsteady aerodynamic effects are introduced through dynamic inflow modelling. Dynamic stall and reverse flow effects are not included.

In this work, the model is of order 24 or 27 depending on whether dynamic inflow is included for a better modelling of unsteady aerodynamics. The fuselage has six degrees of freedom: vertical, longitudinal, and lateral translation, pitch, roll, and yaw motions, each associated with two state variables. The equations of motion are formulated in such a way that they can be extended to N degrees of freedom to include the effects of flexibility between fuselage and the hub without any change in the blade motion part of the model. Each blade has 2 degrees of freedom, flapping and lagging, each corresponding to two state variables. When the blade motion is converted to the fixed frame through the use of multiblade coordinates, six degrees of freedom result (e.g. coning, lateral and longitudinal tilt of the rotor plane for flap) each associated with two state variables. Dynamic inflow adds three more state variables. Control inputs are collective pitch of the blade, lateral and longitudinal cyclic pitch of the blade, and collective pitch of the tail rotor. Rotor RPM is assumed constant. Blade pitch changes due to flapping, lagging, and fuselage deformation and motion by the rotor hub geometry and elastic coupling can be taken into account.

The equations of the system are obtained by algebraic manipulation performed with the symbolic system REDUCE on the IBM computer at computer center at Princeton University, and is checked with the symbolic system MACSYMA at the Laboratory for Control and Automation at Princeton.

2.3 Reference Frames

Because we use a Lagrangian approach, we have to begin our systems of coordinates in an inertial frame, the E system, the earth axis. The basic systems of coordinates are the F_1 and F_2 systems which are shown in Fig. 2-1 and Fig. 2-2. The origins of these systems are placed at undisturbed and disturbed hub centers respectively while Z_f coincide with the shaft direction, and X_f points toward the rear of the helicopter. These are systems which do not rotate with

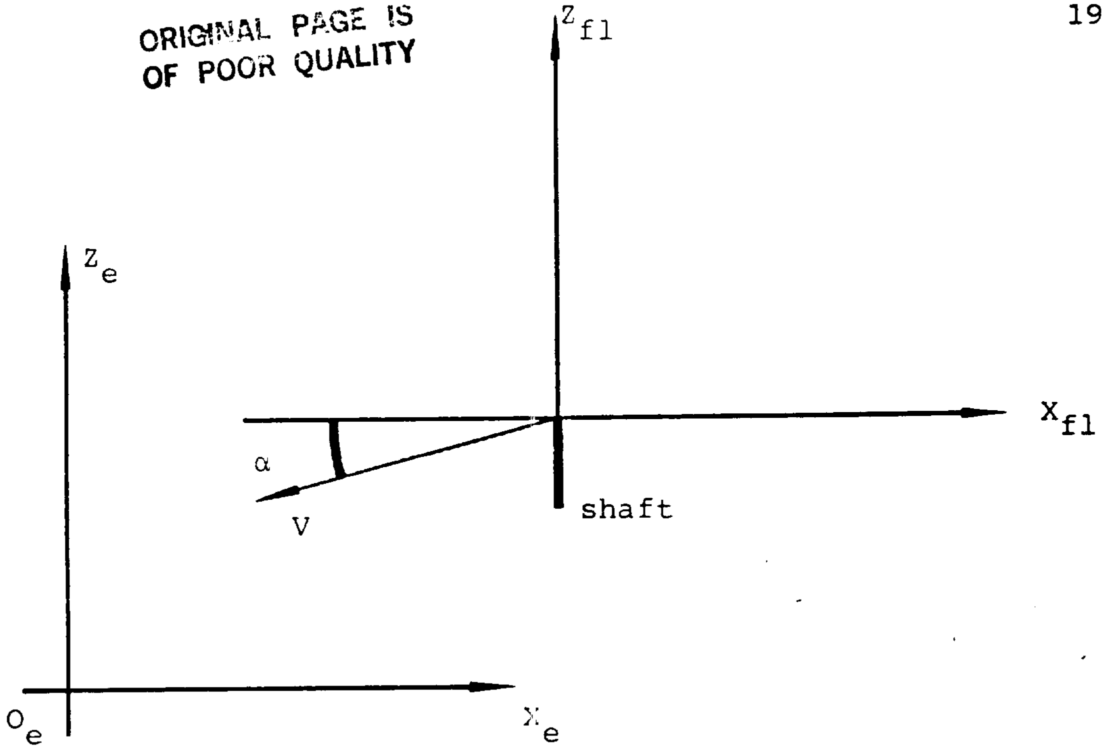

Fig. 2-1 The F_1 System of Coordinates

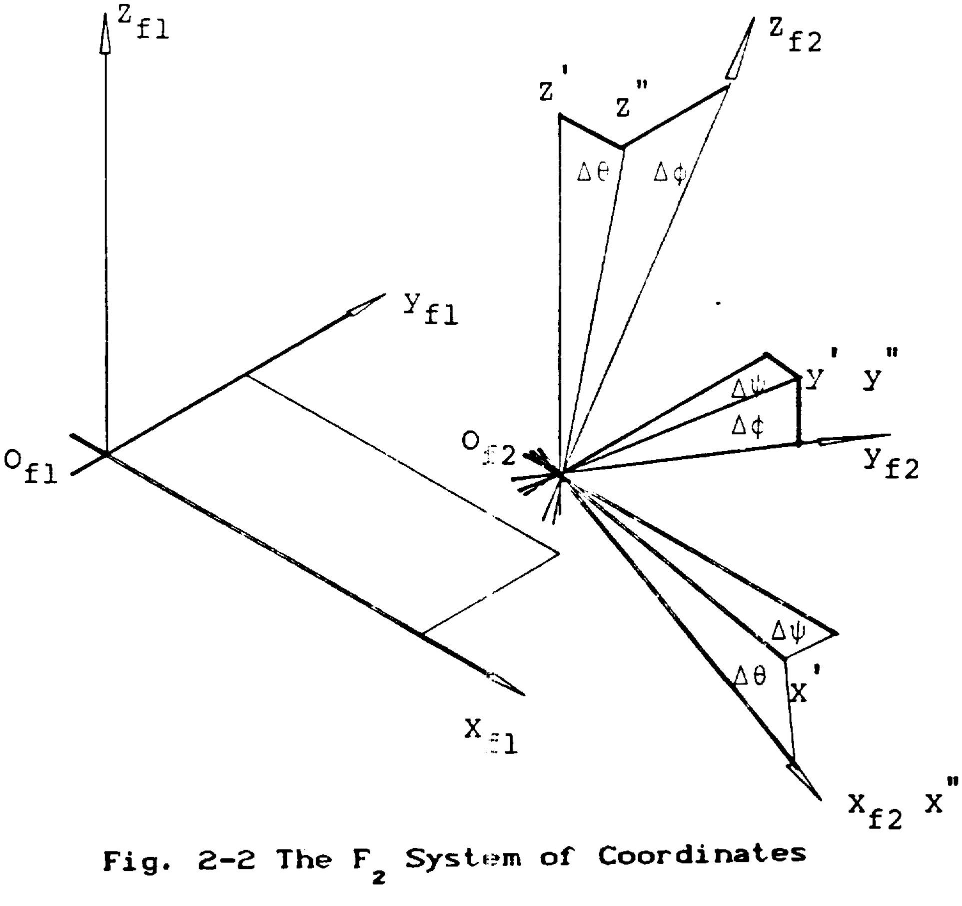

Fig. 2-2 The F_2 System of Coordinates

the hub. The F_1 system moves due to the fuselage trim motion without perturbation, a Galilean frame. The F_2 system moves relative to F_1 due to small perturbations which result from disturbed fuselage rotations and translations. The equations are formalized so that the elastic deformations may also be included, depending on the definition of a transformation expressing the hub motion relative to the fuselage in terms of the generalized coordinates. In the linearization of the system, this transformation is also linearized under an assumption of small perturbations and is assigned as a set of system input parameters to offer more flexibility for the model. By selection of the set of the input parameters, it is possible to investigate the dynamics of a rotor on a flexible shaft or the free motion of a helicopter like that in this thesis, or some combinations of the two.

The third system of coordinates is the H (hub) system, which is rotating with the hub (See Fig. 2-3). The coordinate axes Z_h and Z_{f2} coincide, while the H system rotates about the Z_{f2} axis with an constant angular velocity, relative to the F_2 system. When the azimuthal angle of the H system relative to the F_2 system is zero, the two systems coincide. The next system of co-ordinates is the blade system B (See Fig. 2-4), which is fixed to the rigid blade and is displaced from the H system by offset and rotates due to lag and flap. See Appendix A for more detail.

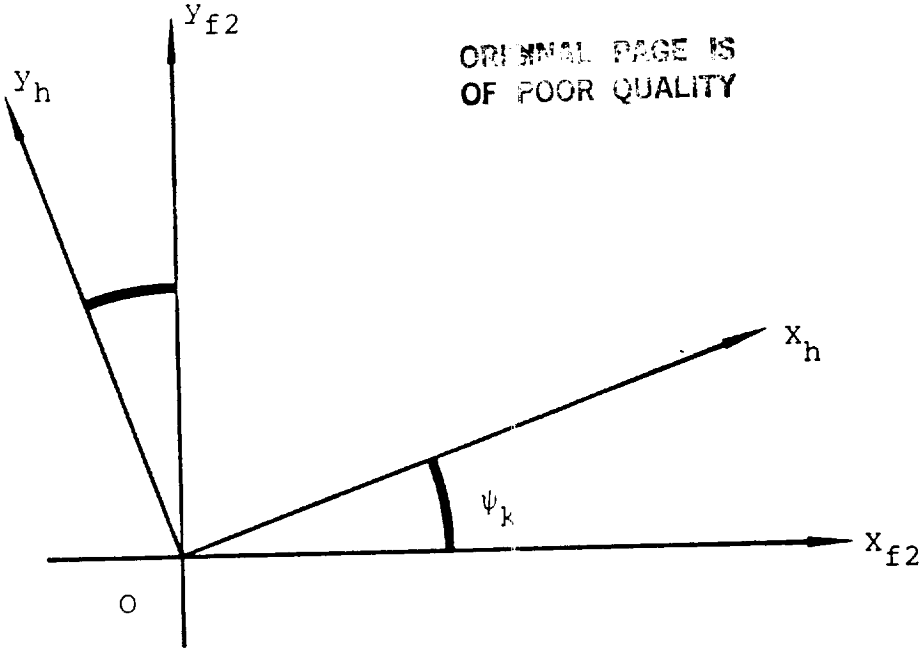

Fig. 2-3 The H System of Coordinates

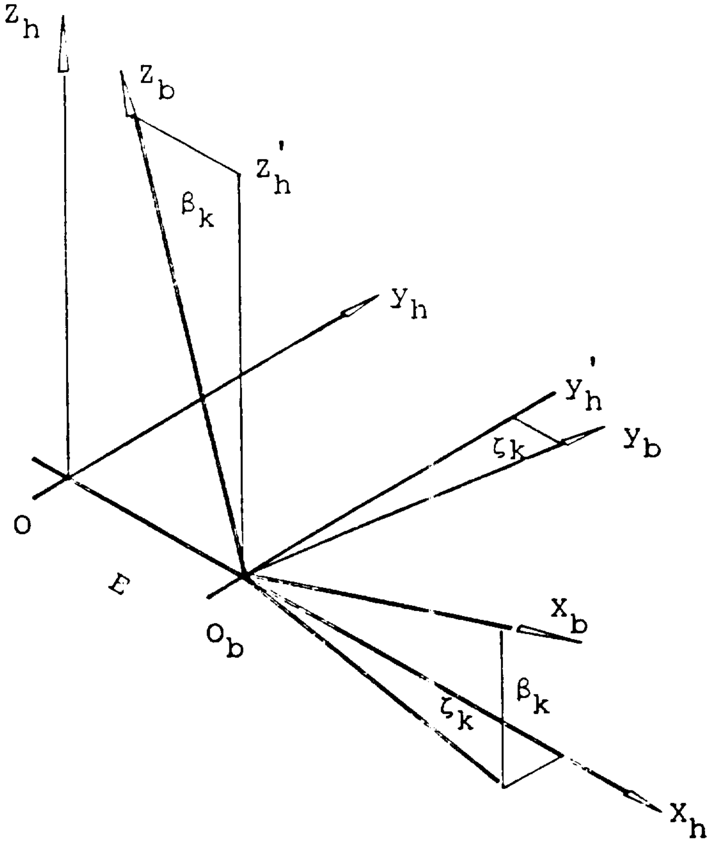

Fig. 2-4 The B System of Coordinates

2.4 Rotor Blade Model

The rotor blade is assumed to be a rigid beam with an offset hinge for a fully articulated rotor. A proper combination of a hinge offset and springs about the hinge can be used to represent a hingeless rotor. This model can incorporate the effects of blade and hub stiffness by two sets of springs inboard and outboard of the hinge. Furthermore, flap-lag-pitch-fuselage structural coupling can be easily incorporated, Spring restrained hinges can be used to model a bearingless rotor.

The coning angles both for flapping and lagging are considered as variables because in forward flight there is coupling between the coning and the first harmonic terms.

2.5 Inertial Analysis

The position of an element of a blade first is written in the B frame. It is assumed that the blade can be modelled as a slender rod with all of its mass located on $[X_b, 0, 0]$. Using a series of transformations, we can express the position of the blade element in the inertia axis, the E system. Then, it is straightforward to obtain the local velocity and the kinetic energy. The same approach applies to the fuselage as well. After integrating along the blade, combining the blade with the fuselage and taking required differentiations, the contribution of the kinetic energy to the equations of motion is obtained The kinetic energy contribution of the tail rotor is neglected.

For the potential energy, the terms due to the gravity of the blades are neglected but those from the fuselage are included. To model a hingeless or bearingless rotor, two other spring potential terms are added for including the elastic potential resulting from the deformations of the flapping and lagging.

2.6 Rotor Blade Aerodynamic Model

First, we get expressions of the normal and tangential velocities at a blade element in the B frame, then apply strip theory to obtain the lift and drag at local blade sections. After integration along the blade and a transformation, we get expressions of the aerodynamic forces and moments of the blade in the hub axis H. The same approach applies to the tail rotor, the vertical tail and the horizontal tail as well, the only difference is that a little algebra is used to treat the delta 3 feedback of the tail rotor. Only the thrust of the tail rotor is considered in this work.

The tail rotor and fixed tail surfaces can experience aerodynamic interference effects from many sources. Only the components of flow from the main rotor are included in this model. However, the equations are formulated to allow easy insertion of other components. The total velocity components for the tail rotor and fixed tail surfaces are made up of contributions from the basic body axes translational and angular velocities and rotor wash. Dynamic pressure loss is introduced by factoring the components of the free stream flow. The actual total dynamic pressure is calculated from the resultant velocity at tail rotor and fixed tail surfaces. This allows a more representative definition of dynamic pressure at low speeds where the downwash velocities predominates.

Then the total virtual work due to the aerodynamic forces is expressed as a function of the generalized coordinates by summarizing all virtual work done by each aerodynamic force or moment, in which extreme care must be exercised because any inconsistency with the corresponding inertia term will result in large errors at final dynamic equations after the linearization. Taking required differentiations, we get the generalized forces for the equations of motion.

2.7 Dynamic Inflow

The rotor blade operates in an unsteady environment; consequently unsteady aerodynamics can have a significant influence on the aeroelastic and aeromechanical stability characteristics of helicopters. To describe the low frequency unsteady aerodynamic behaviour of the rotor, there are relatively simple unsteady aerodynamic models, known as inflow models, which agree with experiment and can be conveniently incorporated in aeromechanical and aeroelastic stability and control analyses of helicopters. These simple models are based upon the definition of certain inflow parameters which represent essentially the unsteady wake-induced flow through the rotor disk.

The induced flow-field acting on a helicopter rotor affects both rotor equilibrium (trim loadings) and rotor response (transient loadings). Hence, it is reasonable to expect that the induced flow will also be affected by the oscillations of the rotor. Following this assumption, the inflow is written as a combination of a steady inflow for trim loadings and a dynamic perturbation for transient loadings. Then, the total induced velocity normal to the rotor disk is expressed as

$$V_n = V_{no} + V_o(t) + V_c(t)\cos\psi + V_s(t)\sin\psi \qquad (1)$$

where v_o, v_c, and v_s are components of the dynamic inflow perturbation. The dynamic inflow components can be related to the perturbed thrust ΔF, the perturbed pitch and roll moments ΔM_y, ΔM_x. The equations are written in form

$$[L]\ [M]\ \{V'\} + \{V\} = [L]\ [D]\ \{\Delta F\} \qquad (2)$$

where $\{V\}^T = [V_o, V_c, V_s]$ and $\{\Delta F\}^T = [\Delta T, \Delta M_y, \Delta M_x]$

The matrix [L] is the static coupling matrix between induced velocity and aerodynamic loads, the matrix [M] assumes the role of an inertia of the air mass, the product of [L][M] is a matrix of time constants, and the matrix [D] is a dimension adjustor.

A number of such inflow models are available in the literature. In this work, the steady inflow is obtained from momentum theory for hover and from classical vortex theory for forward flight. It has a first harmonic distribution as a function of wake skew angle. The dynamic model, i.e. the [M], [L], and [D] matrices, come from Pitt's model based on a rigorous solution to actuator-disk theory. The details of the model can be found in Ref.21.

There is no simple method available to include the effects of the unsteady wake of the rotor on the tail rotor and horizontal tail. Considering the dynamic inflow models represent the global effects of the unsteady wake, the effects of the unsteady wake on the horizontal tail and the tail rotor are included by directly extending the dynamic inflow components out of the rotor plane, which is done by assuming that the dynamic inflow at tail rotor and tail surfaces are of two times of the value on the line $X_{fz}=R$, $Z_{fz}=0$.

2.8 Linearization

The nonlinear equations of motion are of the form:

$$Q'' = F(Q, Q', U, T) \qquad (3)$$

Introducing multiblade coordinates, which transforms the blade-fixed generalized coordinates to nonrotating hub-fixed generalized coordinates, and omitting periodic higher harmonic terms, a constant coefficient approximation to the original periodic system is obtained:

$$Q'' = F(Q, Q', U) \qquad (4)$$

The process of linearization consists of expressing the time dependence of the generalized coordinates and inputs as the sum of the steady-state value and the time-dependent perturbation about the former.

$$Q_i(t) = Q_{io} + \Delta Q_i(t) \qquad (5)$$

$$U_i(t) = U_{io} + \Delta Q_i(t) \qquad (6)$$

Equations (5) and (6) are substituted into the nonlinear equations of motion, and terms containing squares of the perturbation quantities are neglected. The perturbation quantities are set equal to zero to obtain the steady-state values of the generalized coordinates and the control inputs in the trim condition.

$$F(Q_o, U_o) = 0 >> Q_o \; U_o \qquad (7)$$

The final form of the dynamic equations can be symbolically written as

$$M(Q_o, U_o)\Delta Q'' + C(Q_o, U_o)\Delta Q' + K(Q_o, U_o)\Delta Q = B(Q_o, U_o)\Delta U \quad (8)$$

This linear time-invaring system can be written in first order form:

$$X' = A\,X + B\,U \qquad (9)$$

X and U are the state variables and control input vector:

$$X = [\, \beta_o, \beta_1, \beta_2, \zeta_o, \zeta_1, \zeta_2, \theta, -\phi, -\psi, y, x, z$$

$$\dot{\beta}, \dot{\beta}, \dot{\beta}, \dot{\zeta}, \dot{\zeta}, \dot{\zeta}, \dot{\theta}, -\dot{\phi}, -\dot{\psi}, \dot{y}, \dot{x}, \dot{z}, Vo, Vc, Vs\,]^T$$

$$U = [\, A_{1s}, B_{1s}, \theta_t\,]^T$$

The collective pitch angle of the main rotor is not included in the control vector of the perturbation equations because collective input were not investigated.

Chapter III

INFLUENCE OF THE ROTOR WAKE ON THE TAIL ROTOR AND FIXED TAIL SURFACES

3.1 Introduction

It has been found from wind tunnel tests that the rotor wake influences the aerodynamics of the tail rotor in forward flight [22] and that the effect of rotor wake on the horizontal tail produces a significant contribution to yaw pitch coupling [23], which arises because of the angle of attack distribution across the span of the horizontal tail. The angle of attack can vary by as much as 10 degrees from one tip to the other.

In this work it has been found that the transient response in forward flight, especially the pitch response, is very sensitive to the treatment of the influence of the rotor wake on the vertical tail, the horizontal tail, and the tail rotor. A simple theory based on a flat vortex wake model has been employed to obtain estimates of vertical variation of the sidewash at the tail rotor and vertical tail and the horizontal variation of the nonuniform downwash at the horizontal tail. The mathematical details of the wake model used in this work are discussed in Ref.24 and are also given in Appendix C. Only a brief description is given here.

3.2 Theory of Lifting Airscrews with a Flat Vortex System

The flat vortex wake model is based upon the following assumptions:

(1) The vortex wake formed by free vortices leaving the rotor blades moves downstream without any downward motion. This should be a good approximation for helicopters with sufficiently high flight speeds. Experience and theoretical considerations indicate that this assumption is reasonable for a considerable range of flight speeds of helicopters.[25]

(2) The intensity of the free vortices leaving the same section of the blade at various azimuth angles is constant. This means that an average value of the circulation at a given radius r of the blade is used to replace the time varying circulation value, which depends on the azimuth angle.

(3) The free vortices in the rotor wake form a continuous surface of vorticity. This is due to the fact that for most helicopters the cruise tip speed is at least 2.5 times higher than the velocity of flight, and the rotor has 3 or 4 blades so that the density of free vortices would be high enough to be considered as a continuous surface.

Under these three assumptions, consider a free vortex layer which springs from the blade at a given radius r with a constant circulation. One can find, after some simple mathematical derivation, the final vorticity surface is consisted by a lateral vorticity surface within a circle of radius r and centred at hub, and a longitudinal vorticity surface which coincides with the whole wake surface. The circulation per unit length of the lateral vortex layer is a constant, which is proportional to the intensity of the free vortex layer, and inversely proportional to the advance ratio and rotor radius. The circulation per unit length of the longitudinal vortex layer is a function of lateral position y, which is also proportional to the intensity of the free vortex layer, and inversely proportional to the advance ratio and rotor radius. Then under the assumption that the circulation distribution along the rotor radius, averaged over the azimuth, is parabolic, the distribution of vortex strength can be determined and the induced velocity at any point in space can be calculated by applying the Biot-Savart law, and integrating over the whole blade. This model produces lateral and vertical components of the induced velocity.

3.3 Influence of the Rotor wake on the Tail Surfaces

To estimate the influence of the rotor wake on the tail rotor and fixed tail surfaces, it is assumed that the downwash and sidewash distributions in the trim condition are given by distributions calculated relative to the centerline of the wake at X = R. Perturbations in sideslip and angle of attack cause the centerline to move changing the corresponding aerodynamic forces and the moments.

The vertical induced velocity contribution in the plane of the rotor disk due to the lateral vortices is physically equivalent to the fore and aft variation produced by the classical vortex theory, and the average induced velocity due to the longitudinal vortices is equivalent to the uniform part from the classical vortex theory. These contributions are obtained by directly extending the classical vortex results out the rotor plane to the required location. The variable part of the vertical induced velocity contribution due to the lateral vortices is symmetric with respect to the vertical plane, as a result its first order variation in the lateral direction will be zero. In addition, the lateral vortices do not produce a contribution to the lateral component of the induced velocity. Therefore, in this work only the nonuniform contribution of the longitudinal vortices is included as follows.

The normalized nonuniform vertical induced velocity distribution along the lateral axis at the position of horizontal tail in forward flight with zero sideslip angle at an advance ratio of 0.22 (100 KTS) for UH-60A is shown in Fig. 3-1. The antisymmetric part produces a steady rolling moment and a pitch moment variation with the sideslip angle. The symmetric part produces a steady pitch moment and a roll moment variation with the sideslip angle.

The shape of the distribution explains the phenomena observed in the wind tunnel test of Ref.23: (1)the left hand

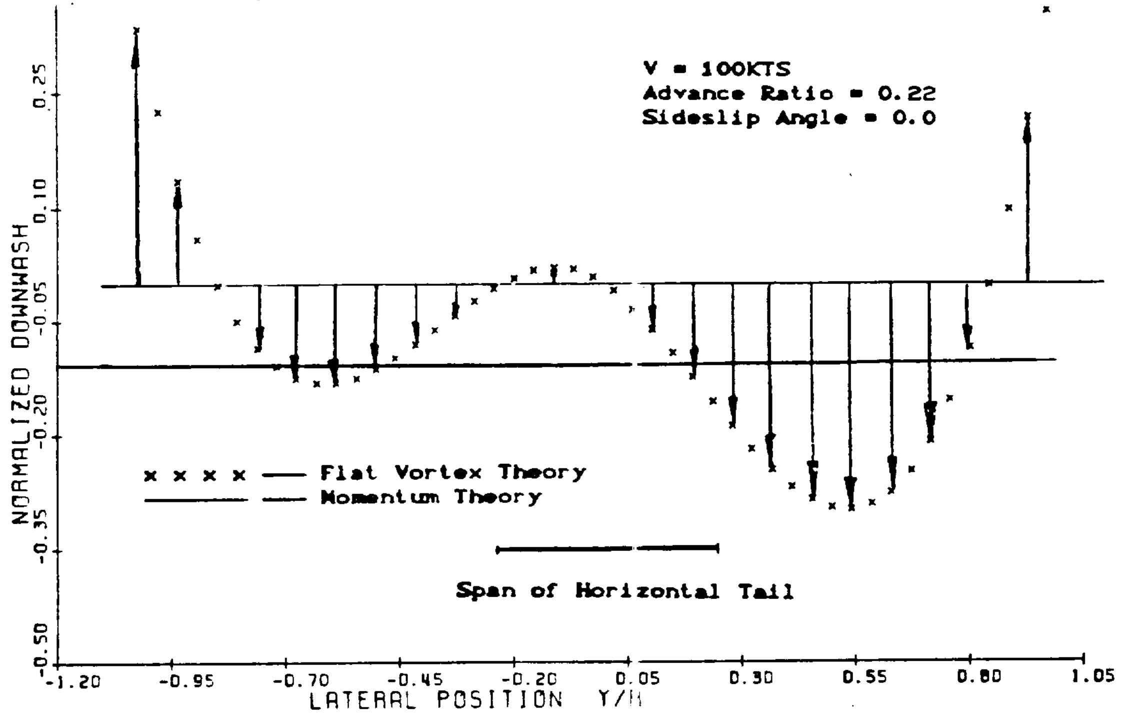

Fig. 3-1 Lateral Distribution of Downwash

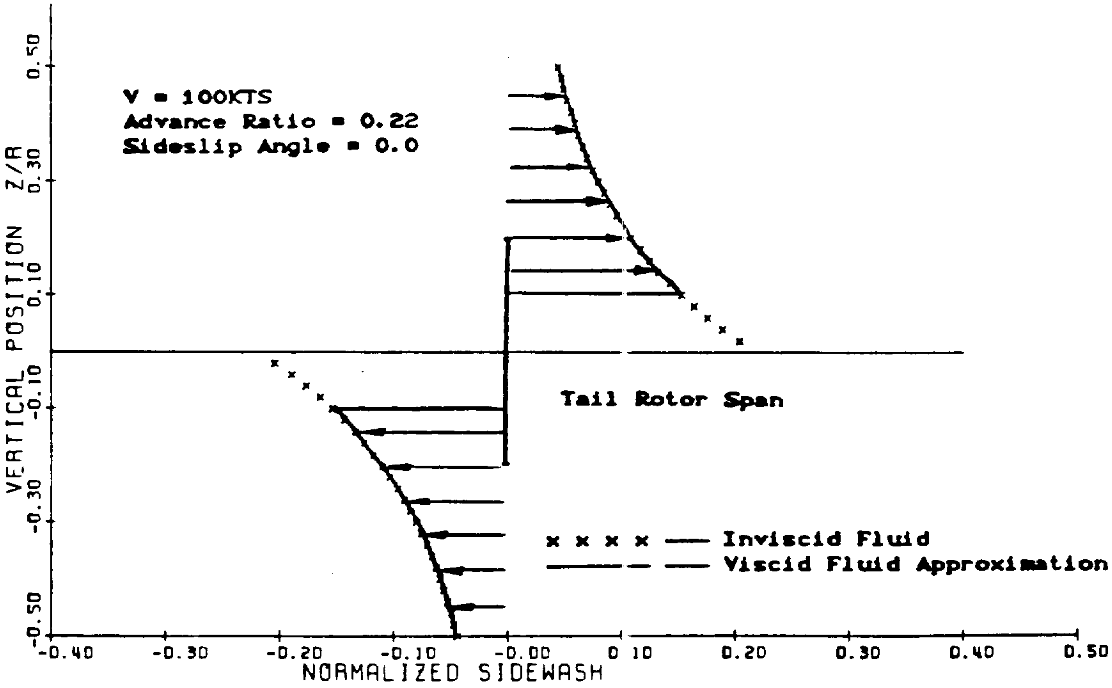

Fig. 3-2 Vertical Distribution of Sidewash

panel encounters relative positive rotor induced angles and the right hand panel encounters negative values, (2)the yaw-pitch coupling is generally worse for a nose left slip than for a nose right slip, (3)the right hand panel produces considerably more coupling than the left hand panel when tested separately.

The vertical variation of the lateral component of the induced velocity at the tail rotor in the zero sideslip case for the same helicopter at the same flight condition at advance ratio of 0.22 is shown in Fig. 3-2. As a consequence the local angle of attack of the tail rotor and vertical tail will vary with the angle of attack of the helicopter, producing roll and yaw moments. It can be seen that there is a discontinuity on the wake, which is due to the inviscid fluid assumption in the theory and is smoothed out by taking the viscosity of the airflow into account. Because the real distribution is unknown and nonlinear, and the assumption of tail rotor center located on the surface of the wake is extremely poor for most flight conditions, the corresponding derivatives are determined by correlation with flight test. The derivatives used in this paper are determined in one trim condition at advance ratio of 0.14 (60 KTS). It has been found that the response prediction is not sensitive to the value of these derivatives, however the overall effect is important.

Although the effects of nonuniform induced velocity are strong nonlinear functions of the sideslip and angle of attack, only the steady contribution and first order variation of these effects are included. For example, the overall roll and pitch moment contributions by horizontal tail as functions of the sideslip angle and their linear approximations are given in Figs. 3-3 and 3-4 for the helicopter at the same flight condition as the induced velocities. As can be seen, these nonlinear effects behave like linear effects only in a small neighborhood about the equilibrium point. Therefore, the model is limited to the case of small sideslip motion.

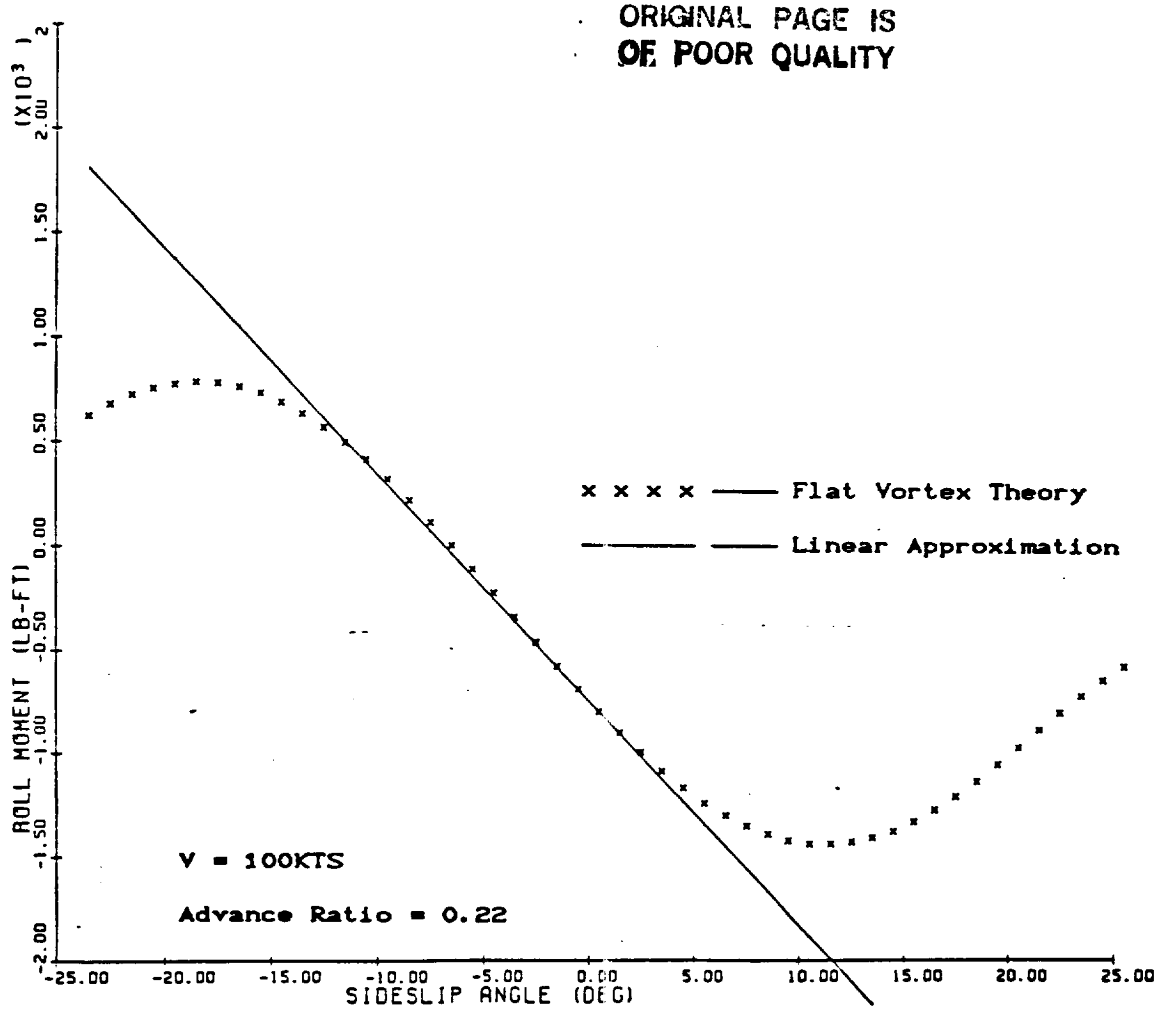

Fig. 3-3 Roll Moment Produced by Horizontal Tail as a Function of Sideslip Angle

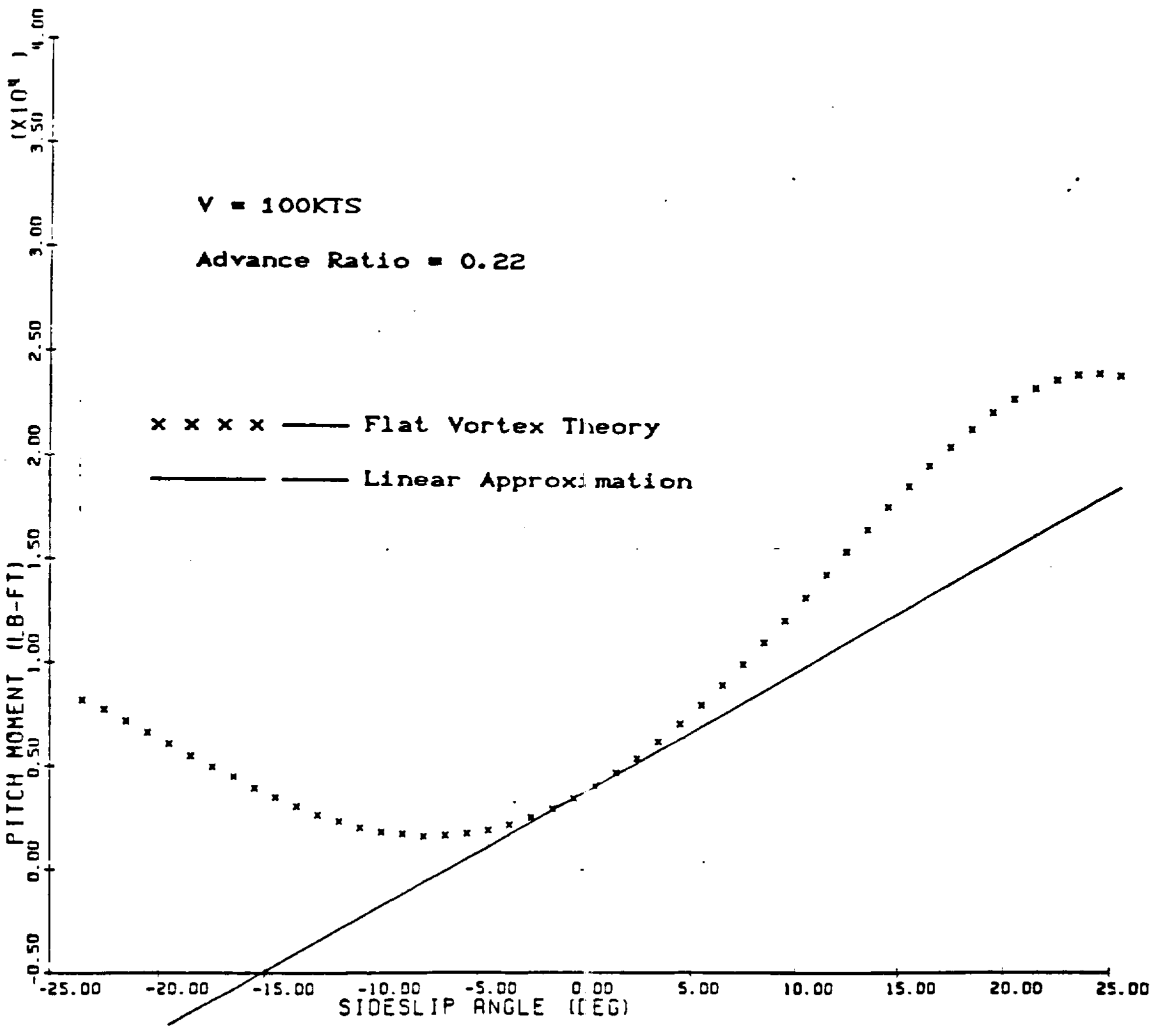

Fig. 3-4 Pitch Moment Produced by Horizontal Tail as a Function of Sideslip Angle

Chapter IV

VERIFICATION OF THE MODEL

4.1 Introduction

To correlate the model, the transient response of an articulated rotor helicopter to small step-inputs of each control at various trim conditions has been calculated and compared with a large nonlinear model currently used in a simulator and with flight test data. The flight test results are obtained by a flight test program solely for the purpose of validating mathematical models of the helicopter.

The helicopter is a UH-60A Black Hawk, which has a fully articulated rotor having four blades with lead-lag dampers. The helicopter configuration, structural and aerodynamic properties are given in Ref.10. The trim conditions are hover, 60 KTS level flight, 100 KTS level flight, and 140 KTS level flight. The time histories of the control inputs, the test conditions, and the transient responses obtained from flight test and the simulation are presented in Ref.18.

The trim values and the initial control settings used in the simulation are directly obtained from flight test data. After trimming to the test conditions, the time-histories of the perturbed input, which are the differences between the time-histories of test-aircraft control and its initial control positions, were used as direct input to the simulation. In this way, the simulation begins each transient response in the actual trim condition; therefore, the trim errors have a minimal influence on dynamic response comparisons. All simulation performed in this work used a time step of 0.05 sec. The simulation output was recorded every 0.15 sec to reduce the cost of plotting.

The calculated response time-histories are compared to flight test data for small control inputs in Figs. 4-1 to 4-27. Correlations are discussed in terms of the fuselage angular rate response since their quantities are of primary interest in handling qualities. Calculated results from models both with and without dynamic inflow are presented in hover so as to illustrate the role of dynamic inflow in response prediction. In forward flight, a third model, the model including not only dynamic inflow but also the effect of the rotor wake on the fixed tail surfaces and tail rotor, is added.

4.2 Hover

Figs. 4-1, 4-2 and 4-3 present the roll, pitch and yaw rate responses of UH-60A at hover to a 1-inch right cyclic input, compared to flight test data of Ref.18. The results obtained from this simulation including dynamic inflow produce very good agreement with the flight test data, and also represent an improvement over the nonlinear simulation

ORIGINAL PAGE IS
OF POOR QUALITY

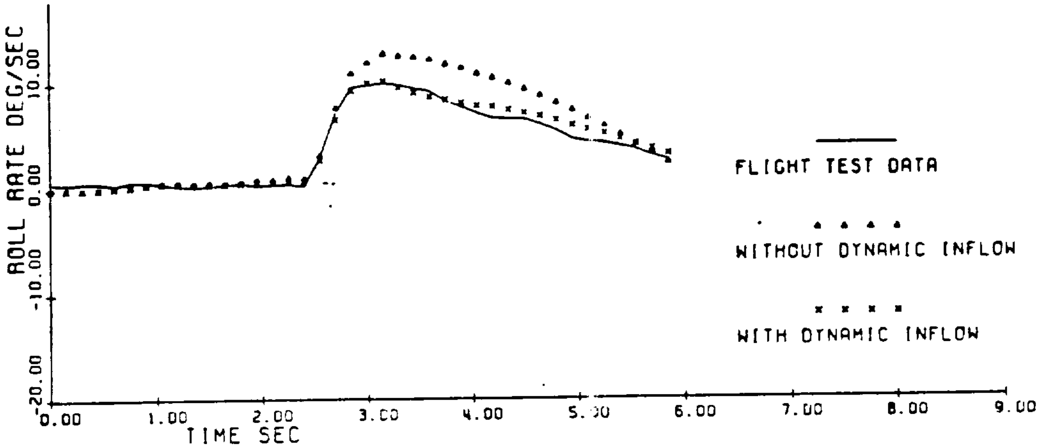

Fig. 4-1 Comparison of Calculated Responses and Flight-Test Data (Roll Rate Response to 1-in Right Cyclic Input, Hover)

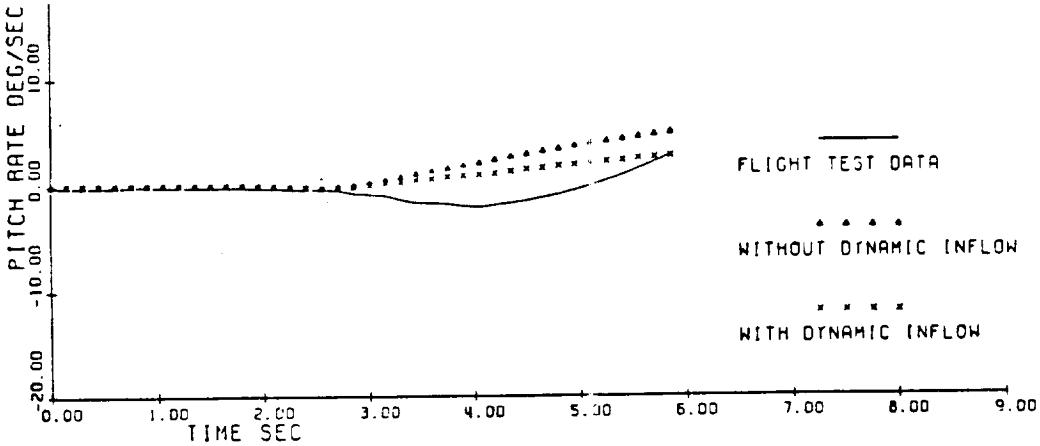

Fig. 4-2 Comparison of Calculated Responses and Flight-Test Data (Pitch Rate Response to 1-in Right Cyclic Input, Hover)

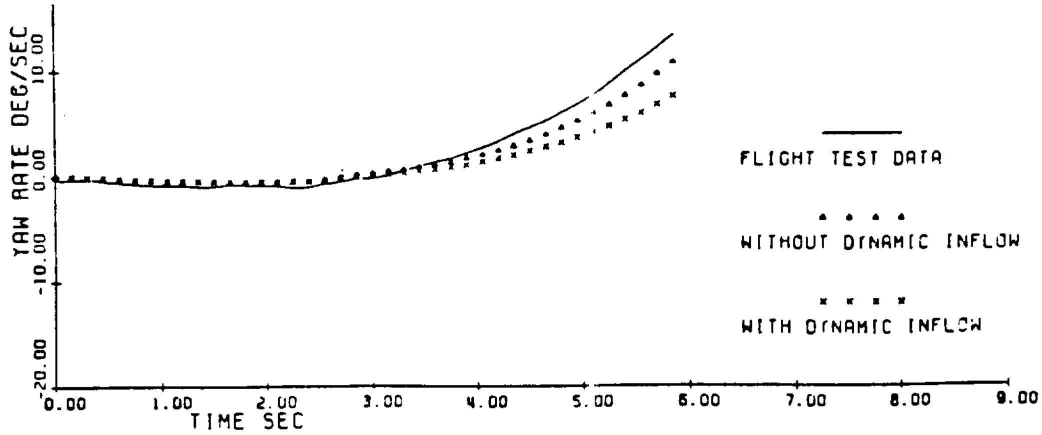

Fig. 4-3 Comparison of Calculated Responses and Flight-Test Data (Yaw Rate Response to 1-in Right Cyclic Input, Hover)

model of Ref.18. For the on-axis response, the addition of dynamic inflow gives a significant improvement in the agreement between experiment and theory. The roll rate response to the right cyclic input almost coincides with the flight test data and reduces the error in the prediction of the roll rate peak to zero from 25% for the model without dynamic inflow. The nonlinear simulation indicates about 40% error in this important characteristic[18]. For the off-axis response, the calculated results are also quite close to the flight test data, although dynamic inflow has little influence on these responses. It is of interest to note that even though this is an articulated rotor helicopter, dynamic inflow has a significant influence on the response.

Figs. 4-4, 4-5 and 4-6 present the pitch, roll and yaw rate responses of UH-60A at hover to 0.5-inch forward cyclic input. Although for the on-axis response, the model including dynamic inflow gives a significant improvement, the agreement in pitch rate response to the forward cyclic input is not as good as in the lateral case. This discrepancy implies that the effective pitch damping is under-estimated, tending to indicate that there is a significant additional source of damping not accounted for in the theory probably due to the rotor wake horizontal tail interaction since the good agreement for the lateral axis shows that the rotor damping contribution is accurately estimated. For the off-axis response, the calculated results are close to the

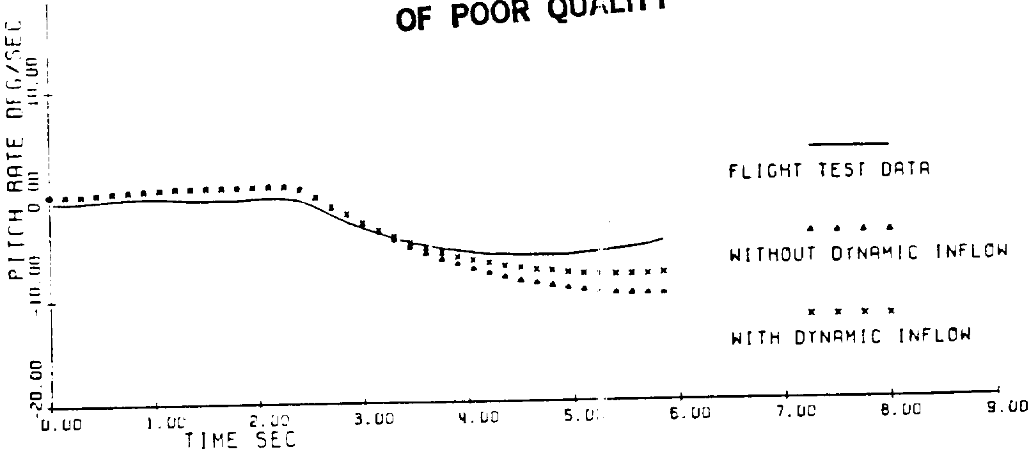

Fig. 4-4 Comparison of Calculated Responses and Flight-Test Data (Pitch Rate Response to 0.5-in Forward Cyclic Input, Hover)

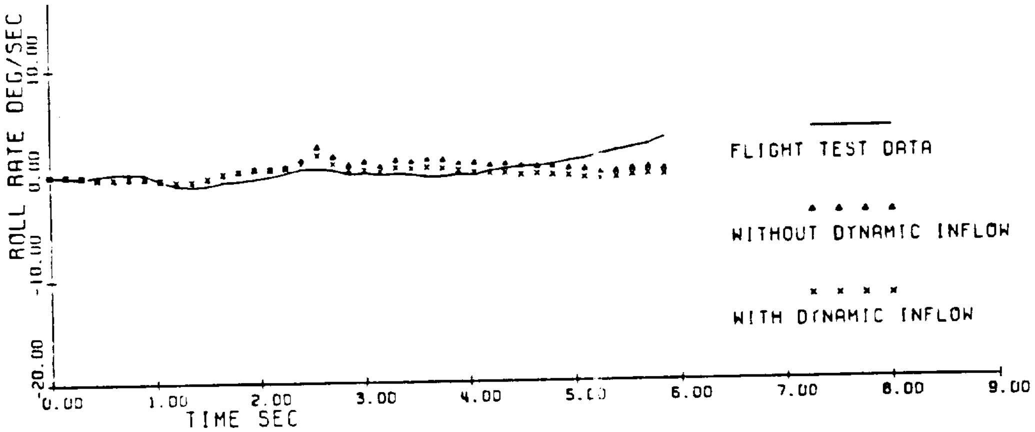

Fig. 4-5 Comparison of Calculated Responses and Flight-Test Data (Roll Rate Response to 0.5-in Forward Cyclic Input, Hover)

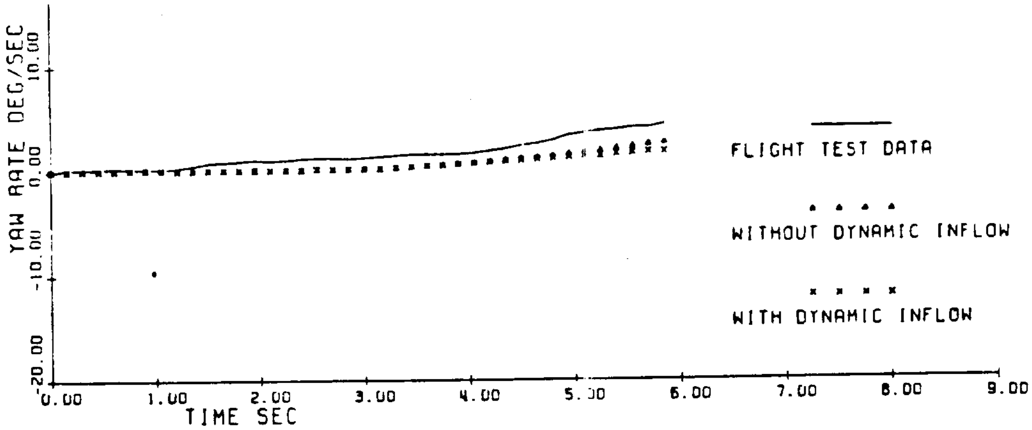

Fig. 4-6 Comparison of Calculated Responses and Flight-Test Data (Yaw Rate Response to 0.5-in Forward Cyclic Input, Hover)

flight test data, and as for the lateral input, dynamic inflow does not give a significant change.

Figs. 4-7, 4-8 and 4-9 present the responses at hover to 1-inch left pedal input. The initial yaw acceleration is under-estimated, and the roll rate response is close to the flight test result. The pitch rate response is quite different from the flight test result, again indicating a rotor-tail interaction.

For each control input, the dynamic inflow has little effect on the yaw rate response because the dynamic inflow is related only to downward inflow components. In addition, because of pilot difficulty in maintaining trim of the unaugmented aircraft, in many cases flight test data drifts from trim before the control input, causing differences between the test data and the simulation responses, especially in the small amplitude off axis responses. This can be clearly seen in Fig. 4-6, in which the control input starts at 2.4 seconds; however at that time the yaw rate response has drifted away a little more than 1 deg./sec, which is almost equal to the difference between the flight test and the simulation for the simulation period.

Generally speaking, the agreements obtained for the lateral and directional responses by including dynamic inflow are quite satisfactory. However the longitudinal responses are not so good. The likely source of this discrepancy is the interaction of the rotor wake with the large horizontal

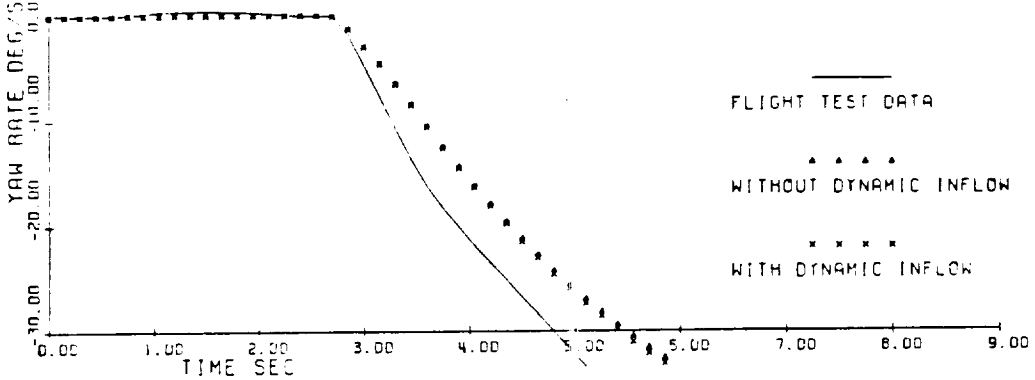

Fig. 4-7 Comparison of Calculated Responses and Flight-Test Data (Yaw Rate Response to 1-in Left Pedal Input, Hover)

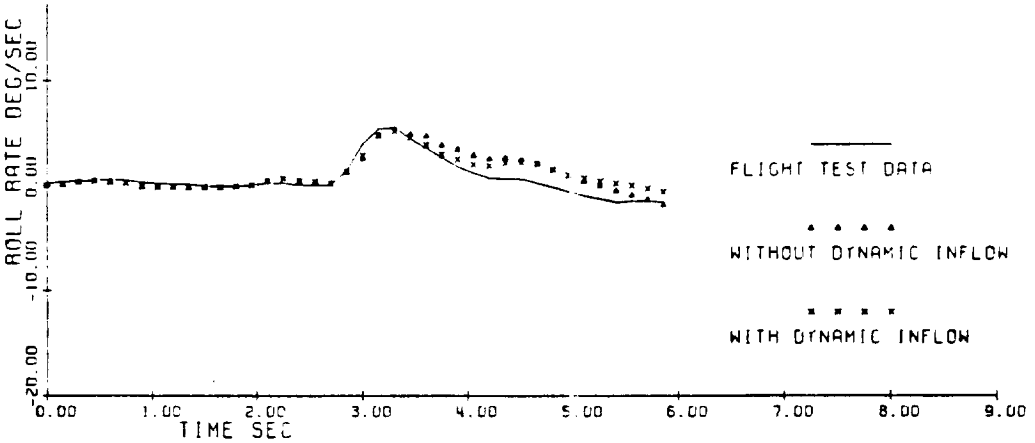

Fig. 4-8 Comparison of Calculated Responses and Flight-Test Data (Roll Rate Response to 1-in Left Pedal Input, Hover)

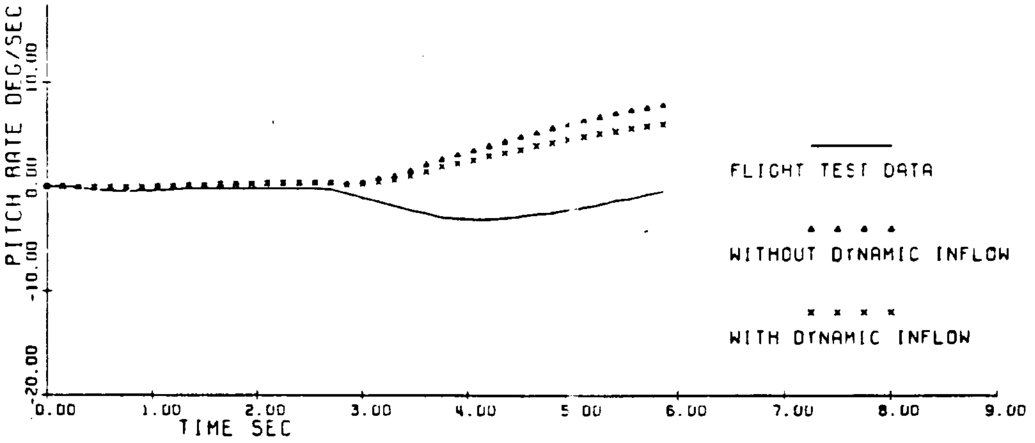

Fig. 4-9 Comparison of Calculated Responses and Flight-Test Data (Pitch Rate Response to 1-in Left Pedal Input, Hover)

tail, which is difficult to estimate due to lack of experimental data. Even so, the longitudinal responses calculated show better agreement than the nonlinear model of Ref.18.

4.3 Forward Flight

Figs. 4-10, 4-11 and 4-12 present the pitch, yaw and roll rate responses of the UH-60A at 60 KTS level flight to 0.5-inch right pedal input. The traces of Fig. 4-11 show that the yaw rate responses, the on-axis response, obtained by the models without dynamic inflow and with only dynamic inflow predict a larger peak yaw rate and a higher damping. Including the effect of the rotor wake on the tail surfaces improves the correlation producing excellent agreement. In Fig. 4-10, the predicted pitch rate responses with and without dynamic inflow depart from the flight test data to the same degree as the nonlinear simulation. Considerable improvement in the agreement is obtained by including the effect of the rotor wake. The improvement arises primarily from the addition of yaw pitch coupling due to nonuniform downwash at the horizontal tail. The roll rate response is shown in Fig. 4-12. The main rotor wake has a significant effect on the response; however this simulation predicts a significantly larger roll coupling. The initial roll acceleration due to application of rudder is over-estimated by the theory, resulting in a larger amplitude roll rate response. In this case, the model including the effect of

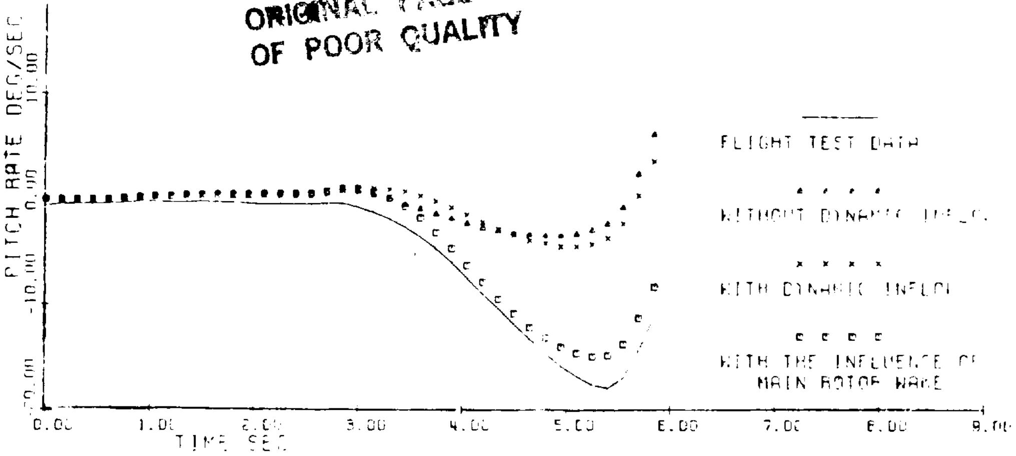

Fig. 4-10 Comparison of Calculated Responses and Flight-Test Data (Pitch Rate Response to 0.5-in Right Pedal Input, 60 KTS)

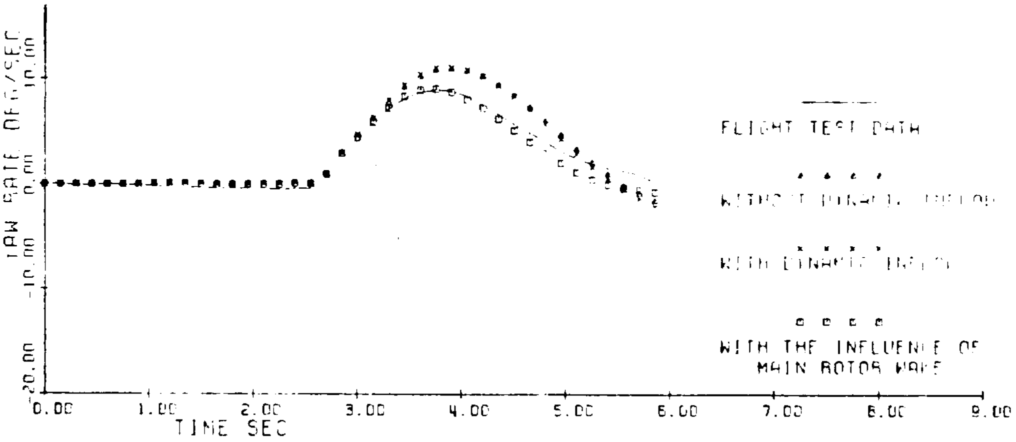

Fig. 4-11 Comparison of Calculated Responses and Flight-Test Data (Yaw Rate Response to 0.5-in Right Pedal Input, 60 KTS)

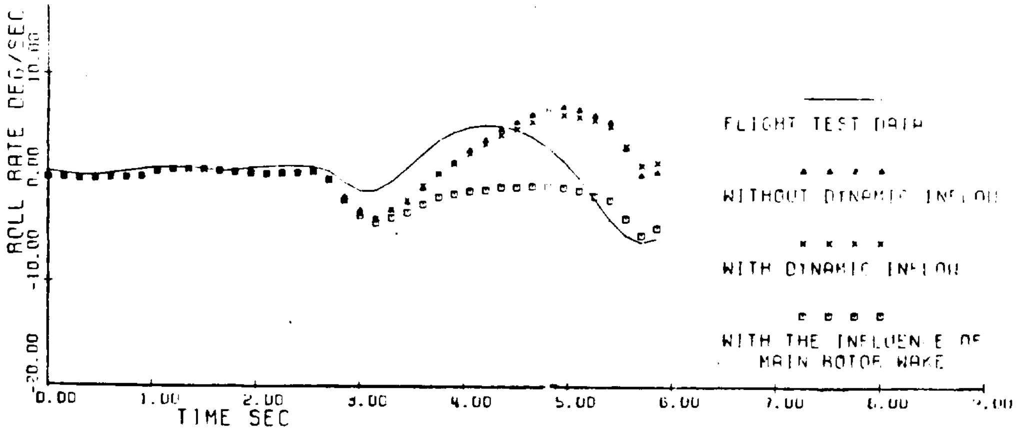

Fig. 4-12 Comparison of Calculated Responses and Flight-Test Data (Roll Rate Response to 0.5-in Right Pedal Input, 60 KTS)

the rotor wake indicates excellent performance by predicting the yaw-pitch coupling. Dynamic inflow has less effect at this translational flight condition than in hover.

Figs. 4-13, 4-14 and 4-15 show the roll, pitch and yaw rate responses to 1-inch left cyclic input. The roll rate response, the on-axis response in this case, shows very good agreement for the initial roll rate with some drift away with time. Note that for the pitch response, the model without dynamic inflow does not give the right direction for the response. Adding the dynamic inflow reverses the sign of the response and including the influence of the rotor wake gives a response very close to the flight test. For the yaw rate response, although all three are close to the flight test data, the model including the influence of the rotor wake shows no improvement over others. However, the shape of these traces suggests that trim drift may be present in the flight test as mentioned earlier. Therefore, generally speaking, the correlation between theory and experiment including the influence of the rotor wake still is much better in this case; it not only gives a correct pitch rate response by taking the yaw pitch coupling into account, but also gives a improvement in roll rate correlation.

Figs. 4-16, 4-17 and 4-18 show the angular rate responses at 100 KTS level flight to 1-inch forward cyclic input. Once again the pitch rate responses, the on-axis response, obtained by the models with and without dynamic inflow drift

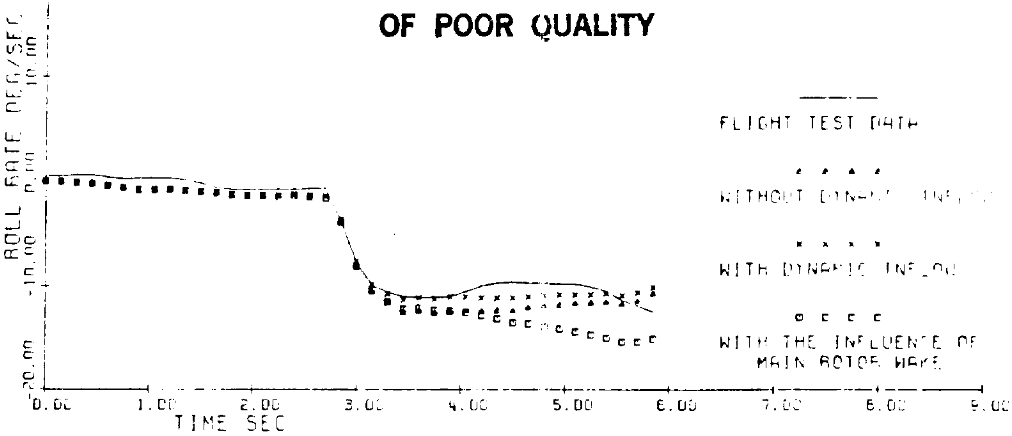

Fig. 4-13 Comparison of Calculated Responses and Flight-Test Data (Roll Rate Response to 1-in Left Cyclic Input, 60 KTS)

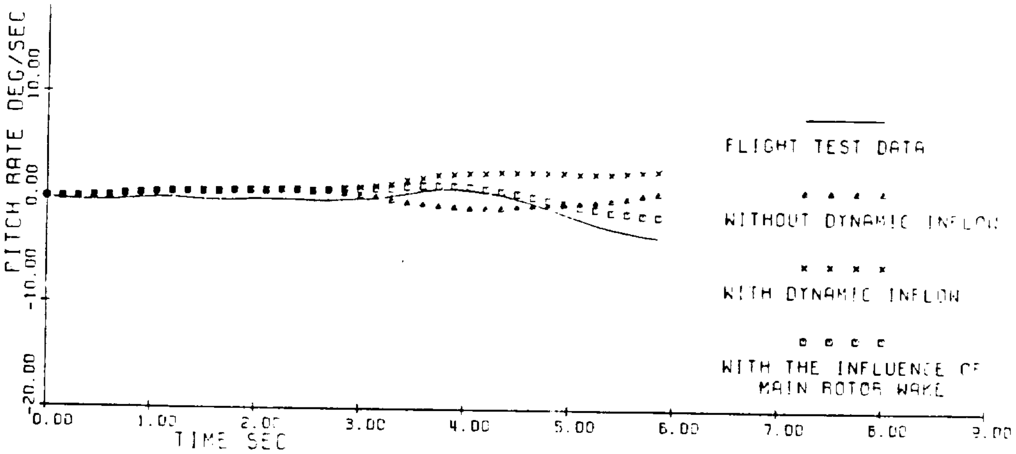

Fig. 4-14 Comparison of Calculated Responses and Flight-Test Data (Pitch Rate Response to 1-in Left Cyclic Input, 60 KTS)

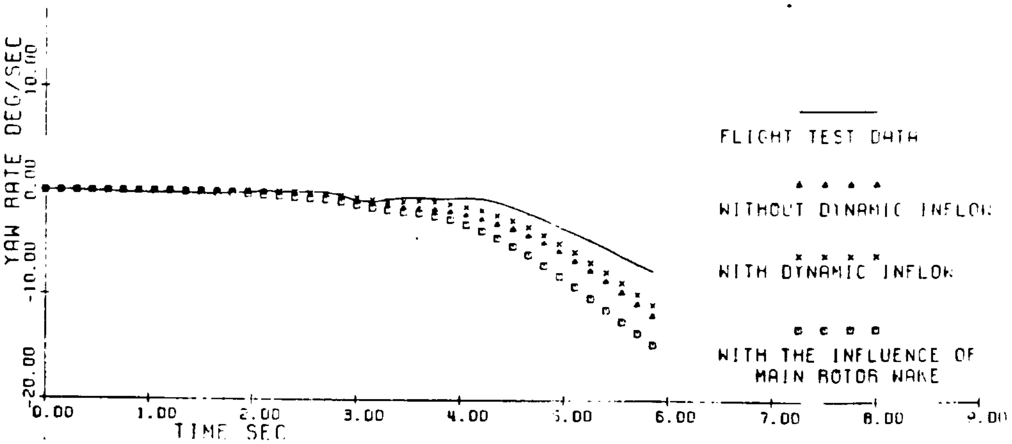

Fig. 4-15 Comparison of Calculated Responses and Flight-Test Data (Yaw Rate Response to 1-in Left Cyclic Input, 60 KTS)

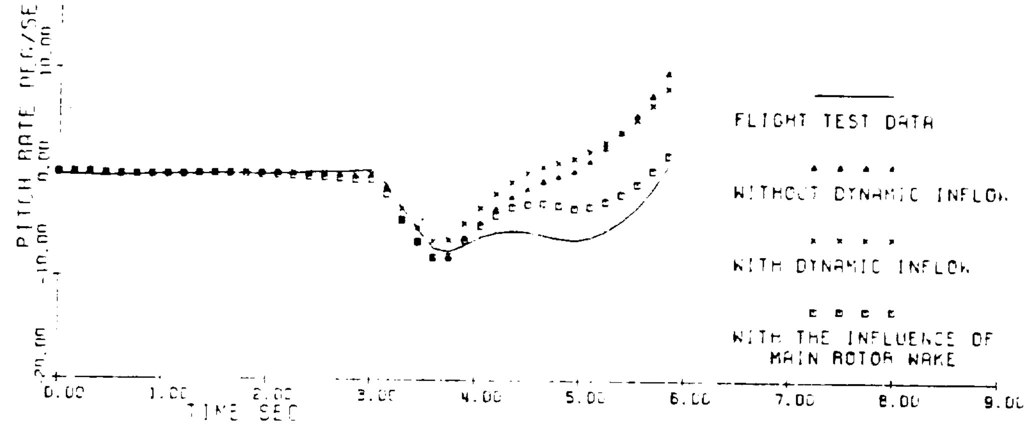

Fig. 4-16 Comparison of Calculated Responses and Flight-Test Data (Pitch Rate Response to 1-in Forward Cyclic Input, 100 KTS)

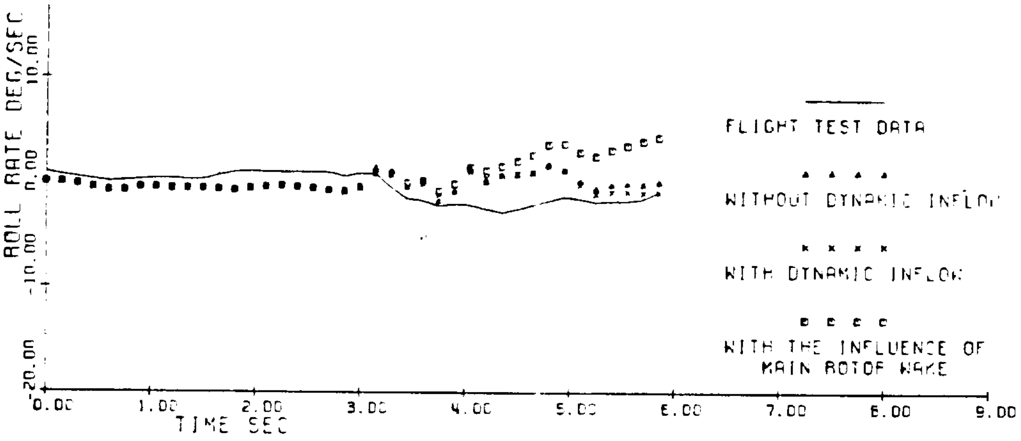

Fig. 4-17 Comparison of Calculated Responses and Flight-Test Data (Roll Rate Response to 1-in Forward Cyclic Input, 100 KTS)

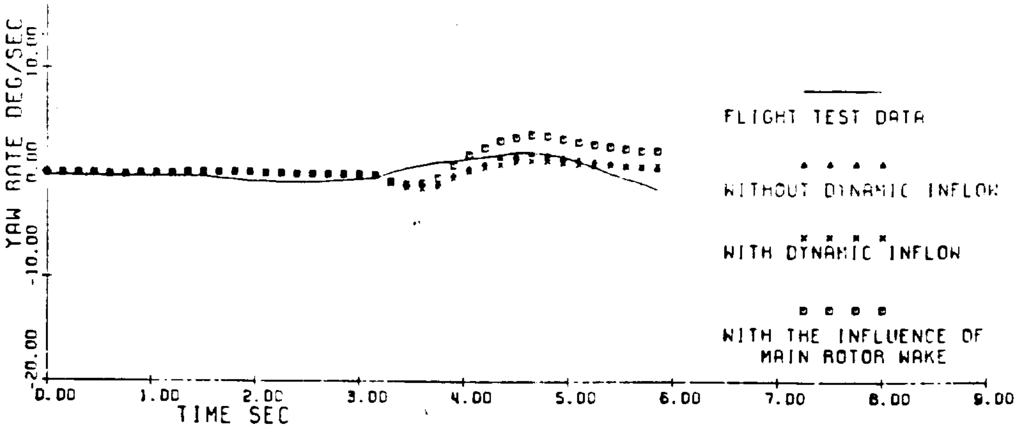

Fig. 4-18 Comparison of Calculated Responses and Flight-Test Data (Yaw Rate Response to 1-in Forward Cyclic Input, 100 KTS)

away from the flight test data. The effect of dynamic inflow is quite small at this airspeed. Considerably improved correlation of pitch rate is obtained by including the effect of the rotor wake. It has a similar shape to the flight test data, which has two peaks instead of one. For the yaw rate response, the model including the influence of the rotor wake presents a better shape but still an overshoot, which is believed due to the lack of the dynamic inflow modelling for the tail rotor. The overshoot of yaw rate response, through the yaw roll coupling by the horizontal tail caused by the nonuniform downwash, results in a small wrong positive roll rate response. Even so, it is still reasonable to say that the model including the effect of the rotor wake is better because it can predict the second peak in the primary response.

Figs. 4-19, 4-20 and 4-21 present responses of UH-60A at 100 KTS level flight to 1-inch right pedal input. The traces of Fig. 4-20 show that for the yaw rate response, the on-axis response, the models without the effect of the main rotor wake show poor agreement after the first peak. After 3.5 seconds, both of the responses drift away from the flight test data, there is an error in dominant frequency. Including the influence of the rotor wake gives a much better agreement with flight test data for the 6 second test period. In Fig. 4-19, once again the pitch rate response which shows best agreement to the flight test data comes

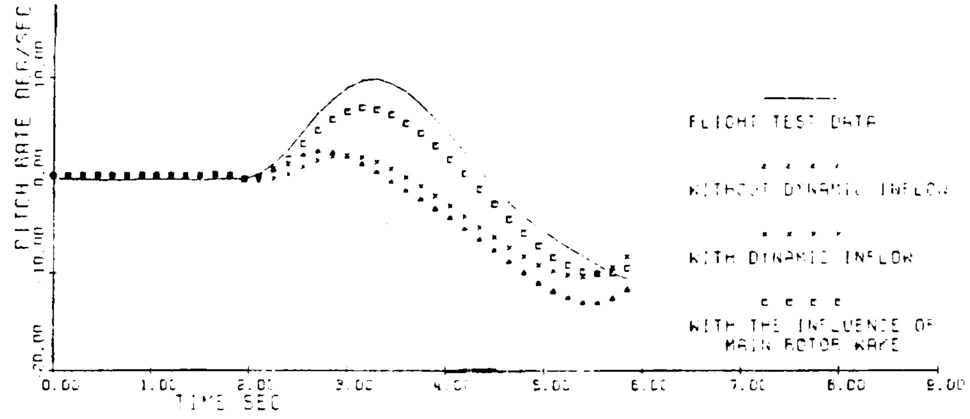

Fig. 4-19 Comparison of Calculated Responses and Flight-Test Data (Pitch Rate Response to 1-in Right Pedal Input, 100 KTS)

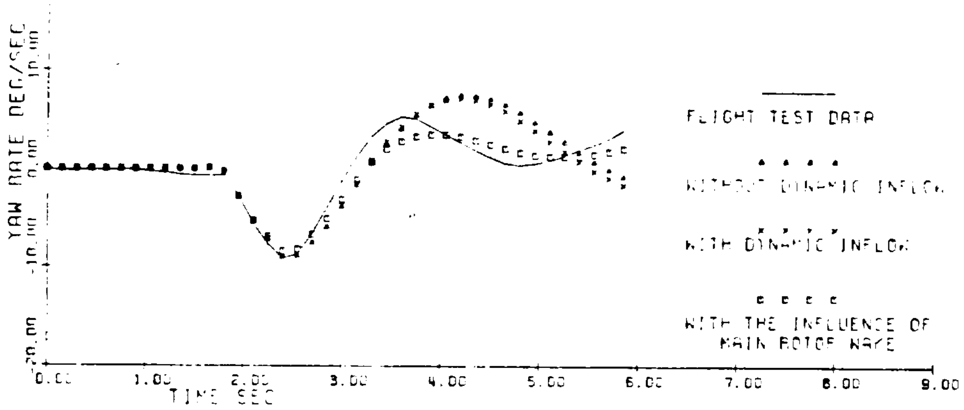

Fig. 4-20 Comparison of Calculated Responses and Flight-Test Data (Yaw Rate Response to 1-in Right Pedal Input, 100 KTS)

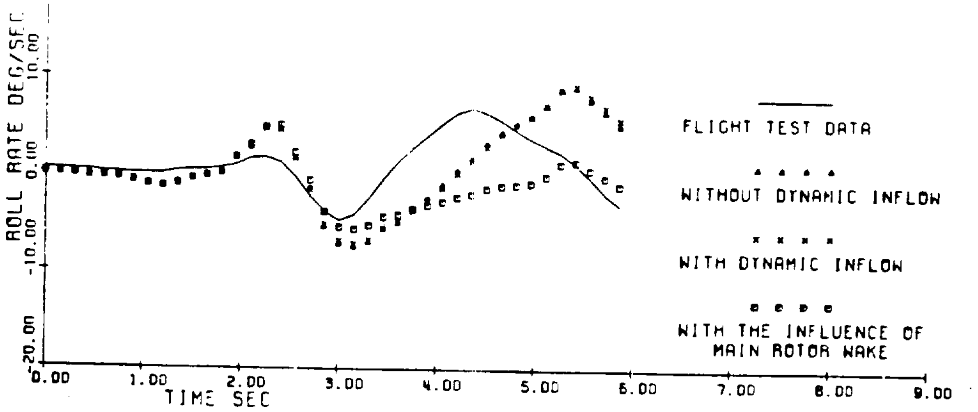

Fig. 4-21 Comparison of Calculated Responses and Flight-Test Data (Roll Rate Response to 1-in Right Pedal Input, 100 KTS)

from the model including the effect of the rotor wake on the tails and tail rotor. The same improvement also can be seen at Fig. 4-21 for the roll rate response, but again as in the 60 KTS case the initial roll acceleration due to pedal input is over-estimated by about a factor of two. A similar discrepancy appears in the nonlinear simulation model of Ref.18.

Figs. 4-22, 4-23 and 4-24 show the responses of UH-60A at 140 KTS level flight to 1-inch lateral cyclic input. In this case, the responses obtained by all three models show very good agreement with the flight test data, the model including the influence of the rotor wake produces only a little improvement in long term trends.

Figs. 4-25, 4-26 and 4-27 give the responses of UH-60A at 140 KTS level flight to 0.5-inch doublet pedal input. The traces of Fig. 4-25 show that the yaw rate responses, the on-axis response, obtained by all models are very close to the flight test. In this case, the improvement including the effect of the rotor wake is significant for both yaw and pitch rate. The roll rate responses are shown in Fig. 4-27, and again the roll acceleration due to pedal input is over-estimated by this model.

It should be pointed out that in these six forward flight cases the variations of the sideslip angle are all within 15 degrees, and the reason for only one longitudinal input case being chosen is that the longitudinal inputs usu-

**ORIGINAL PAGE IS
OF POOR QUALITY**

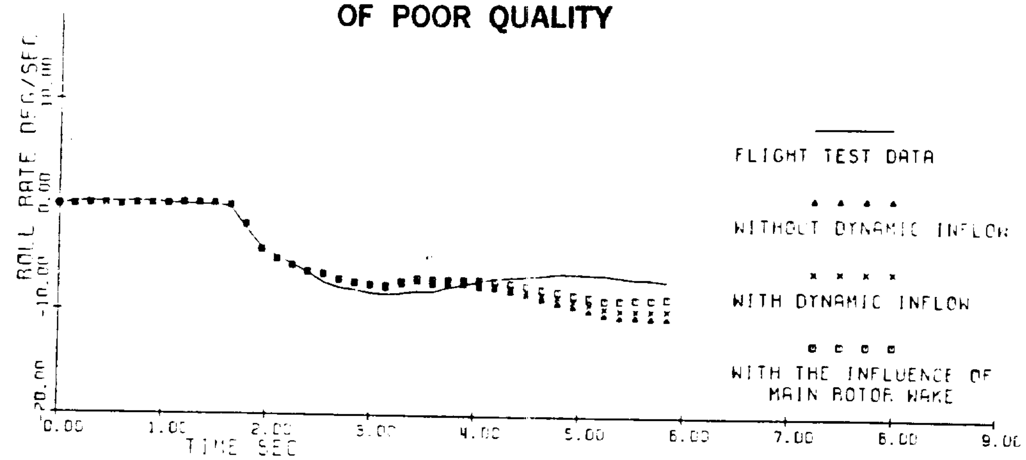

Fig. 4-22 Comparison of Calculated Responses and Flight-Test Data (Roll Rate Response to 1-in Lateral Cyclic Input, 140 KTS)

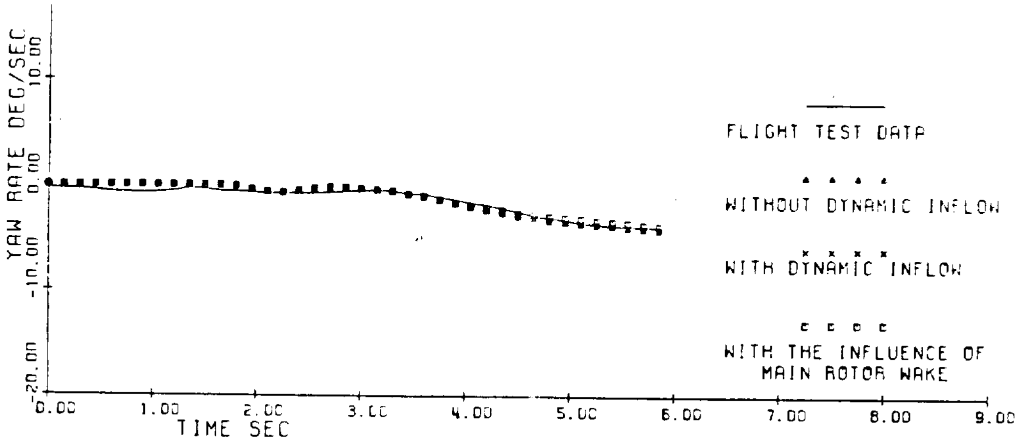

Fig. 4-23 Comparison of Calculated Responses and Flight-Test Data (Yaw Rate Response to 1-in Lateral Cyclic Input, 140 KTS)

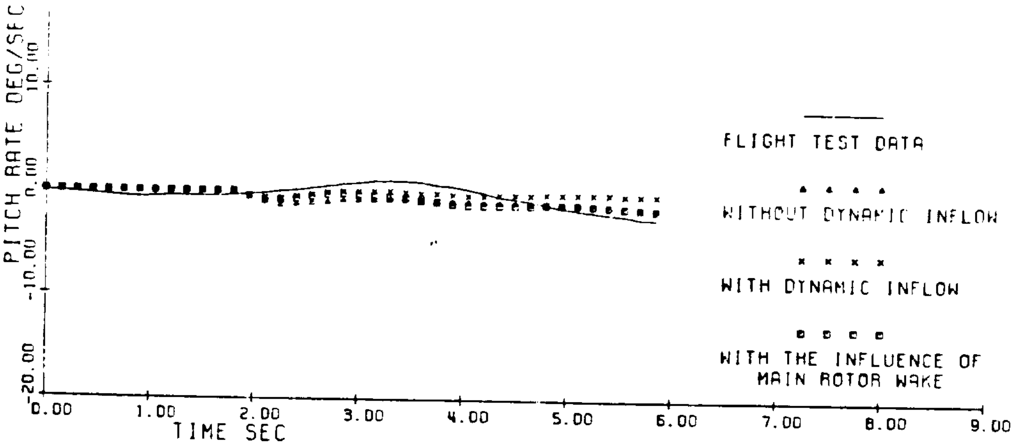

Fig. 4-24 Comparison of Calculated Responses and Flight-Test Data (Pitch Rate Response to 1-in Lateral Cyclic Input, 140 KTS)

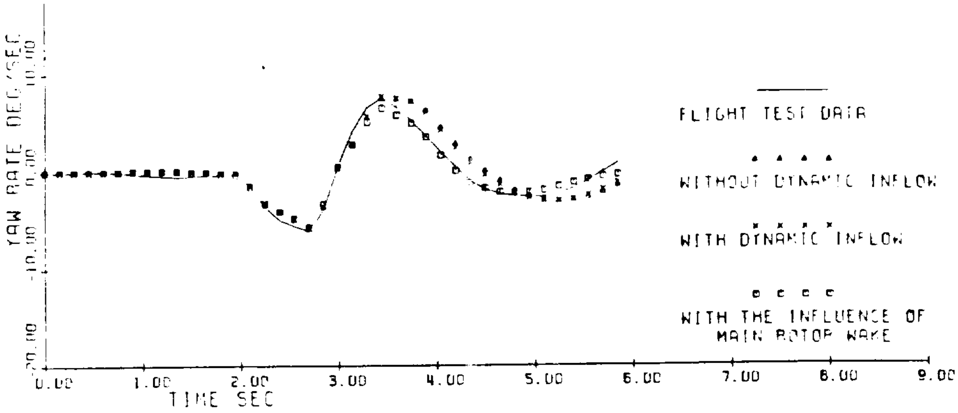

Fig. 4-25 Comparison of Calculated Responses and Flight-Test Data (Yaw Rate Response to 0.5-in Pedal Input, 140 KTS)

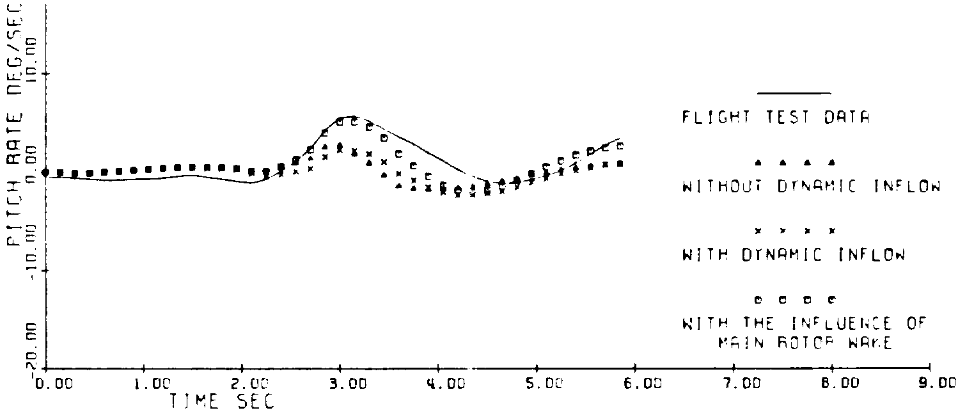

Fig. 4-26 Comparison of Calculated Responses and Flight-Test Data (Pitch Rate Response to 0.5-in Pedal Input, 140 KTS)

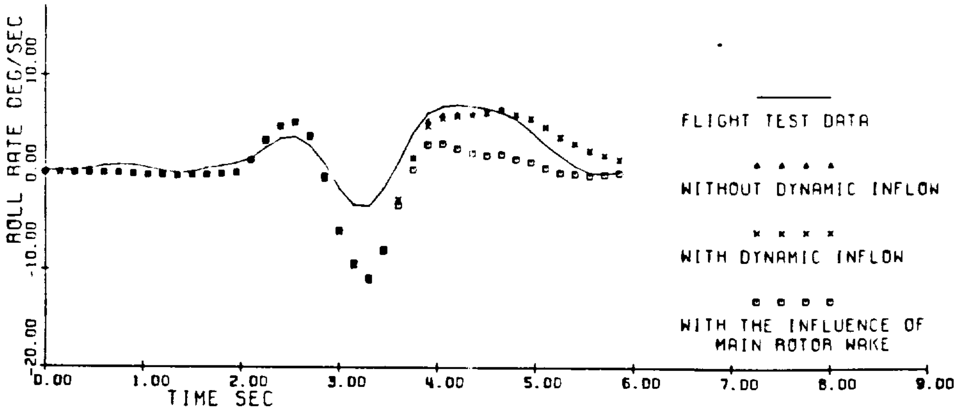

Fig. 4-27 Comparison of Calculated Responses and Flight-Test Data (Roll Rate Response to 0 5-in Pedal Input, 140 KTS)

ally result in a significant variation of rotor speed, which is not included in this model.

Generally speaking, the calculated results are close or very close to the flight test data for all three models used in the correlation study. The on-axis directional responses to the pedal input show excellent agreement with flight test data for all three models, although taking the effect of the rotor wake on the tail rotor and fixed tails into account is still beneficial. The longitudinal off-axis response to pedal input is strongly influenced by the effect of the main rotor wake on the tail rotor and fixed tails. The models without the effect of the rotor wake give the similar discrepancies as the nonlinear model used in Ref.18. The model including the effect of the rotor wake gives significant improvement and shows excellent agreement with flight test data, especially at low speed. In general the roll acceleration due to pedal input is over-estimated at all airspeeds. The agreement is reasonable only in hover but in this case the yaw acceleration is under-estimated. The reason for this discrepancy is not clear. A possible source of error could be the estimation of the inertial characteristics of the vehicle. The on-axis lateral response and off-axis directional response to lateral cyclic input show very good agreement with the flight test data for all of three models. The model including the effect of rotor wake shows a little improvement in long term trends. The off-axis longitudinal response to lateral cyclic input is also strongly influenced by the main rotor wake, the model including this effect works quite well, offering noticeable improvement. As for the longitudinal input, if there is not much variation in the main rotor speed, the models show good agreement with flight test data as well.

The pitch-yaw coupling mentioned in Ref.23 is estimated by the flat vortex model of the rotor wake at moderate speeds and at high speeds. The estimate of yaw-roll coupling is not so obvious because the roll rate responses due to pedal input are not satisfactory. In contrast to the hover cases, the addition of dynamic inflow has a small effect in both moderate speed and high speed flight.

Finally, to illustrate the nonlinear nature of the coupled rotor/fuselage system and the nonlinear nature of the influence of the rotor wake on the tail rotor and fixed tails, transient responses of the helicopter for two moderate 1-inch pedal inputs at 100 KTS are calculated. The variations of sideslip angle in two cases are all 20 degrees. The yaw rate, pitch rate, and roll rate responses are presented in Figs. 4-28, 4-29, and 4-30 for the right pedal input and in Figs. 4-31, 4-32 and 4-33 for the left pedal input. For both cases, the sideslip angle reached 15 deg. at the fourth second[18]. Before that time the model including the influence of the rotor wake gives very good responses for all three rates. After that, the yaw-pitch coupling

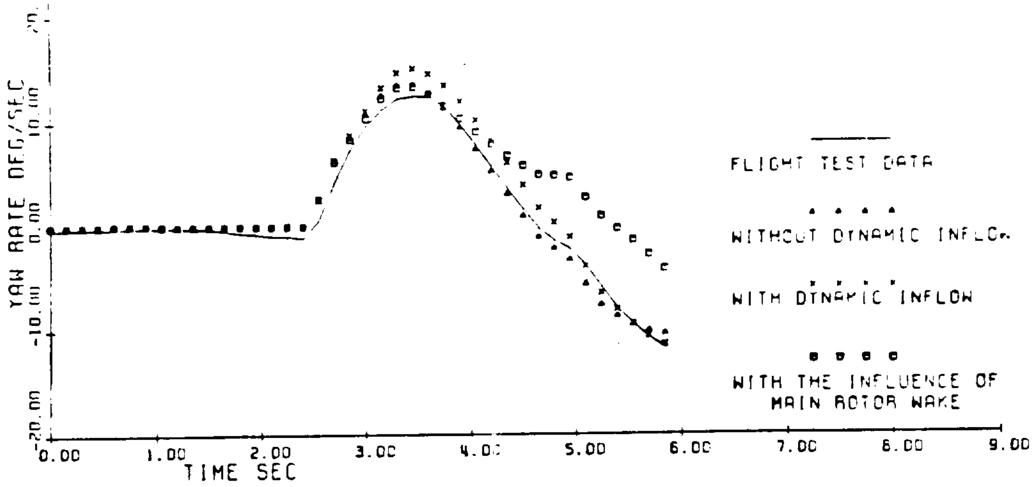

Fig. 4-28 Comparison of Calculated Responses and Flight-Test Data (Yaw Rate Response to 1-in Right Pedal Input, 100 KTS)

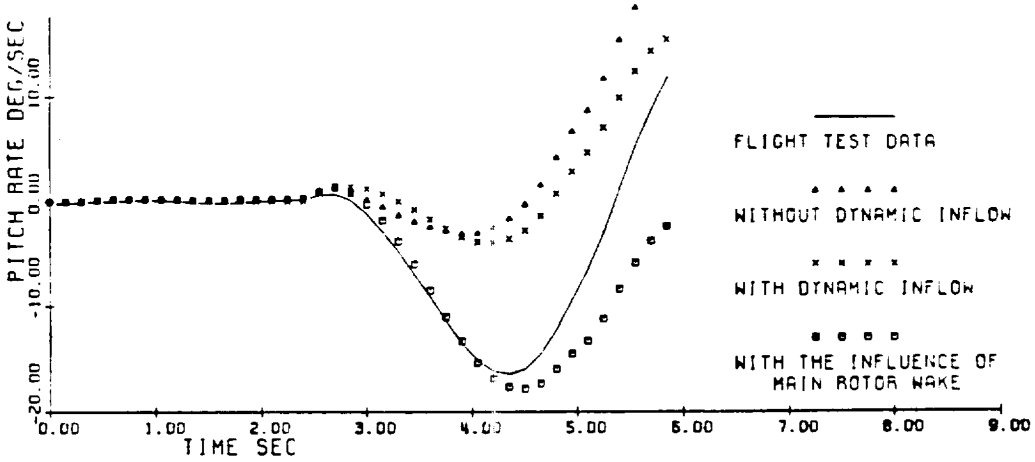

Fig. 4-29 Comparison of Calculated Responses and Flight-Test Data (Pitch Rate Response to 1-in Right Pedal Input, 100 KTS)

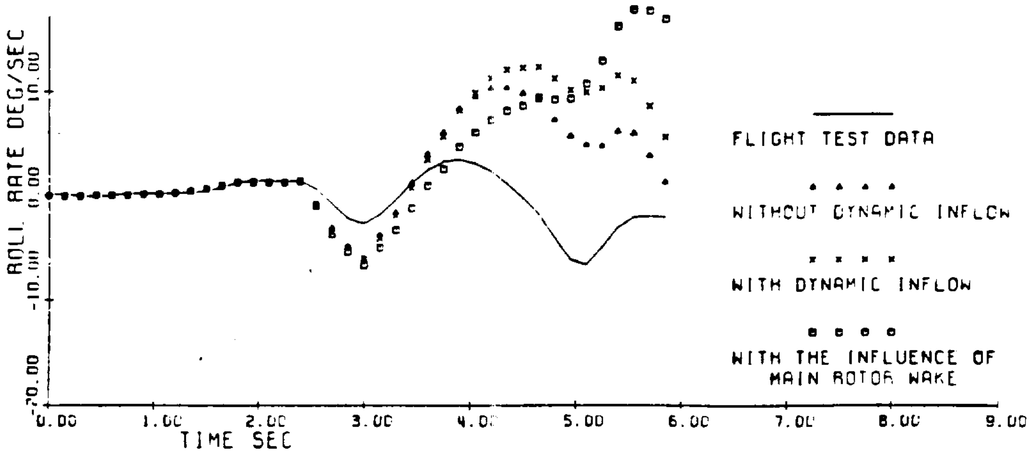

Fig. 4-30 Comparison of Calculated Responses and Flight-Test Data (Roll Rate Response to 1-in Right Pedal Input, 100 KTS)

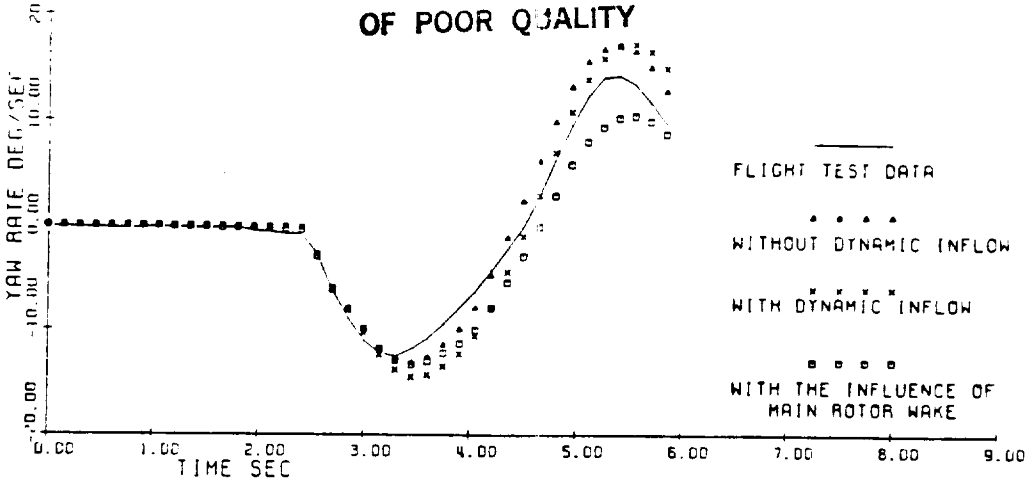

Fig. 4-31 Comparison of Calculated Responses and Flight-Test Data (Yaw Rate Response to 1-in Left Pedal Input, 100 KTS)

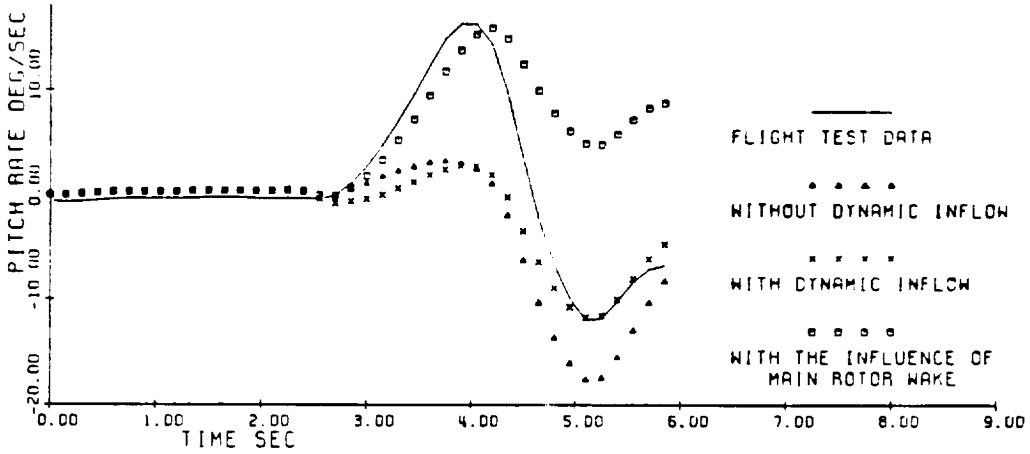

Fig. 4-32 Comparison of Calculated Responses and Flight-Test Data (Pitch Rate Response to 1-in Left Pedal Input, 100 KTS)

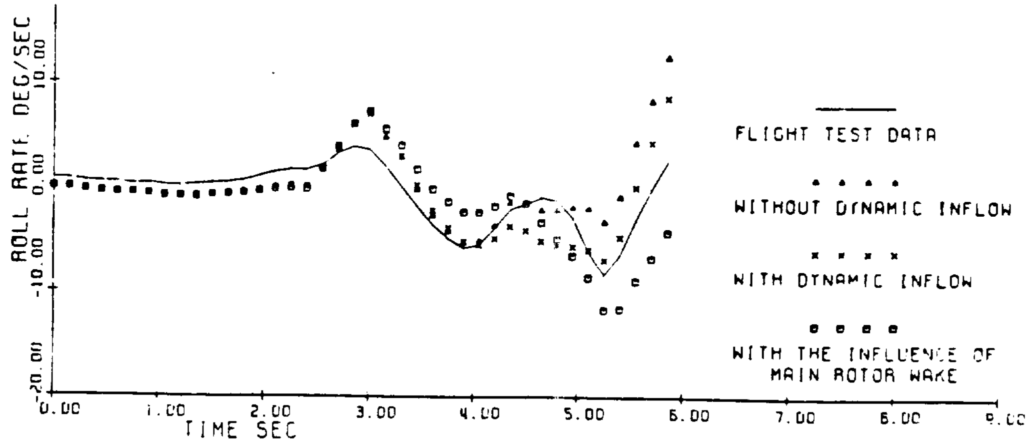

Fig. 4-33 Comparison of Calculated Responses and Flight-Test Data (Roll Rate Response to 1-in Left Pedal Input, 100 KTS)

and the yaw-roll coupling are overestimated as expected. For the left pedal input, the overestimation mainly happenes in pitch rate response, and for the right pedal, the roll rate has the largest overshoot in all three over responses. Consequently it is concluded that the linearized approximation to the nonuniform down wash and sidewash at tails is not valid when the sideslip angle variation is larger than 15 degrees.

On the other hand, it should be noticed that all three responses obtained by the models without considering the influence of the rotor wake have the same accuracy and similar shape or trend with the nonlinear dynamic model used in Ref.18. Therefore, it seems that even under moderate control inputs, the simulation deficiencies still mainly are results of insufficient modelling of the rotor/tail interaction, and have little to do with the small perturbation assumption under which the system is linearized and the approximation by replacing the periodic term with its time average.

4.4 Conclusions

From the correlation results given in the last section, it is clear that the linearized model of helicopter dynamics developed in this work is a good description for helicopter free-flight dynamic characteristics in both hover and translational flight trim conditions. The flight test data confirmed the analytic predictions with excellent accuracy for small inputs.

The comparison of the transient responses with flight test data shows that in hover the effects of dynamic inflow are significant and can be correctly taken into account by momentum theory, and that the inclusion of dynamic inflow is not important as expected in forward flight. The rough agreement of the transient responses between the models without considering rotor tail interaction in this work and the nonlinear simulation model used in Ref.18 for small and moderate control suggested that for the flight dynamical analysis the coupled rotor/fuselage system still can be considered as linear time invariant in a wide range of flight conditions. The significant improvement obtained by the model including the influence of the rotor/tail interaction suggested that for forward flight the sidewash variation at tail rotor and vertical tail and the nonuniform downwash at horizontal tail are more important for flight dynamic analysis than the inertia nonlinear coupling, the mechanical nonlinearities associated with moderate elastic deflections, the servo dynamics, the effects of sweep, the compressibility, and the nonlinear lag damping, all of them are included in the nonlinear simulator model. Therefore, the inclusion of the static influences of the rotor wake on the tail rotor and fixed tail surfaces are very important and may be the most important factor for forward flight dynamical analyses after the basic configuration modelling. It also has been shown from the comparison that the simple linear flat vortex

theory employed here is a good description of the phenomenon and its linearized approximation can be used in a wide range of flight speed for small control inputs.

Chapter V

INFLUENCE OF THE BLADE DYNAMICS ON THE FEEDBACK CONTROL SYSTEM DESIGN

5.1 Introduction

In the design of high-gain control systems for the helicopter, it is essential to consider the influences of the blade dynamics. Although it has been recognized for quite some time that the flapping dynamics of an articulated rotor system imposes limitations in the design of automatic control systems for rotorcraft, and a significant amount of analytical research has been performed to investigate their impact on the design of automatic control systems, only a limited number of studies take the lag degrees of freedom into account. Furthermore, all investigations to date are based on incomplete system modelling under assumptions that yaw motion and vertical motion of the helicopter are uncoupled, the fuselage center of gravity is on the shaft, and the effects of the tail rotor are not included. In Ref.26, R.T.N.Chen and W.S.Hindson investigated the limitations in control gain encountered when flapping dynamics are included and presented experimental verification of these trends. In Ref.5, H.C.Curtiss investigated the high frequency characteristics of the transfer functions describing the response of helicopters associated with the rotor degrees of freedom including the lag degrees of freedom and examined the impact of those on the design of automatic control systems in hover. The results showed that if the simple roll attitude or roll rate feedback is employed on the helicopter model with rotor dynamics neglected, there is no gain limitation. For a model including flapping dynamics, there will be limitations for roll rate feedback due to the effect of the feedback on the regressing flap mode, and for the roll attitude feedback due to the effect of the feedback on the advancing flap mode. When both flapping and lagging dynamics are included in the model, the maximum allowable gain of the roll rate feedback is much smaller, and the corresponding unstable mode is advancing lag instead[5]. This study extends these results by an analysis on a complete system model described in Chapter 3 which includes all the low frequency degrees of freedom, the effects of center of gravity location, the effects of the tail rotor and fixed tail surfaces, and the unsteady aerodynamics through dynamic inflow modelling, for forward flight trim conditions as well as hover.

Due to the multivariable nature of the helicopter system, linear optimal regulator theory has also been used to design stability augmentation systems for helicopters. Although successful flight control systems[27,28] have been designed by optimal control procedures based on conventional quasi-static stability derivative models. These studies are limited to helicopters that have relatively high fuselage inertia and small hinge offset. Therefore the rotor-body coupling is small. And these designs do not reflect the more demanding bandwidth requirement for very agile rotorcraft. Attempts to design a model-following flight control system for a hingeless rotor helicopter to achieve moderately high bandwidths have worked well in ground-based simulation, but have been less successful in flight[29,30]. Since the ground-based simulation, which is based on a stability derivative model, and flight results do not agree, it must be assumed that better models of such rotor-system dynamics are required. Several investigators have shown that for the application of the linear optimal regulator theory to high-gain, full-authority controller, the inclusion of the flapping dynamics is essential. In particular, Miyajima has found that the blade regressing flap mode should be included in the stability and control augmentation system design[4]. Hall has shown that if an optimal control system devised based on the quasi-static flapping assumption is applied to a model with flap dynamics included, instabilities result[6]. This study extends previous studies by examining the closed-loop responses of the model including both flap and lag when the controller design is based on a model which includes only flapping dynamics, and the closed-loop controller is designed by standard and frequency-shaped performance indexes. The latter is shown to be very effective for eliminating the destabilizing effect of unmodelled dynamics. It has been found that in addition to rotor dynamics, the sensor dynamics, the actuator dynamics, and the transport delay associated with the digital implementation also can severely limit the usable values of feedback gain[26]. One investigation[31] has found that the simulation of the feedback controller design based on the semi-empirical stability derivative model shows an instability due to interaction between actuator dynamics and sensor dynamics. However, these open-loop modes have higher damping and frequency than the rotor lag dynamics. Therefore, it seems more reasonable to include the lag dynamics in the basic model before examining the destabilizing effects of the actuator and sensor dynamics. For the requirement of better modelling, some semi-empirical models are obtained by numerically adjusting time constants, damping factors, and natural frequencies in an assumed model structure untill the frequency response of the model matched flight test data [32]. This approach may be useful in the design of feedback control system for a specific aircraft, but it can not provide the physical insight to the helicopter designer for improving the basic configuration design for next step in the development. Furthermore, a series of simplified controllers are developed through successive reduction in the number of feedback loops while using the feedback gain factors obtained for the optimal control, which makes it possible to reduce significantly the number of feedback loops required by optimal control design without any noticable effect on the overall system dynamics.

All the active control simulations in this study were performed on a UH-60A Black Hawk helicopter. All the results use the complete model which includes the dynamic inflow at hover and both dynamic inflow and the influences of rotor wake on the tail rotor and empennage at forward flight unless noted.

5.2 Simple Feedback Control

Although a variety of output variables are possible sources of closed loop feedback information for control actuation, the rotation attitude and rotation rate variables have been considered to be highly effective for stabilizing helicopters by some investigations [33,34], and are most frequently used in practice. Therefore, both have been chosen as feedback variables.

In this section, the influences of rotor dynamics and dynamic inflow have been studied by examining the root loci and the closed loop frequency response characteristics of the system with simple state feedback. The eigenvalue and eigenvector analysis has been used to promote physical insight.

5.2.1 Attitude feedback at hover

Fig. 5-1 shows the eigenvalues of the helicopter at hover, their numerical values are listed in Table 5-1. It can been seen that the regressing flap mode, roots 17 and 18, has moved away from the position directly below the coning flap, which suggests that it is strongly coupled with the fuselage modes. Fig. 5-2 shows the eigenvalues associated with free-flight stability-and-control-characteristics in detail. According to eigenvector analysis, the left complex conjugate pair, roots 17 and 18, represents the mode coupled by regressing flap and body roll motion. The two right complex conjugate pairs near each other, roots 22, 23 and 24, 25, represent modes having coupled pitch and longitudinal velocity, and coupled roll and lateral velocity, the two so-called longitudinal and lateral phugoid modes. Four zero roots, roots 1, 2, 3, and 27, are associated with vertical, lateral, longitudinal and yaw position each. The root 27 is not exactly zero due to a lack of complete cancellation of terms, and should be a zero if the equations are derived explicitly for the coupled system. The smallest negative real root near zero, root 26, is associated with yaw damping, and the one next to it, root 21, is associated with the vertical damping; the left two roots, roots 19 and 20, represent the modes coupling body pitch and regressing flap. All of them are coupled together through the canted tail rotor.

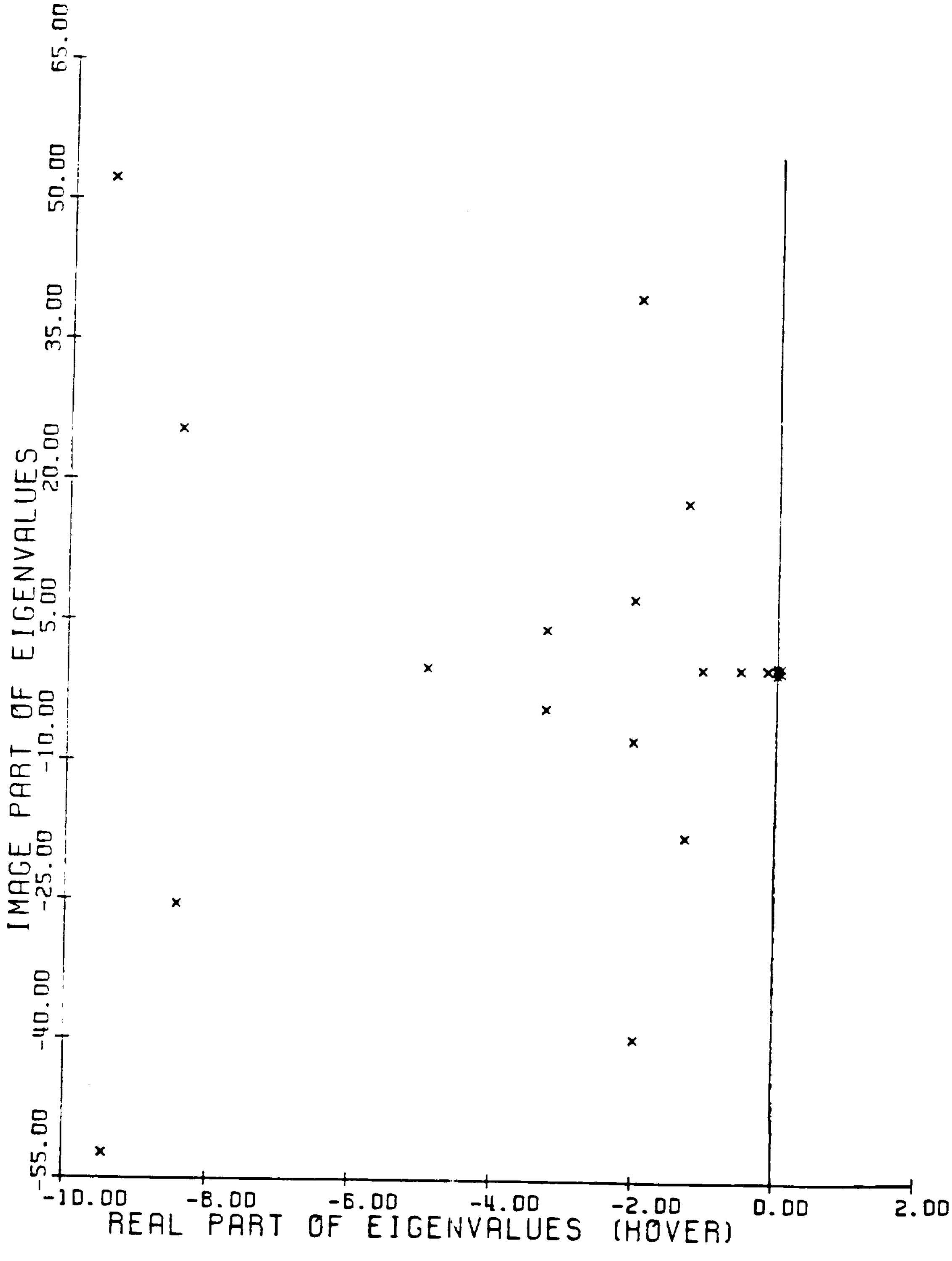

Fig. 5-1 The Helicopter Rotor/Fuselage System Open Loop Roots at Hover

ORIGINAL PAGE IS
OF POOR QUALITY

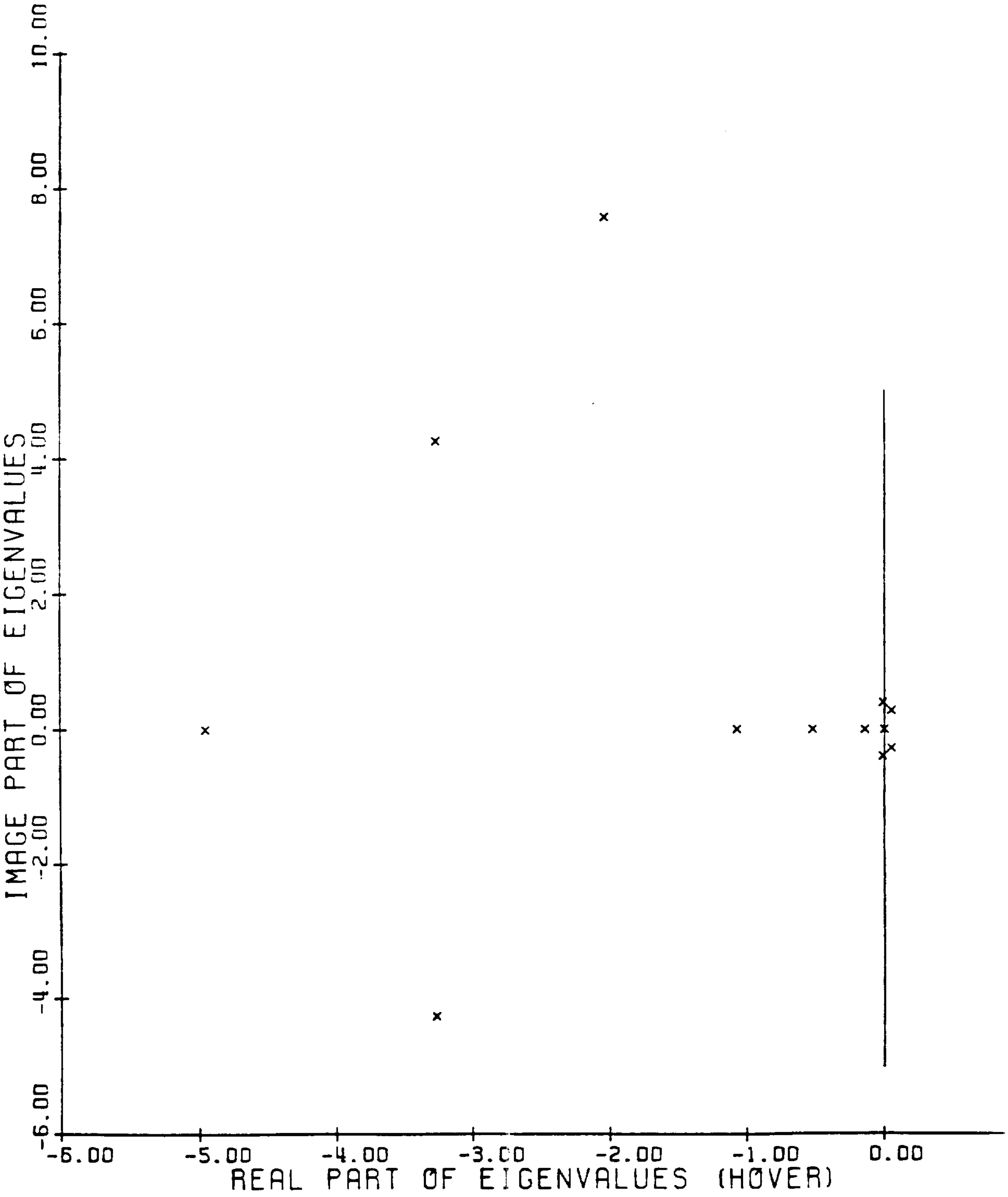

Fig. 5-2 The Helicopter Rotor/Fuselage System Open Loop Roots at Hover (Detail)

The root loci of the helicopter with roll attitude feedback with in a range from zero to 1.5 Deg/Deg are shown in Fig. 5-3. The modes shown in the figure are those locations that are significantly affected by the feedback. Those include the body roll/regressing flap, roll/lateral velocity and yaw damping. The longitudinal modes, lag modes and coning and advancing flap modes are hardly affected by the feedback.

Roll attitude feedback stabilizes the roll/lateral velocity mode very effectively at low gain, and makes it overdamped at gain K = 0.12. This will improve the helicopter lateral dynamic characteristics because the roll/lateral velocity mode dominates the low frequency lateral dynamics.

However, the body roll/regressing flap mode is destabilized and finally becomes unstable at feedback gain a little higher than critical gain K = 1.0 Deg/Deg, which has been predicted to be the theoretical feedback limitation by a simple model used in Ref.5. This is physically reasonable because the model here includ extra damping contributed by the tail rotor. The roll attitude feedback destabilizes the yaw damping mode as well, implying there is a sizeable coupling between the lateral and directional dynamics at hover.

The pole-zero locations of open-loop roll angle to lateral cyclic transfer function at hover were also calculated. The results are shown in Table 5-1. As can be seen, the

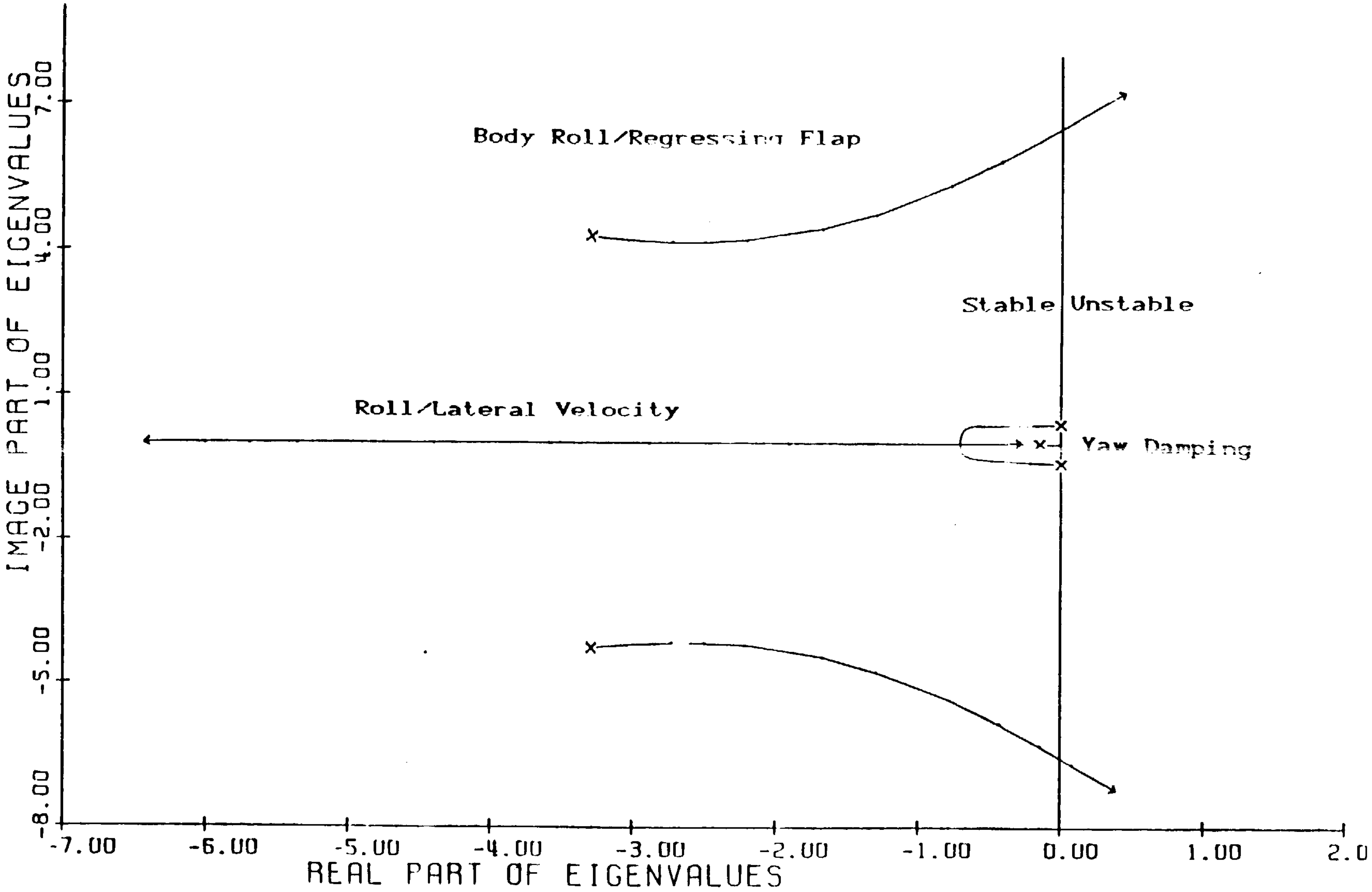

Fig. 5-3 The Root Loci of The Helicopter With Roll Attitude Feedback to Lateral Cyclic Input at Hover

	POLES		ZEROS	
1	0.0000E+00	0.0000E+00		
2	0.0000E+00	0.0000E+00		
3	0.0000E+00	0.0000E+00	-0.3843E+01	0.1179E+03
4	-0.9427E+01	0.5229E+02	-0.3843E+01	-0.1179E+03
5	-0.9427E+01	-0.5229E+02	0.2413E+01	0.5588E+02
6	-0.1973E+01	0.3974E+02	0.2413E+01	-0.5588E+02
7	-0.1973E+01	-0.3974E+02	-0.8447E+01	0.2545E+02
8	-0.8447E+01	0.2545E+02	-0.8447E+01	-0.2545E+02
9	-0.8447E+01	-0.2545E+02	-0.2617E+02	0.0000E+00
10	-0.2375E+02	0.2171E+01	-0.1960E+02	0.0000E+00
11	-0.2375E+02	-0.2171E+01	-0.2258E+02	0.0000E+00
12	-0.1275E+01	0.1791E+02	0.1474E+01	0.1739E+02
13	-0.1275E+01	-0.1791E+02	0.1474E+01	-0.1739E+02
14	-0.1960E+02	0.0000E+00	-0.2011E+01	0.7574E+01
15	-0.2028E+01	0.7586E+01	-0.2011E+01	-0.7574E+01
16	-0.2028E+01	-0.7586E+01	-0.1149E+02	0.0000E+00
17	-0.3258E+01	0.4257E+01	-0.4905E+01	0.0000E+00
18	-0.3258E+01	-0.4257E+01	-0.1026E+01	0.0000E+00
19	-0.4947E+01	0.0000E+00	-0.5178E+00	0.0000E+00
20	-0.1065E+01	0.0000E+00	0.6182E-01	0.2928E+00
21	-0.5168E+00	0.0000E+00	0.6182E-01	-0.2928E+00
22	-0.8410E-02	0.4062E+00	-0.2112E+00	0.0000E+00
23	-0.8410E-02	-0.4062E+00	-0.3537E-02	0.0000E+00
24	0.5203E-01	0.2813E+00	0.1961E-05	0.0000E+00
25	0.5203E-01	-0.2813E+00	-0.5199E-10	0.0000E+00
26	-0.1380E+00	0.0000E+00	-0.1342E-12	0.0000E+00
27	0.5839E-06	0.0000E+00	0.1893E-11	0.0000E+00

APPROXIMATE TRANSFER FUNCTION :

$$\frac{\mathrm{Roll}(s)}{\mathrm{Als}(s)} = \frac{2.057(S+0.003537)(S+0.2212)}{(S+0.138)(S+0.00841+j0.4062)(S+0.00841-j0.4062)} \cdot \frac{(S+11.49)}{(S+3.258+j4.257)(S+3.258-j4.257)}$$

TABLE 5-1 Poles, Zeros and Approximate Transfer Function of Lateral Helicopter Dynamics at Hover longitudinal low frequency poles have very close zeros and hence will be canceled in the overall transfer function. The low-frequency modes remaining after the cancellation will be the body roll/regressing flap, the roll/lateral velocity and the yaw damping. In Table 5-1, a reduced-order approximate transfer function consisting of the remaining low-frequency modes is also presented. From the frequency response of the helicopter roll attitude to the lateral cyclic input with roll attitude feedback shown in Fig. 5-4, it can be clearly seen there are significant improvements by both reducing the resonance ratio of the system and increasing the bandwidth in the Bode amplitude characteristics and by reducing the phase shift in the phase characteristics. Due to the presence of several nonminimum phase poles and zeros, the standard interpretation of gain margin and phase margin is not valid here, and there is a phase lead at low frequencies. In addition, the root loci using the approximate transfer function with same feedback will coincide with the root loci shown in Fig. 5-3. This implies that the roll response is primarily determined by the lateral modes of fuselage and the mode of regressing flap and is coupled with the mode of directional damping. The cross coupling from longitudinal dynamics to the roll attitude response is one order smaller.

The longitudinal root loci of the helicopter with pitch attitude feedback in the same gain range is shown in Fig.

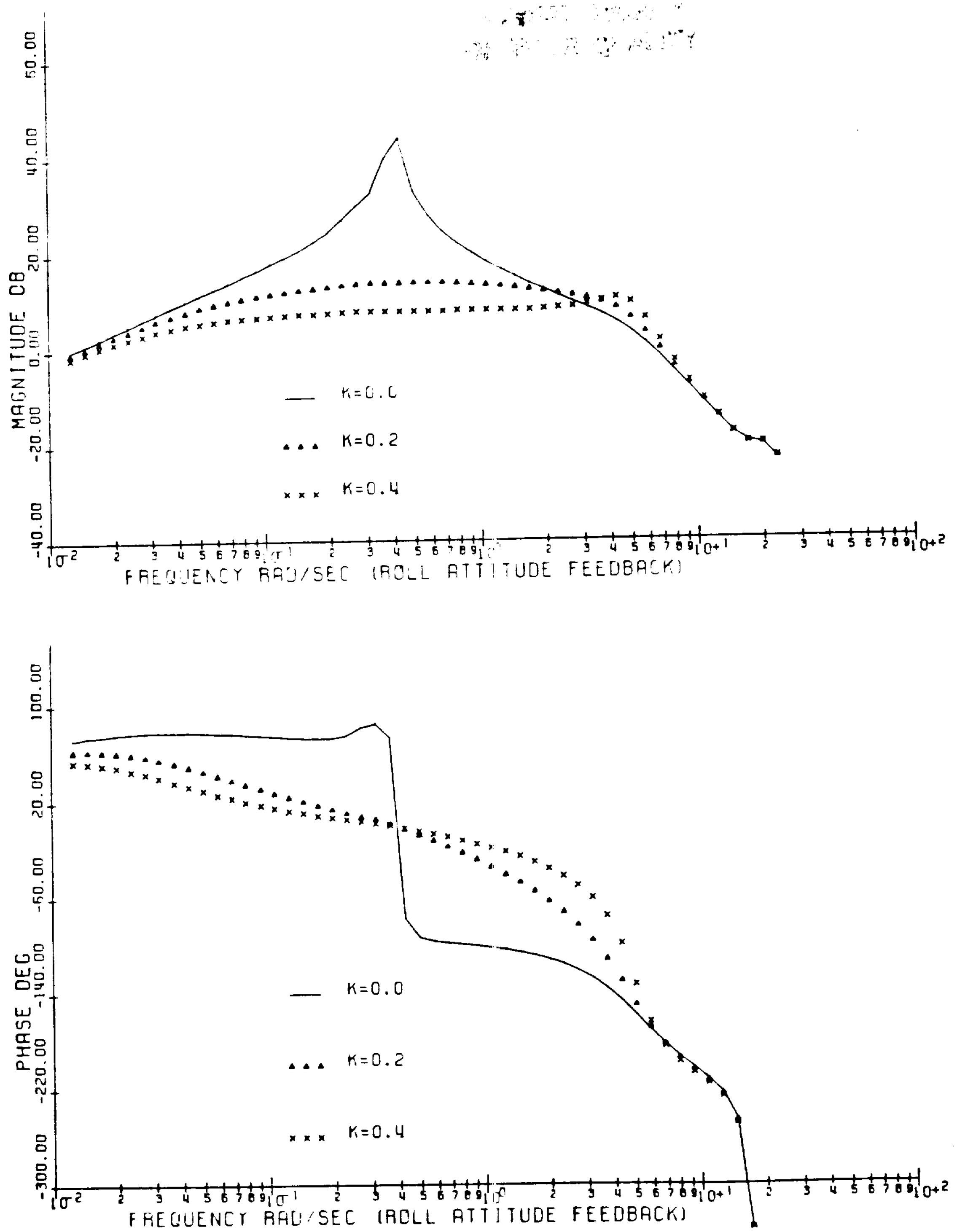

Fig. 5-4 Frequency Response of ϕ/A_{1s} With Roll Attitude Feedback to Lateral Cyclic Input, Hover

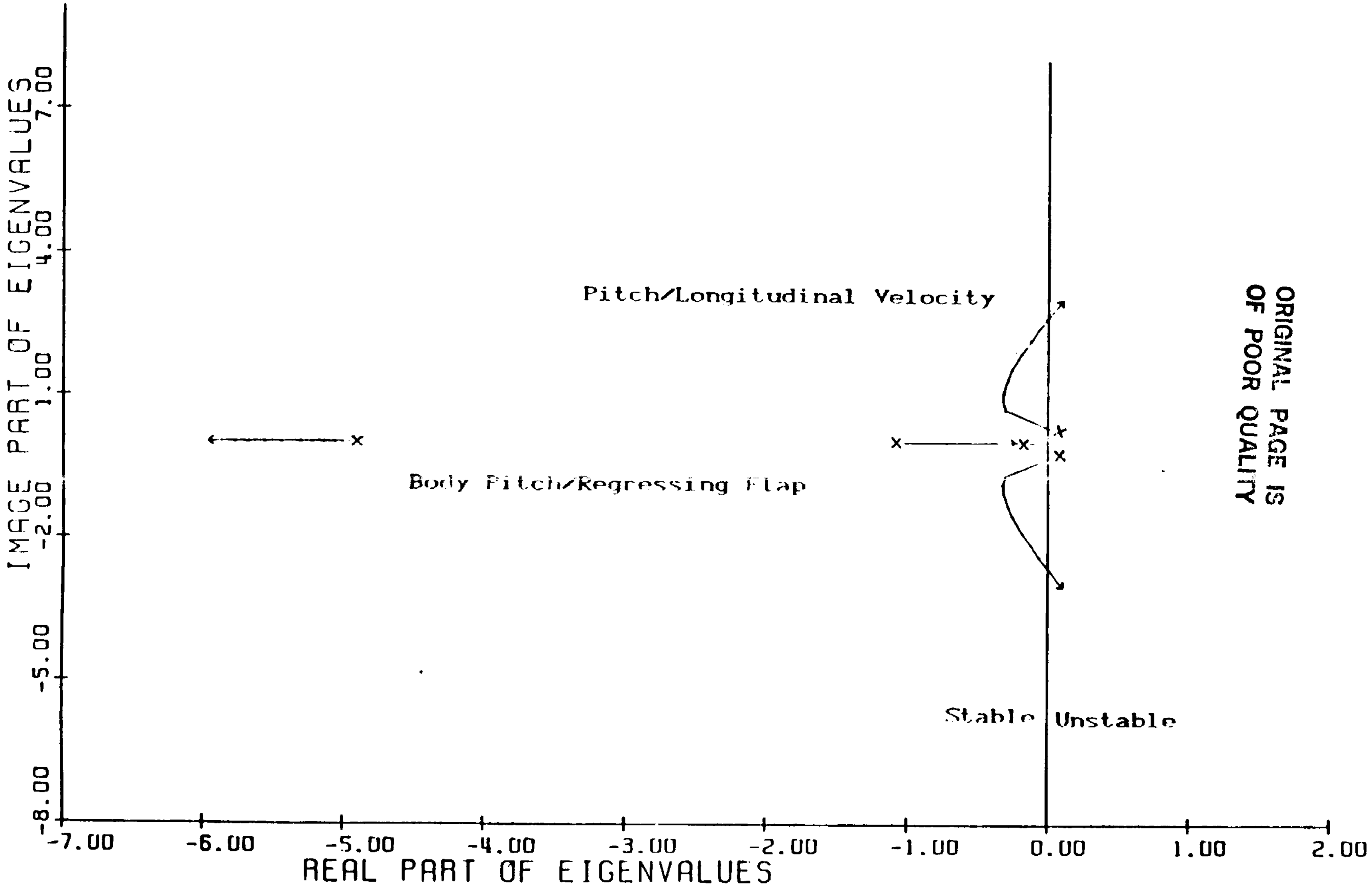

Fig. 5-5 The Root Loci of The Helicopter With Pitch Attitude Feedback to Longitudinal Cyclic Input at Hover

5-5. The modes shown in the figure are those whose locations in the complex plane are significantly affected by the feedback. They include the body pitch/regressing flap, the pitch/longitudinal velocity and the yaw damping modes. In addition, the damping ratio of the roll/lateral velocity mode is also significantly changed by the pitch attitude feedback, from -0.18 at K=0.0 Deg/Deg to 0.0132 at K=1.5 Deg/Deg, although this variation of the damping is too small to be shown in the root loci map. The pitch attitude feedback stabilizes the longitudinal oscillatory mode at gain K<0.15 Deg/Deg; destabilizes it thereafter; makes it unstable about K=1.4 Deg/Deg; and increases the oscillatory frequency quite rapidly. The flapping velocity component in the corresponding eigenvector is increased rapidly with the feedback, suggesting that the feedback limitation physically results from the coupling with the flapping dynamics. The pitch attitude feedback decreases the damping of the right body pitch/regressing flap mode and increases the damping of the left one.

The pole-zero locations of open-loop pitch angle to longitudinal cyclic transfer function at hover are presented in Table 5-2. For this case, only the vertical damping and regressing lag have a very close zero, hence will be canceled in the overall transfer function. Therefore the simplified transfer function, presented in the table, is much more involved. This implies that the pitch response of the

	POLES		ZEROS	
1	0.0000E+00	0.0000E+00		
2	0.0000E+00	0.0000E+00		
3	0.0000E+00	0.0000E+00	-0.9378E+00	0.1239E+03
4	-0.9427E+01	0.5229E+02	-0.9378E+00	-0.1239E+03
5	-0.9427E+01	-0.5229E+02	0.1431E+01	0.5591E+02
6	-0.1973E+01	0.3974E+02	0.1431E+01	-0.5591E+02
7	-0.1973E+01	-0.3974E+02	-0.8453E+01	0.2543E+02
8	-0.8447E+01	0.2545E+02	-0.8453E+01	-0.2543E+02
9	-0.8447E+01	-0.2545E+02	-0.2609E+02	0.0000E+00
10	-0.2375E+02	0.2171E+01	-0.2254E+02	0.0000E+00
11	-0.2375E+02	-0.2171E+01	-0.1960E+02	0.0000E+00
12	-0.1275E+01	0.1791E+02	0.1485E+01	0.1694E+02
13	-0.1275E+01	-0.1791E+02	0.1485E+01	-0.1694E+02
14	-0.1960E+02	0.0000E+00	-0.1148E+02	0.0000E+00
15	-0.2028E+01	0.7586E+01	-0.2025E+01	0.7593E+01
16	-0.2028E+01	-0.7586E+01	-0.2025E+01	-0.7593E+01
17	-0.3258E+01	0.4257E+01	-0.1189E+01	0.4844E+01
18	-0.3258E+01	-0.4257E+01	-0.1189E+01	-0.4844E+01
19	-0.4947E+01	0.0000E+00	-0.3728E+01	0.0000E+00
20	-0.1065E+01	0.0000E+00	-0.5275E+00	0.0000E+00
21	-0.5168E+00	0.0000E+00	-0.2315E+00	0.0000E+00
22	-0.8410E-02	0.4062E+00	-0.3231E-01	0.0000E+00
23	-0.8410E-02	-0.4062E+00	-0.2872E-02	0.0000E+00
24	0.5203E-01	0.2813E+00	0.9957E-06	0.0000E+00
25	0.5203E-01	-0.2813E+00	-0.4581E-10	0.0000E+00
26	-0.1380E+00	0.0000E+00	0.2050E-11	0.0000E+00
27	0.5839E-06	0.0000E+00	-0.2433E-11	0.0000E+00

APPROXIMATE TRANSFER FUNCTION :

$$\frac{\mathrm{Pitch}(s)}{\mathrm{Bls}(s)} = \frac{-0.2954(S+0.002872)}{(S-0.05203+j0.2813)(S-0.05203-j0.2813)}$$

$$\frac{(S+0.03231)(S+0.2315)(S+3.728)}{(S+0.00841-j0.4062)(S+0.00841+j0.4062)(S+0.138)(S+1.065)}$$

$$\frac{(S+1.189-j4.844)(S+1.189+j4.844)}{(S+3.258-j4.257)(S+3.258+j4.257)(S+4.947)}$$

TABLE 5-2 Poles, Zeros and Approximate Transfer Function of Longitudinal Helicopter Dynamics at Hover helicopter, which is a key figure for the longitudinal dynamics, is strongly coupled with the lateral and directional dynamics.

As same as roll attitude feedback control, the yaw damping mode is destabilized significantly by the pitch attitude feedback.

5.2.2 Attitude feedback in forward flight

Fig. 5-6 shows the eigenvalues associated with free flight stability and control characteristics of the helicopter for forward flight at 60 KTS and 100 KTS; their numerical values are listed in Tables 5-3 and 5-4. According to eigenvector analysis, the left complex conjugate pair, roots 17 and 18, represent the mode coupled by regressing flap and body roll. The complex conjugate pair in the middle, roots 22 and 23, as well as the left real mode, root 19, represent a short period mode which involves primarily pitch angle and angle of attack and is strongly coupled with the regressing flap. The right complex conjugate pair, roots 20 and 21, represent the dutch roll mode which involves primarily the yaw degree of freedom with a number of small translation velocities; another complex conjugate pair very near zero, roots 24 and 25, is the spiral coupled with an unrealistic yaw mode due to the remainded error mentioned in the introduction about the disadvantage of the matrix displacement method. This mode is the one that is somewhat inaccurate due to a lack of complete cancellation of terms, and

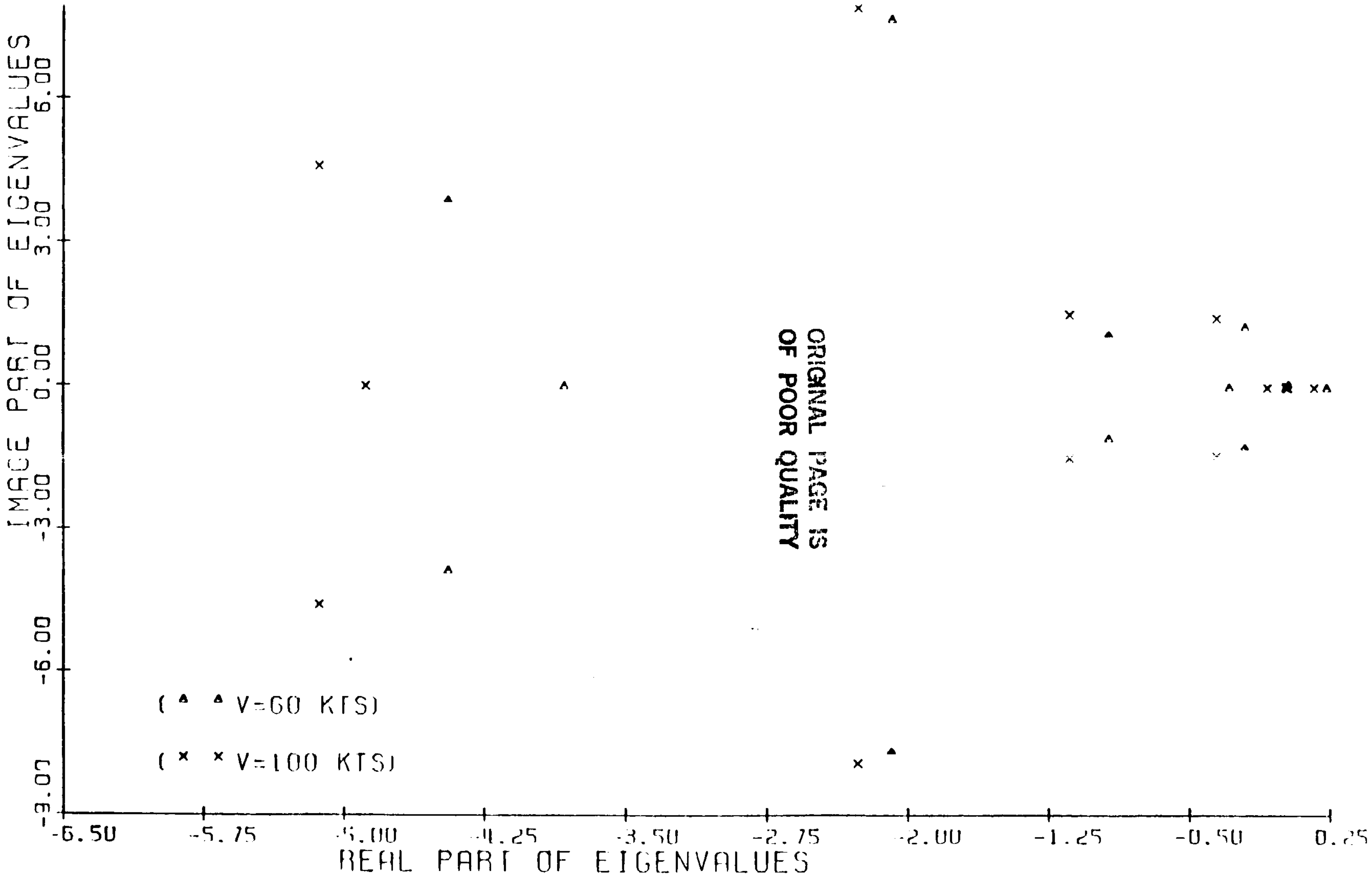

Fig. 5-6 The Helicopter Rotor/Fuselage System Open Loop Roots at 60 KTS and 100 KTS

	POLES		ZEROS	
1	0.0000E+00	0.0000E+00		
2	0.0000E+00	0.0000E+00		
3	0.0000E+00	0.0000E+00	-0.5844E+02	0.9794E+02
4	-0.9359E+01	0.5207E+02	-0.5844E+02	-0.9794E+02
5	-0.9359E+01	-0.5207E+02	0.7133E+01	0.5395E+02
6	-0.2012E+01	0.3954E+02	0.7133E+01	-0.5395E+02
7	-0.2012E+01	-0.3954E+02	-0.5050E+02	0.0000E+00
8	-0.8313E+01	0.2503E+02	-0.8648E+01	0.2530E+02
9	-0.8313E+01	-0.2503E+02	-0.8648E+01	-0.2530E+02
10	-0.2428E+02	0.7011E+01	0.1648E+01	0.1876E+02
11	-0.2428E+02	-0.7011E+01	0.1648E+01	-0.1876E+02
12	-0.1177E+01	0.1774E+02	-0.2276E+02	0.0000E+00
13	-0.1177E+01	-0.1774E+02	-0.1571E+02	0.7746E+01
14	-0.1949E+02	0.0000E+00	-0.1571E+02	-0.7746E+01
15	-0.2092E+01	0.7671E+01	-0.1919E+01	0.7638E+01
16	-0.2092E+01	-0.7671E+01	-0.1919E+01	-0.7638E+01
17	-0.4444E+01	0.3883E+01	-0.3892E+01	0.0000E+00
18	-0.4444E+01	-0.3883E+01	-0.8986E+00	0.1125E+01
19	-0.3830E+01	0.0000E+00	-0.8986E+00	-0.1125E+01
20	-0.2137E+00	0.1254E+01	-0.2731E+00	0.1118E+01
21	-0.2137E+00	-0.1254E+01	-0.2731E+00	-0.1118E+01
22	-0.9324E+00	0.1093E+01	-0.2916E+00	0.0000E+00
23	-0.9324E+00	-0.1093E+01	0.2168E+00	0.0000E+00
24	0.1490E-01	0.5367E-01	0.2771E-03	0.0000E+00
25	0.1490E-01	-0.5367E-01	0.2678E-09	0.0000E+00
26	0.2209E+00	0.0000E+00	0.1802E-12	0.0000E+00
27	-0.3006E+00	0.0000E+00	-0.2330E-12	0.0000E+00

APPROXIMATE TRANSFER FUNCTION :

$$\frac{\mathrm{Roll}(s)}{\mathrm{Als}(s)} = \frac{1.052}{(S-0.0149+j0.05367)(S-0.0149-j0.05367)} \cdot \frac{(S-0.0002771)}{(S+4.44-j3.88)(S+4.44-j3.88)}$$

TABLE 5-3 Poles, Zeros and Approximate Transfer Function of Lateral Helicopter Dynamics at 60KTS

	POLES		ZEROS	
1	0.0000E+00	0.0000E+00		
2	0.0000E+00	0.0000E+00		
3	0.0000E+00	0.0000E+00	-0.2156E+03	0.0000E+00
4	-0.9025E+01	0.5194E+02	-0.2047E+02	0.7327E+02
5	-0.9025E+01	-0.5194E+02	-0.2047E+02	-0.7327E+02
6	-0.2083E+01	0.3897E+02	-0.2612E+01	0.5333E+02
7	-0.2083E+01	-0.3897E+02	-0.2612E+01	-0.5333E+02
8	-0.3312E+02	0.1683E+02	-0.8965E+01	0.2499E+02
9	-0.3312E+02	-0.1683E+02	-0.8965E+01	-0.2499E+02
10	-0.7759E+01	0.2517E+02	-0.2221E+02	0.1608E+02
11	-0.7759E+01	-0.2517E+02	-0.2221E+02	-0.1608E+02
12	-0.2418E+02	0.0000E+00	-0.2660E+02	0.0000E+00
13	-0.1167E+01	0.1738E+02	0.1175E+01	0.1937E+02
14	-0.1167E+01	-0.1738E+02	0.1175E+01	-0.1937E+02
15	-0.2269E+01	0.7914E+01	-0.2016E+01	0.7886E+01
16	-0.2269E+01	-0.7914E+01	-0.2016E+01	-0.7886E+01
17	-0.5138E+01	0.4588E+01	-0.4889E+01	0.0000E+00
18	-0.5138E+01	-0.4588E+01	-0.1146E+01	0.1526E+01
19	-0.4890E+01	0.0000E+00	-0.1146E+01	-0.1526E+01
20	-0.3618E+00	0.1440E+01	-0.3910E+00	0.1312E+01
21	-0.3618E+00	-0.1440E+01	-0.3910E+00	-0.1312E+01
22	-0.1146E+01	0.1503E+01	0.1449E+00	0.0000E+00
23	-0.1146E+01	-0.1503E+01	-0.8595E-01	0.0000E+00
24	0.1137E-01	0.4161E-01	0.1116E-02	0.0000E+00
25	0.1137E-01	-0.4161E-01	0.8511E-11	0.0000E+00
26	0.1528E+00	0.0000E+00	-0.1040E-10	0.0000E+00
27	-0.9152E-01	0.0000E+00	-0.8388E-12	0.0000E+00

```
APPROXIMATE TRANSFER FUNCTION :

Roll(s)                      0.7014
-------  =  ---------------------------------------
Als(s)      (S-0.01137+j0.04161)(S-0.01137-j0.04161)

                          (S-0.001116)
                 -------------------------------
                 (S+5.138-j4.588)(S+5.138-j4.588)
```

TABLE 5-4 Poles, Zeros and Approximate Transfer Function of Lateral Helicopter Dynamics at 100KTS should be a zero and a real root if the equations are derived explicitly for the coupled system. Three zero roots, roots 1, 2, and 3, are associated with vertical, lateral, longitudinal position each; the two real roots at right represent the phugoid mode coupled with lateral damping due to the canted tail rotor.

The root loci of the helicopter dynamics with roll attitude feedback for a gain range from zero to 1.5 Deg/Deg for 60 KTS and 100 KTS forward flight are shown in Fig. 5-7 and Fig. 5-8. The modes shown in the figures are those significantly affected by the feedback, including the body roll/regressing flap, dutch roll and spiral. It is shown that the roll attitude feedback stabilizes the spiral mode very effectively but has very little effect on the dutch roll. The stabilization of the spiral mode improves the low frequency characteristics of the helicopter's lateral dynamics. As can be clearly seen from the frequency responses presented in Figs. 5-9 and 5-10, the feedback reduces the resonance ratio of the system, increases the bandwidth in the Bode amplitude characteristics and reduces the phase shift in the phase characteristics. It should be noticed that the spiral mode is unstable without the feedback. The low frequency response peak shown in the Bode plot is only a measurement about how close to the imaginary axis of the pole, instead of the classical magnitude of steady-state response for a sinusoidal input. This means that the improvement obtained

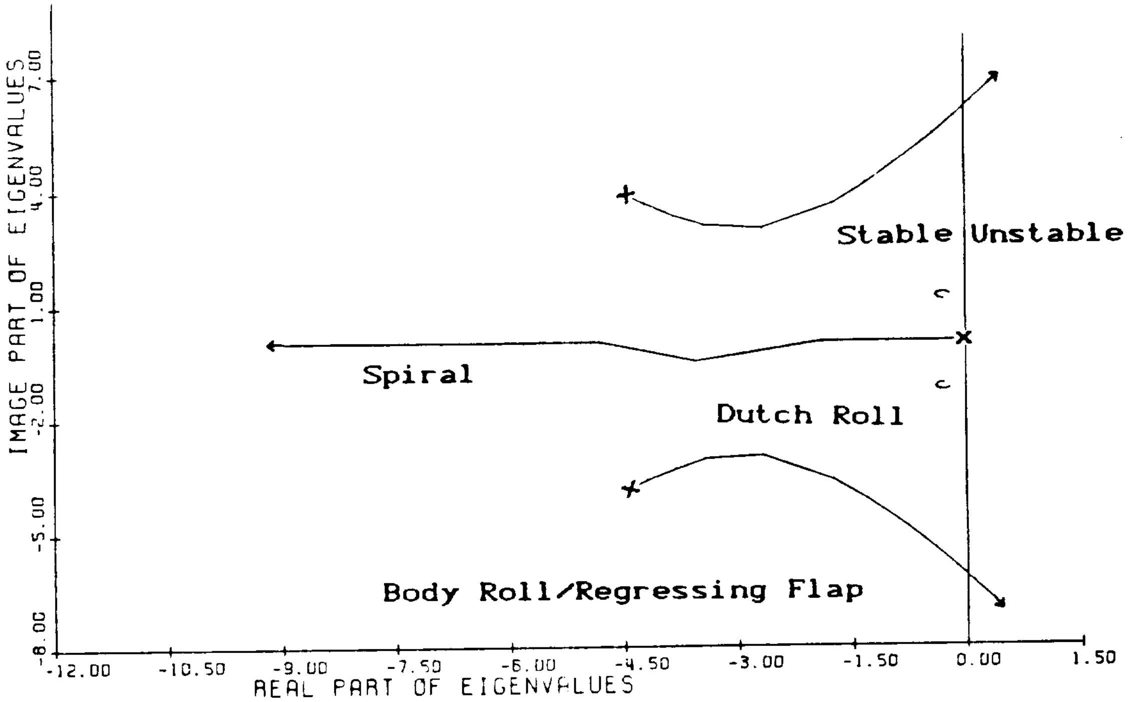

Fig. 5-7 The Root Loci of The Helicopter With Roll Attitude Feedback to Lateral Cyclic Input at 60 KTS

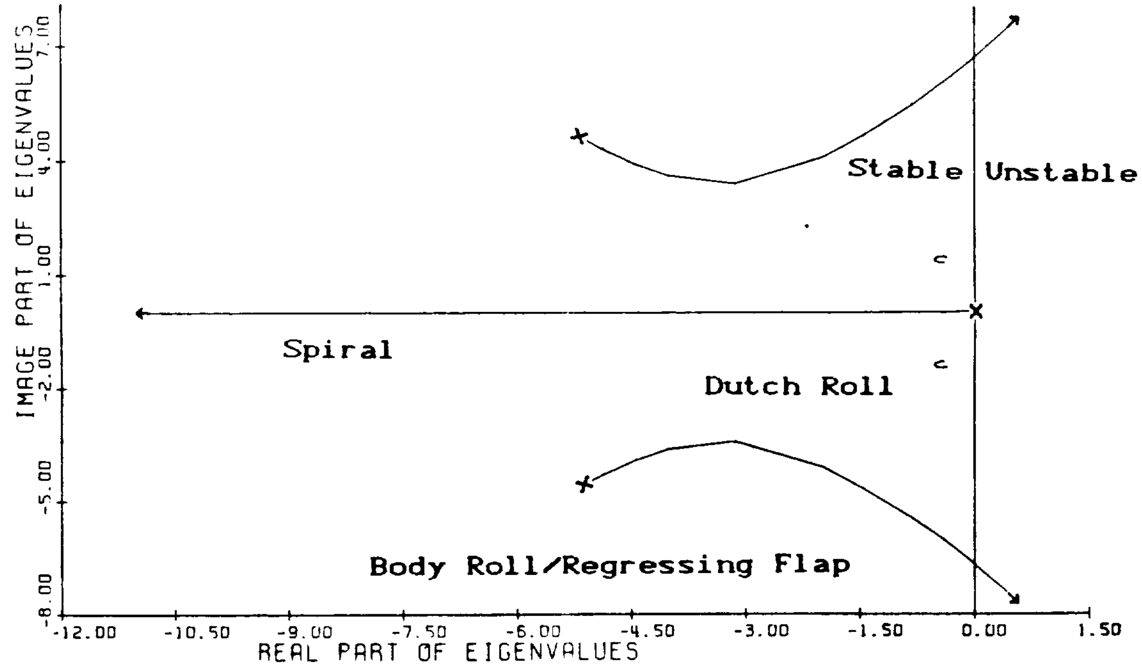

Fig. 5-8 The Root Loci of The Helicopter With Roll Attitude Feedback to Lateral Cyclic Input at 100 KTS

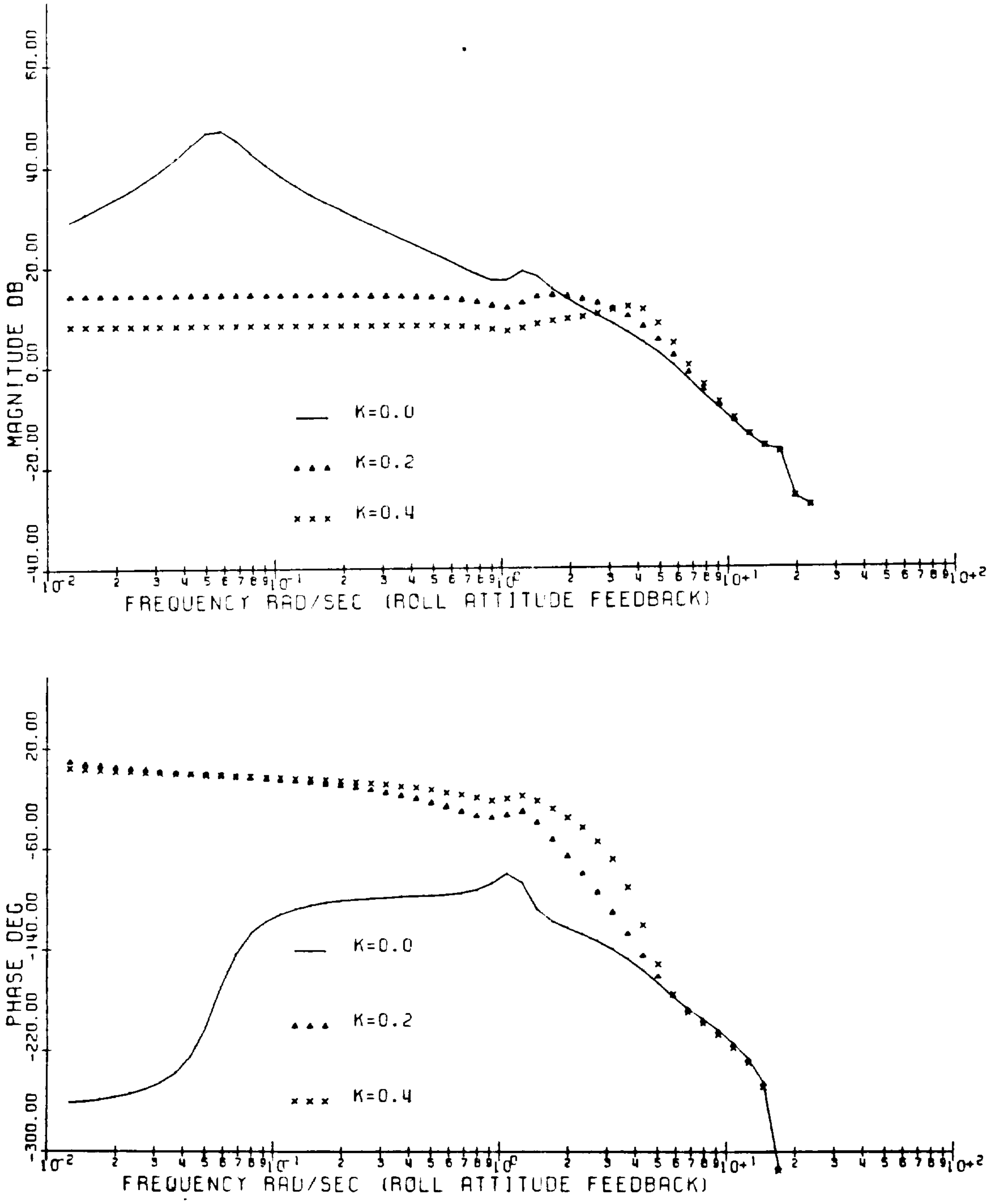

Fig. 5-9 Frequency Response of ϕ/A_{1s} With Roll Attitude Feedback to Lateral Cyclic, 60 KTS

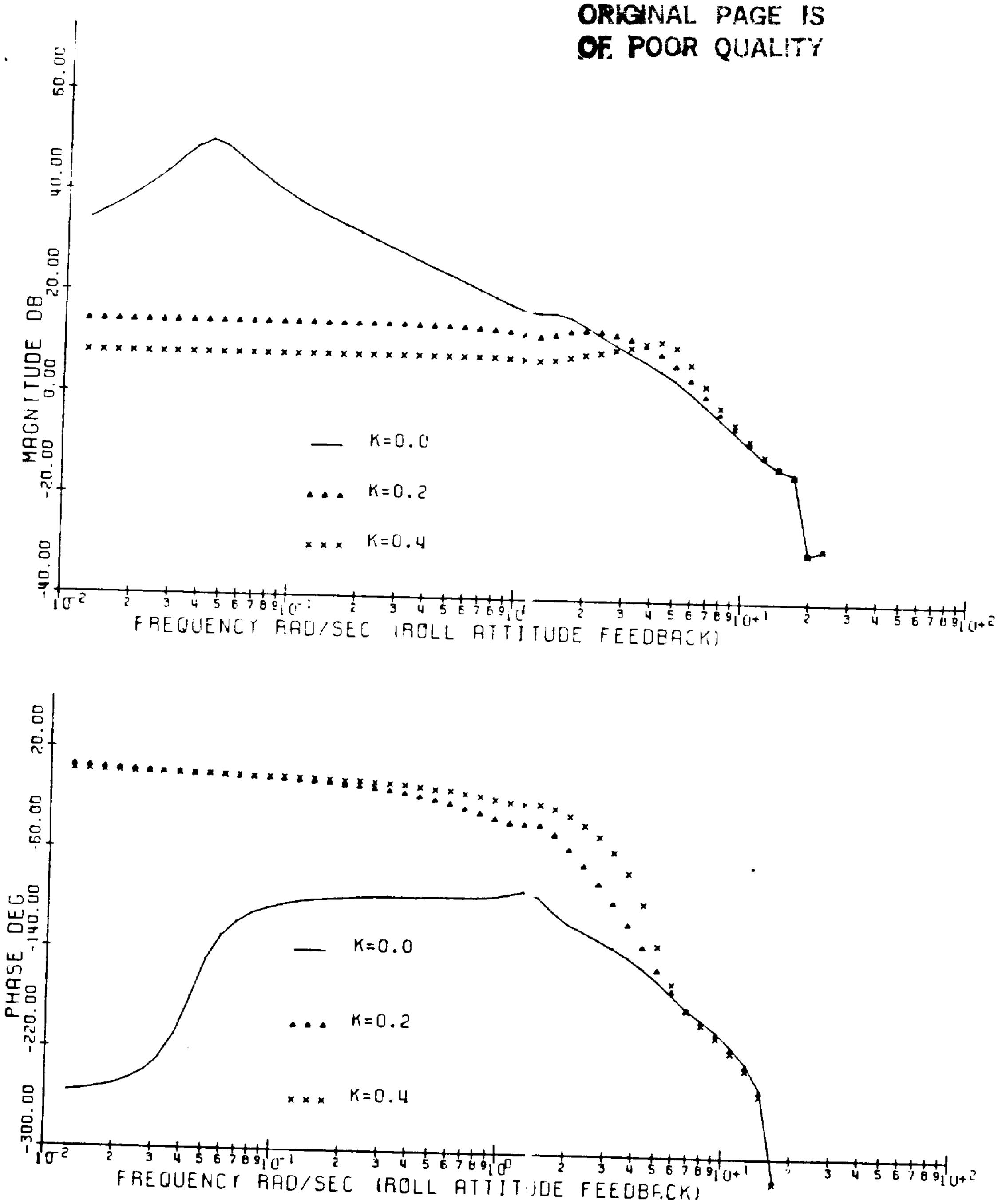

Fig. 5-10 Frequency Response of ϕ/A_{1s} With Roll Attitude Feedback to Lateral Cyclic Input, 100 KTS

by the roll attitude feedback is larger than it seems to be in the frequency responses.

The same as at hover, the roll damping/regressing flap mode is destabilized and finally becomes unstable at feedback gain a little higher than K=1.0 Deg/Deg.

The pole-zero locations of open-loop roll angle to lateral cyclic transfer function at 60KTS and 100KTS are presented in Tables 5-3 and 5-4. The same as at hover, most nonlateral low frequency poles have a very close zero, therefore will be canceled in the overall transfer function. Furthermore, even the dutch roll mode, which traditionly is strongly coupled with the lateral dynamics, has a close zero pair, this explains why the roll attitude feedback hardly affects it's position. Therefore it is suggested that for this helicopter, the low frequency roll response to the lateral cyclic input at forward flight is only determined by the roll damping/regressing flap and spiral modes. The reduced order approximate transfer functions are also presented in Tables 5-3 and 5-4. Also, the root loci of the simplified transfer function with same feedback will have same shapes with those shown in Figs. 5-7 and 5-8. This shows that low frequency lateral dynamics of the helicopter at forward flight is well separated from the longitudinal and directional dynamics but coupled with the flapping dynamics.

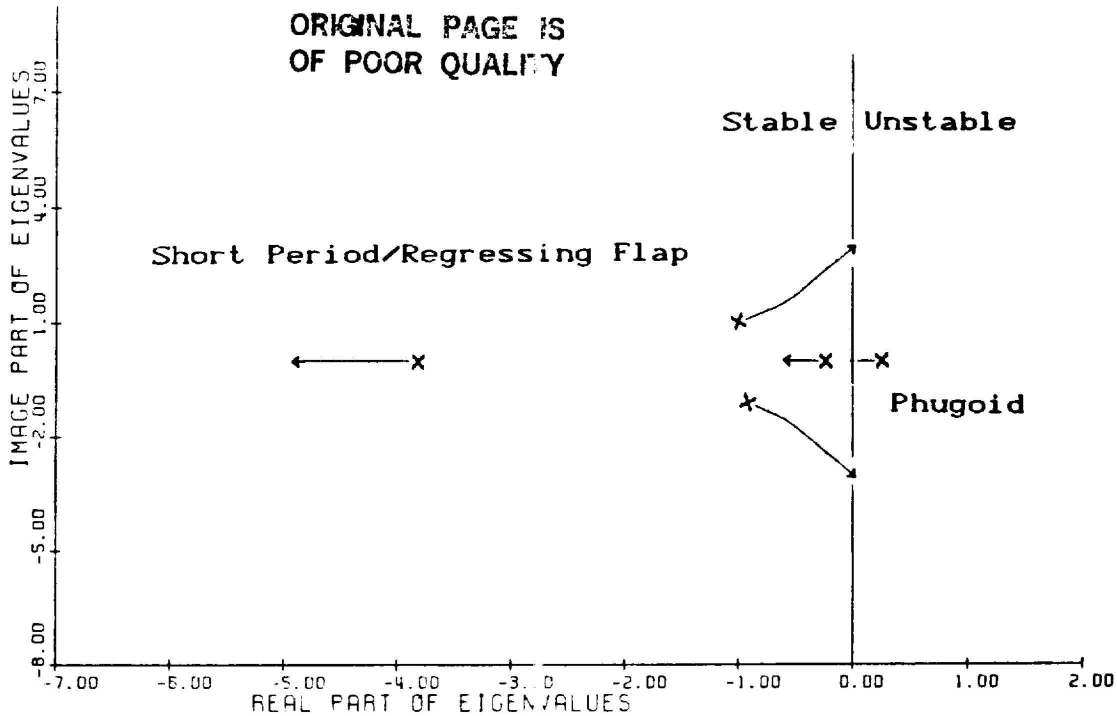

Fig. 5-11 The Root Loci of The Helicopter With Pitch Attitude Feedback to Longitudinal Cyclic Input at 60 KTS

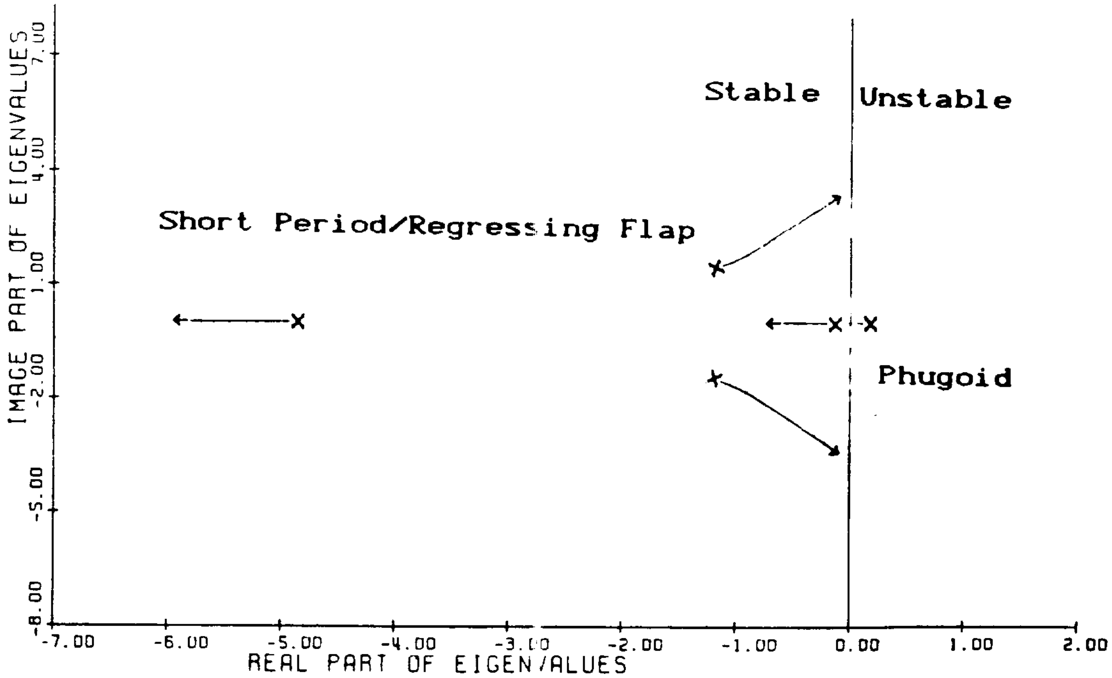

Fig. 5-12 The Root Loci of The Helicopter With Pitch Attitude Feedback to Longitudinal Cyclic Input at 100 KTS

The longitudinal root loci of the helicopter with pitch attitude feedback in the same gain range is shown in Fig. 5-11 and Fig. 5-12. The modes which are significantly affected by the feedback are those traditional longitudinal modes, phugoid and short period. The phugoid mode is two real roots, one divergent; and the short period mode is coupled with the regressing flap. The less damped spiral mode which has coupled with longitudinal velocity is also affected although it's numerical variation is too small to be shown in the figures. The pitch attitude feedback stabilizes the phugoid mode as well as the real root of short period mode but destabilizes the complex pair. The spiral mode is also destabilized at low gain range and is stabilized after the gain K=0.4 for 60KTS and K=0.11 for 100KTS. The final feedback limitation gain due to the destabilized short period mode is increased with forward flight velocity because the stable effect of the horizontal tail on the longitudinal dynamics is increased with flight velocity.

The pole-zero locations of open-loop pitch angle to longitudinal cyclic transfer function at 60KTS and 100KTS are presented in Tables 5-5 and 5-6. There is only one pole-zero close pair, which is associate with regressing lag mode, in the overall transfer function. Hence the simplified transfer function presented in the table is much more involved. As at hover, it is implied that the pitch response of the helicopter which is a key figure for the

	POLES		ZEROS	
1	0.0000E+00	0.0000E+00		
2	0.0000E+00	0.0000E+00		
3	0.0000E+00	0.0000E+00	-0.2293E+03	0.0000E+00
4	-0.9359E+01	0.5207E+02	0.1055E+03	0.0000E+00
5	-0.9359E+01	-0.5207E+02	-0.1500E+01	0.5544E+02
6	-0.2012E+01	0.3954E+02	-0.1500E+01	-0.5544E+02
7	-0.2012E+01	-0.3954E+02	-0.5593E+02	0.0000E+00
8	-0.8313E+01	0.2503E+02	-0.5681E+01	0.2826E+02
9	-0.8313E+01	-0.2503E+02	-0.5681E+01	-0.2826E+02
10	-0.2428E+02	0.7011E+01	0.5003E+00	0.1814E+02
11	-0.2428E+02	-0.7011E+01	0.5003E+00	-0.1814E+02
12	-0.1177E+01	0.1774E+02	-0.1596E+02	0.2315E+01
13	-0.1177E+01	-0.1774E+02	-0.1596E+02	-0.2315E+01
14	-0.1949E+02	0.0000E+00	-0.2118E+01	0.7736E+01
15	-0.2092E+01	0.7671E+01	-0.2118E+01	-0.7736E+01
16	-0.2092E+01	-0.7671E+01	-0.6366E+01	0.1082E+01
17	-0.4444E+01	0.3883E+01	-0.6366E+01	-0.1082E+01
18	-0.4444E+01	-0.3883E+01	-0.1676E+01	0.4423E+01
19	-0.3830E+01	0.0000E+00	-0.1676E+01	-0.4423E+01
20	-0.2137E+00	0.1254E+01	-0.3050E+00	0.1118E+01
21	-0.2137E+00	-0.1254E+01	-0.3050E+00	-0.1118E+01
22	-0.9324E+00	0.1093E+01	-0.6778E+00	0.0000E+00
23	-0.9324E+00	-0.1093E+01	0.1721E-10	0.0000E+00
24	0.1490E-01	0.5367E-01	-0.2397E-02	0.0000E+00
25	0.1490E-01	-0.5367E-01	-0.2378E-01	0.0000E+00
26	0.2209E+00	0.0000E+00	0.5138E-11	0.0000E+00
27	-0.3006E+00	0.0000E+00	0.1640E-13	0.0000E+00

APPROXIMATE TRANSFER FUNCTION :

$$\frac{Pitch(s)}{Bls(s)} = \frac{0.116(S-0.01721)(S+0.002397)(S+0.6778)}{(S-0.0149+j0.05367)(S-0.0149-j0.05367)(S-0.2209)}$$

$$\frac{(S+0.305+j1.118)(S+0.305-j1.118)(S+1.676-j4.423)}{(S+0.9324-j1.093)(S+0.9324+j1.093)(S+0.2137+j1.254)}$$

$$\frac{(S+1.676+j4.423)(S+6.366+j1.082)(S+6.366-j1.082)}{(S+0.2137-j1.254)(S+4.444-j3.883)(S+4.444+j3.883)(S+3.83)}$$

TABLE 5-5 Poles, Zeros and Approximate Transfer Function of Longitudinal Helicopter Dynamics at 60KTS

	POLES		ZEROS	
1	0.0000E+00	0.0000E+00		
2	0.0000E+00	0.0000E+00		
3	0.0000E+00	0.0000E+00	-0.2013E+03	0.0000E+00
4	-0.9025E+01	0.5194E+02	-0.8070E+02	0.0000E+00
5	-0.9025E+01	-0.5194E+02	-0.4372E+01	0.5287E+02
6	-0.2083E+01	0.3897E+02	-0.4372E+01	-0.5287E+02
7	-0.2083E+01	-0.3897E+02	0.3553E+02	0.0000E+00
8	-0.3312E+02	0.1683E+02	-0.2014E+01	0.3259E+02
9	-0.3312E+02	-0.1683E+02	-0.2014E+01	-0.3259E+02
10	-0.7759E+01	0.2517E+02	-0.1983E+02	0.6674E+01
11	-0.7759E+01	-0.2517E+02	-0.1983E+02	-0.6674E+01
12	-0.2418E+02	0.0000E+00	-0.5780E+00	0.1764E+02
13	-0.1167E+01	0.1738E+02	-0.5780E+00	-0.1764E+02
14	-0.1167E+01	-0.1738E+02	-0.2321E+01	0.8041E+01
15	-0.2269E+01	0.7914E+01	-0.2321E+01	-0.8041E+01
16	-0.2269E+01	-0.7914E+01	-0.9728E+01	0.0000E+00
17	-0.5138E+01	0.4588E+01	-0.8057E+01	0.0000E+00
18	-0.5138E+01	-0.4588E+01	-0.1563E+01	0.4835E+01
19	-0.4890E+01	0.0000E+00	-0.1563E+01	-0.4835E+01
20	-0.3618E+00	0.1440E+01	-0.3449E+00	0.1338E+01
21	-0.3618E+00	-0.1440E+01	-0.3449E+00	-0.1338E+01
22	-0.1146E+01	0.1503E+01	-0.9088E+00	0.0000E+00
23	-0.1146E+01	-0.1503E+01	-0.1261E-01	0.0000E+00
24	0.1137E-01	0.4161E-01	-0.1152E-09	0.0000E+00
25	0.1137E-01	-0.4161E-01	-0.1158E-02	0.0000E+00
26	0.1528E+00	0.0000E+00	0.2535E-11	0.0000E+00
27	-0.9152E-01	0.0000E+00	0.4516E-12	0.0000E+00

```
APPROXIMATE TRANSFER FUNCTION :

Pitch(s)        0.3924(S+0.001261)(S+0.01261)
-------- = ------------------------------------------
 Bls(s)      (S-0.01137+j0.04161)(S-0.01137-j0.04161)

         (S+0.9088)(S+0.3449-j1.338)(S+0.3449+j1.338)
-----------------------------------------------------------
(S+0.09152)(S+0.3618+j1.44)(S+0.3618-j1.44)(S+1.146+j1.503)

      (S+1.563-j4.835)(S+1.563+j4.835)(S+8.057)(S+9.728)
   --------------------------------------------------------
   (S+1.146+j1.503)(S+4.89)(S+5.138-j4.588)(S+5.138+j4.588)
```

TABLE 5-6 Poles, Zeros and Approximate Transfer Function of Longitudinal Helicopter Dynamics at 100KTS longitudinal dynamics, is strongly coupled with the lateral and directional dynamics.

5.2.3 Pitch Rate feedback

The longitudinal root loci of the helicopter with pitch rate feedback in a gain range from zero to 1.5 Deg/(Deg/Sec) are shown in Figs. 5-13, 5-14 and 5-15 for the hover, 60KTS and 100KTS forward flight respectively.

At hover the pitch rate feedback increases the damping ratio of the long period mode very effectively by both increasing the damping and reducing the frequency, and stabilized the unstable mode at gain K=0.5 Deg/(Deg/Sec). In contrast to the attitude feedback, the pitch rate feedback moves the two coupled body pitch/regressing flap real roots closing to each other and becoming a complex pair at the gain K=0.18 and finally coupling with the lateral coupled body roll/regressing flap mode, making it more stable. This means that at low gain range, the feedback stabilized the dominant less stable one of the two body pitch/regressing flap modes. Furthermore, the feedback slightly stabilizes the yaw damping mode as well, although the effect is too small to be shown in the root loci. All of these make the pitch rate feedback more beneficial than the corresponding pitch attitude feedback.

For forward flight, the pitch rate feedback offers the same beneficial improvements. The feedback not only increases the damping of the unstable long period mode but also

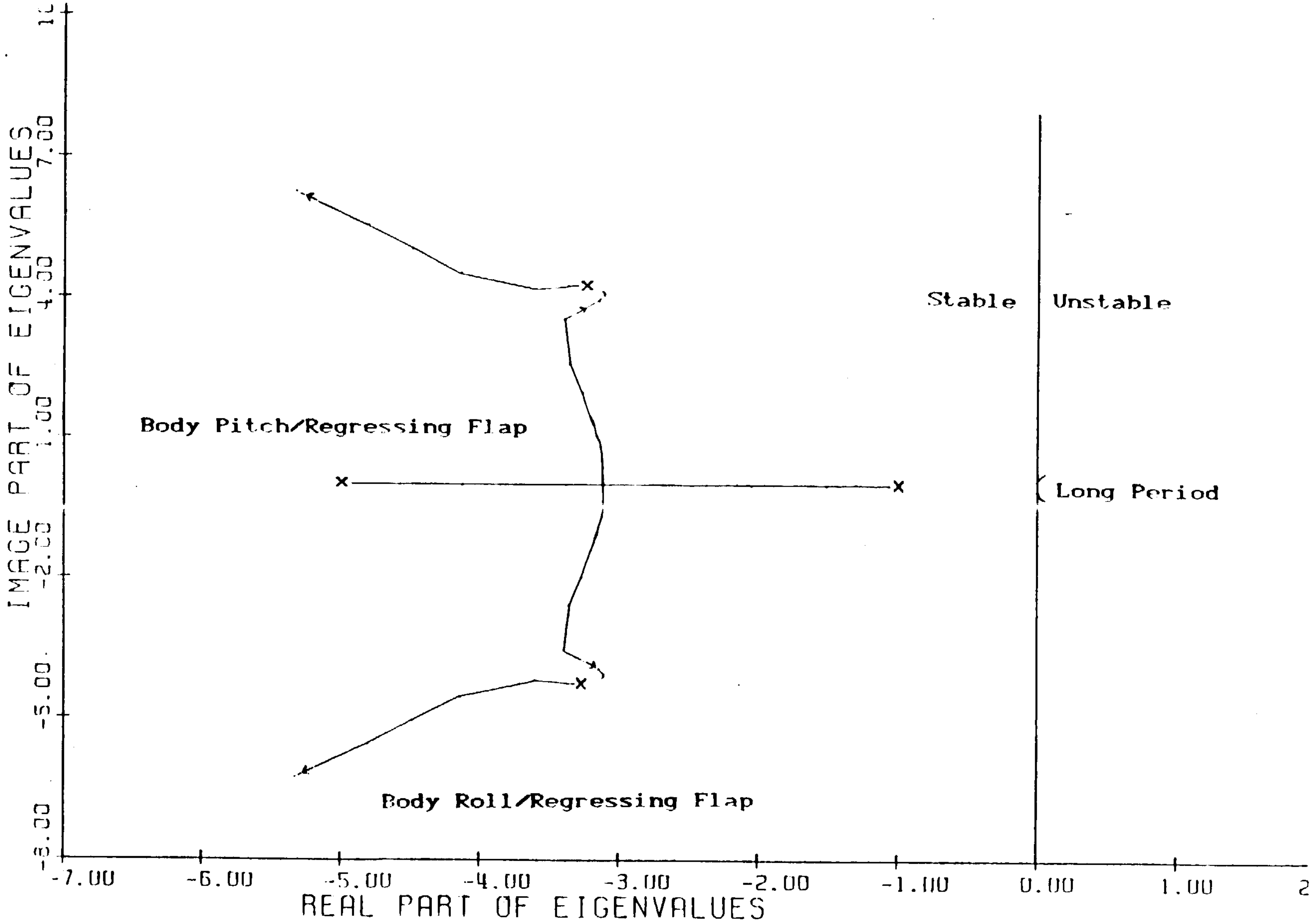

Fig. 5-13 The Root Loci of The Helicopter With Pitch Rate Feedback to Longitudinal Cyclic Input at Hover

ORIGINAL PAGE IS
OF POOR QUALITY

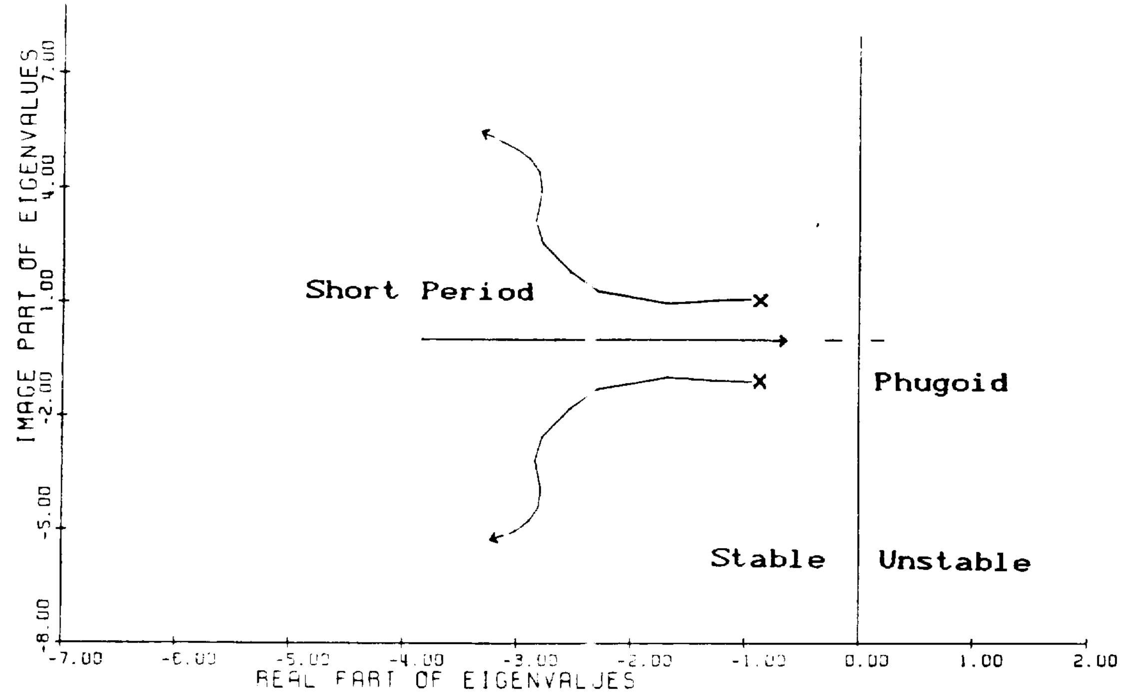

Fig. 5-14 The Root Loci of The Helicopter With Pitch Rate Feedback to Longitudinal Cyclic Input at 60 KTS

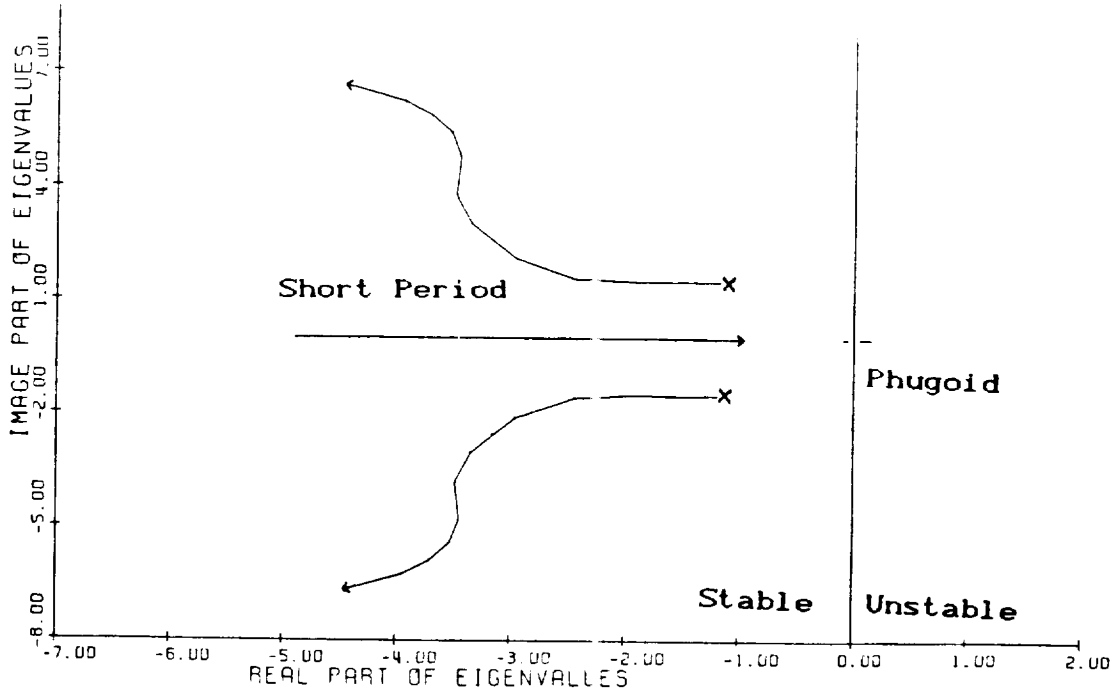

Fig. 5-15 The Root Loci of The Helicopter With Pitch Rate Feedback to Longitudinal Cyclic Input at 100 KTS

increases the damping of the oscillatory short period mode, both of them are dominant modes in the long period response and the short period response respectively, although it decreases the damping of the stable long period mode and the real root of short period mode.

The feedback limitation for pitch rate feedback comes from the destabilized lag motion. The advancing lag mode becomes unstable at feedback gain about K=1.5 Deg/(Deg/Sec) for hover. The effect on the damping of the advanced lag with the pitch rate feedback gain for hover and forward flight are shown in Fig. 5-16. As can be seen, the limitation is relaxed significantly at forward flight.

5.2.4 Roll Rate feedback

So far all of the feedback gain limitations encounted by the rotor/fuselage coupling are quite high compared to those conventionally used in the rotorcraft. However, the gain limitations in roll rate feedback are far lower. At hover the advancing lag mode becomes unstable with a feedback gain 0.23 Deg/(Deg/Sec), in forward flight the coning lag mode becomes unstable at about the same feedback gain at 100 KTS. Figs. 5-17 and 5-18 present the effect of the roll rate feedback on the dampings of the advancing lag mode and the coning lag mode. As can be seen, although the destabilized mode changes from advancing lag at hover to the coning lag at high speed, the limitation in feedback gain which will destabilize the rotor/fuselage system does not change sig-

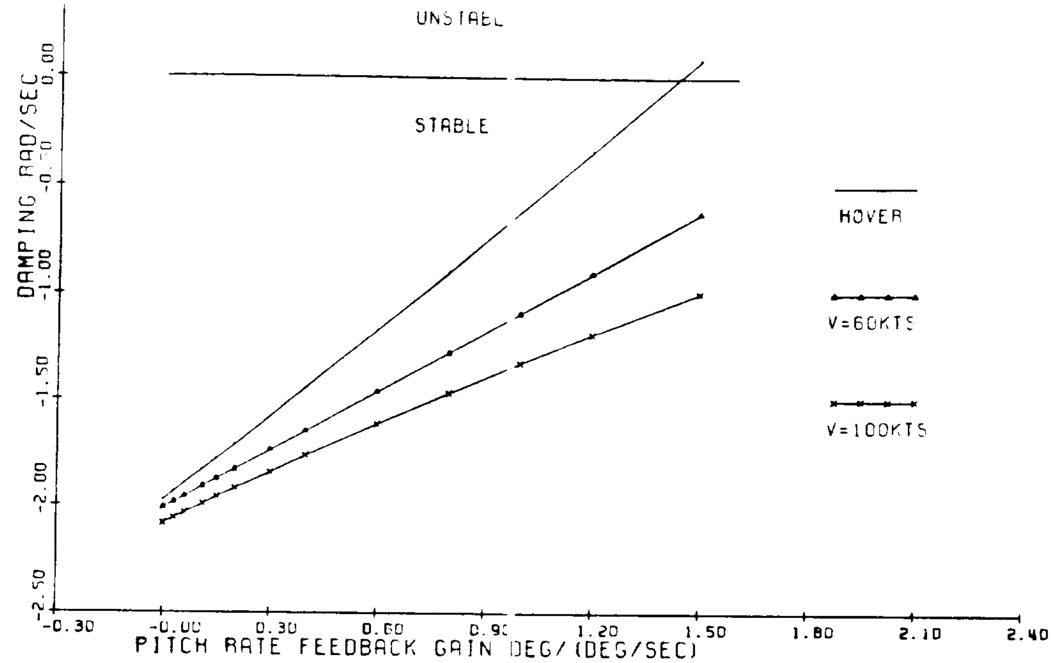

Fig. 5-16 Effect of Pitch Rate Feedback on The Damping of Advancing Lag Mode

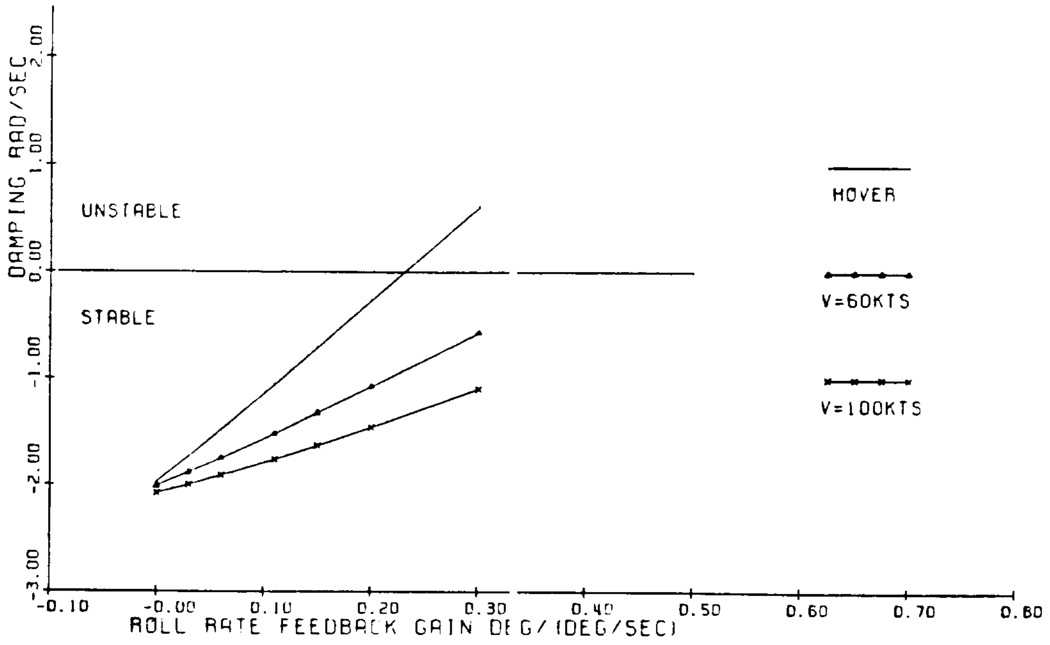

Fig. 5-17 Effect of Roll Rate Feedback on The Damping of Advancing Lag Mode

nificantly. Therefore, the roll rate feedback has to be used with caution in the whole flight speed range.

The precise value of the limiting gain is of course sensitive to the estimation of the mechanical lag damper characteristics. The effect of the estimated mechanical damping on the advancing lag damping is shown in Fig. 5-19 for roll rate feedback near the stability boundary of the helicopter at hover. The increase of the mechanical damping will result in a increase in the allowable rate gain before instability is encountered. Therefore, for the nonlinear damper whose estimated damping increases with the oscillatory velocity, the slightly unstable mode only means a moderate oscillation limit cycle.

Unfortunately the roll rate feedback is very beneficial for the helicopter lateral dynamics. At hover the roll/lateral velocity mode and body roll/regressing flap mode are stabilized by the feedback this can not be done simultaneously by the attitude feedback. In forward flight, the body roll/regressing flap mode, which is unstable for the high gain roll attitude feedback, and dutch roll mode, which can not be stabilized by the roll attitude feedback, are both stabilized by the feedback. The spiral mode, which can be effectively stabilized by the roll attitude feedback, is affected very little by the roll rate feedback. The frequency response of the helicopter roll rate at hover to the lateral cyclic input with roll rate feedback is shown in

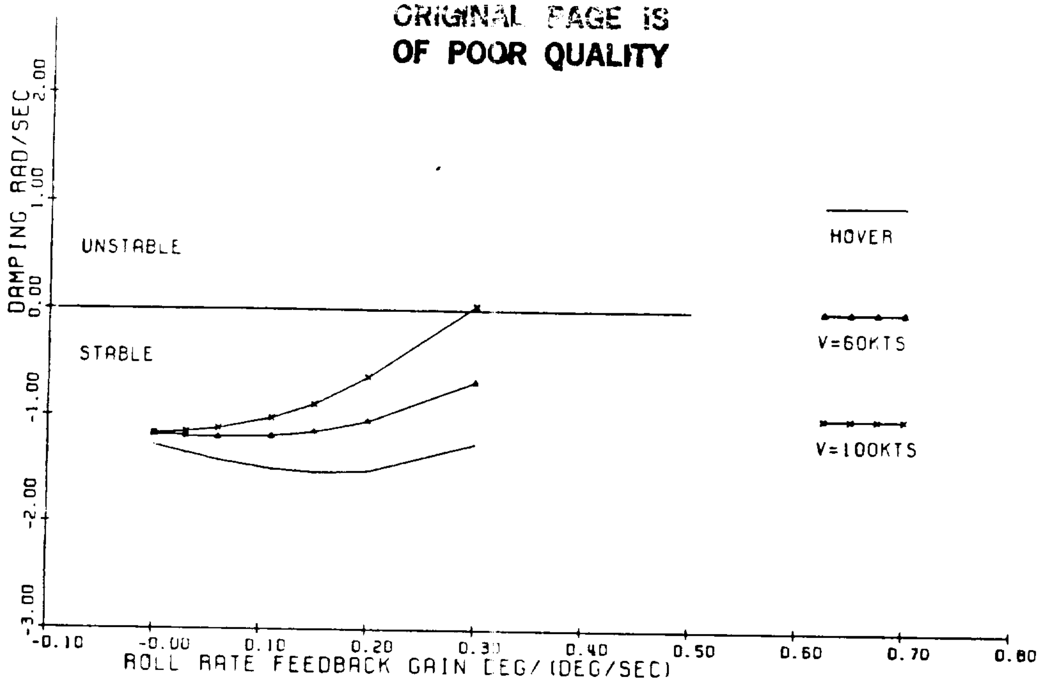

Fig. 5-18 Effect of Roll Rate Feedback on The Damping of Coning Lag Mode

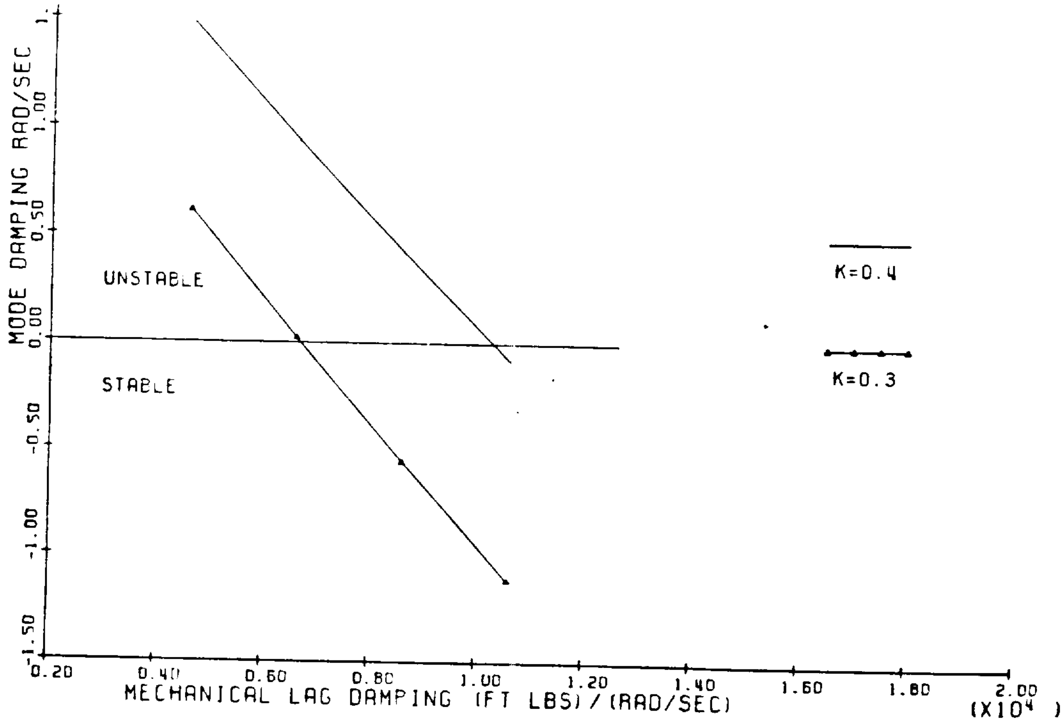

Fig. 5-19 Effect of Mechanical Lag Damping on The Damping of Advancing Lag Mode With Different Roll Rate Feedback Gains

ORIGINAL PAGE IS
OF POOR QUALITY

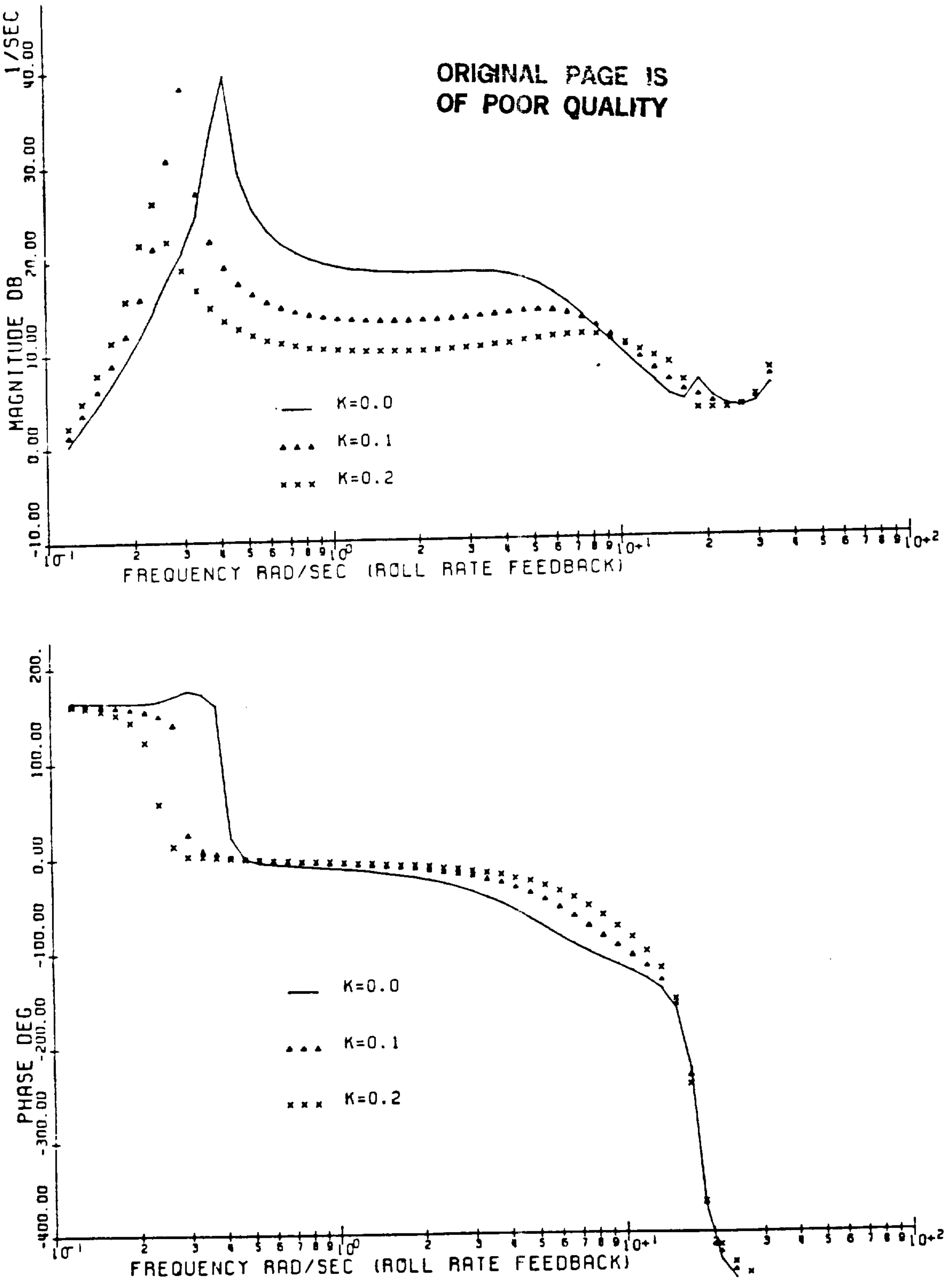

Fig. 5-20 Frequency Response of $\dot{\phi}/A_{1s}$ With Roll Rate Feedback to Lateral Cyclic Input, Hover

Fig. 5-20. As can be seen, the roll rate feedback increases the bandwidth of the rate command system by both moving the low frequency response peak, which associated with lateral phugoid mode, to lower frequency and increasing magnitude of the rate response at high frequencies. This will significantly improve the ablity of the helicopter for the manoeuvre requirement. The corresponding phase characteristics also have the same extension. The frequency response of the helicopter roll rate for forward flight to the lateral cyclic input with roll rate feedback is shown in Figs. 5-21 and 5-22. Although the peak to be smoothed is small itself, the roll rate feedback makes the improvement in the high frequency range, which is the most important for the manoeuvre capability.

5.2.5 Summary

For the simple feedback control, the blade dynamics can severely limit the useable values of the feedback gains, especially for the roll rate feedback. The fuselage attitude gain limitations arise primarily from the stability limits associated with the coupled body-flap modes, the fuselage rate gain limitations arise primarily from the stability limits associated with the lag modes. It should be noted that rate feedback always stabilizes those fuselage/ flap modes which produce the limitations in the attitude feedback. The proper combination with rate feedback will hence increase the attitude feedback limitation, which is

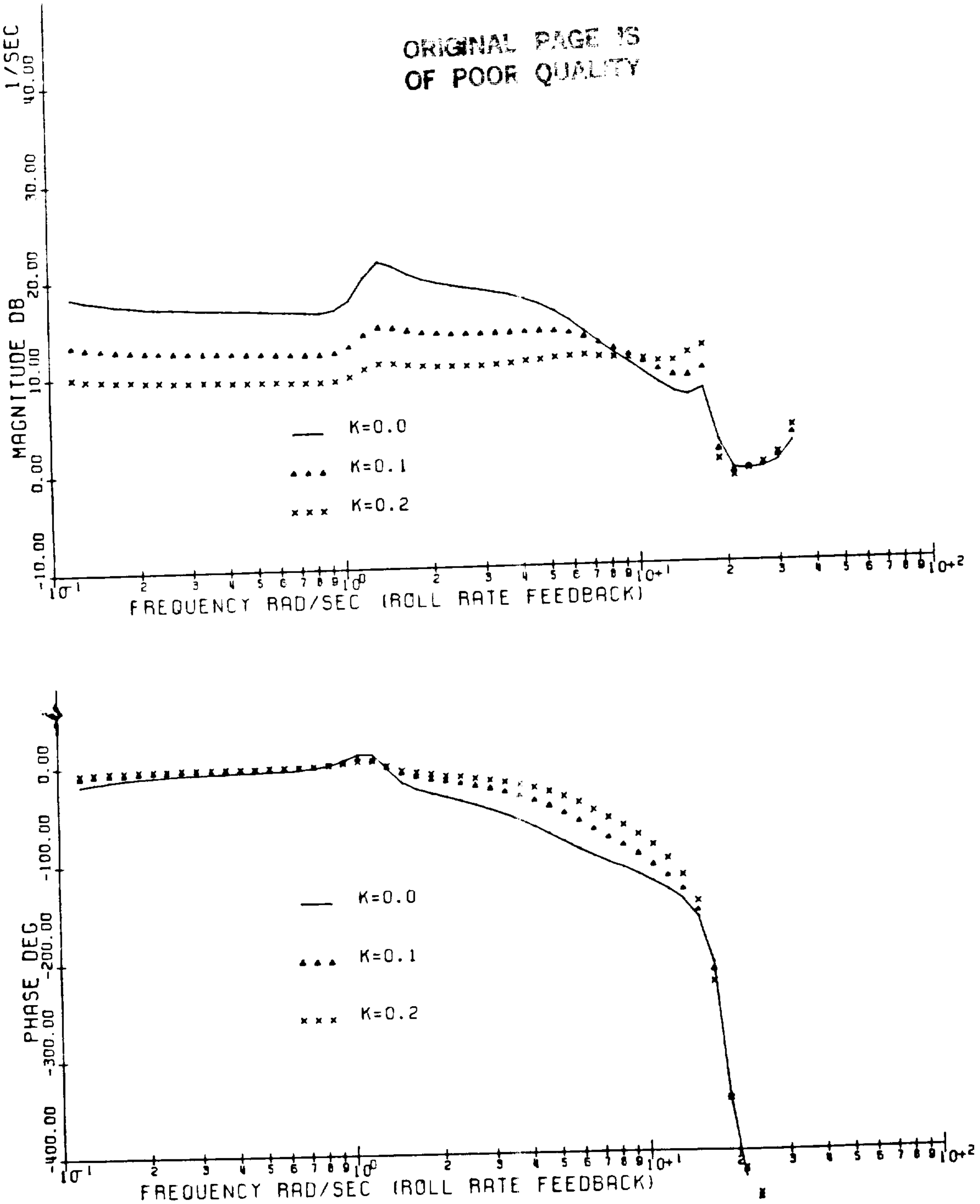

Fig. 5-21 Frequency Response of $\dot{\phi}/A_{1s}$ With Roll Rate Feedback to Lateral Cyclic Input, 60 KTS

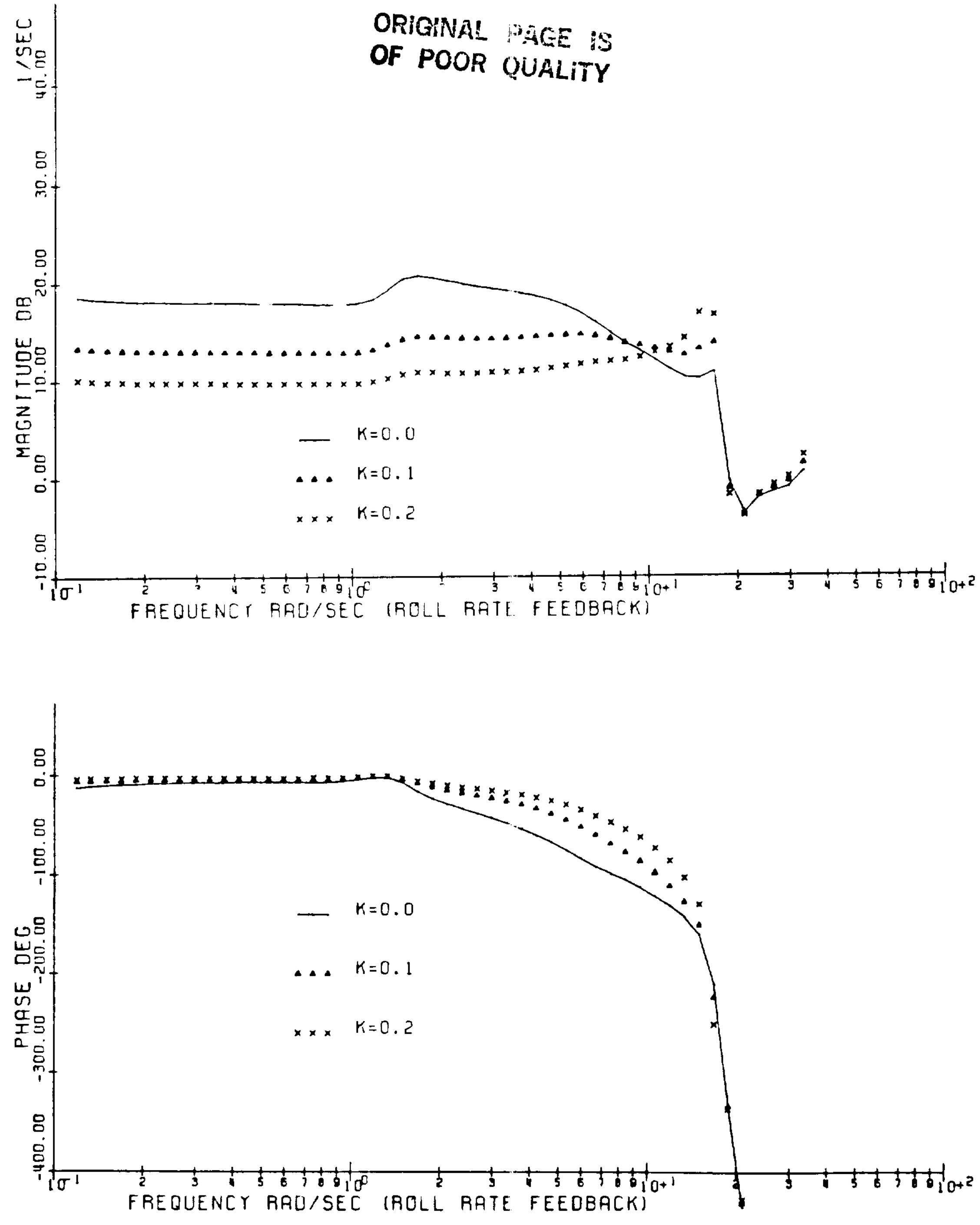

Fig. 5-22 Frequency Response of $\dot{\phi}/A_{1s}$ With Roll Rate Feedback to Lateral Cyclic Input, 100 KTS

already quite high. Therefore the limitation on the attitude feedback should be not a real problem for the automatic control design. However, the effect of attitude feedback on the lag modes is very small, although it is stabilizing. Therefore the limitations on the rate feedback can not be relaxed by addition of attitude feedback. Consequently it can be concluded that reducing the destabilizing effect of the feedback control on the lag dynamics will be required to raise the feedback gain limitations.

For the low frequency longitudinal dynamics, the improvement obtained by the pitch attitude and/or pitch rate feedback is limited because of the coupling with the lateral dynamics. It seems that good lateral dynamics, especially a stable spiral mode, is essential to achieve satisfactory longitudinal dynamics. The gain limitations due to the blade dynamics are not critical for their relative high values. For the lateral dynamics, in contrast, the simple roll attitude or roll rate feedback offers a significant improvement to the lateral dynamics. The proper combination of both can give perfect lateral dynamical characteristics.

5.3 Multivariable Optimal Control

Active control considered in this section is based on the deterministic linear optimal regulator problem[35,36]. The purpose of the present study is to show the effect of the lag dynamics on the overall system controller design. For the sake of clarity, it is assumed that all of the states, including the dynamic inflow, are available for measurement.

Optimal control theory is applied to the linear, constant coefficient differential Eq.(8) written in first order form

$$X' = A X + B U \tag{9}$$

$$Y = C X \tag{10}$$

The objective is now to find controls U, that is the cyclic control inputs to the swashplate and the collective control input to the tail rotor, which will minimize the quadratic cost function.

$$J = \int_0^\infty Y^T Q Y + U^T R U \ dt \tag{11}$$

where the weighting matrices Q and R are assumed to be symmetric and positive definite. The solution is the deterministic optimal controller with linear feedback of all state variables.

$$U = K X \tag{12}$$

where

$$K = - R^{-1} B^T S \tag{13}$$

and the matrix S is the constant, symmetric, positive definite solution of the algebraic Riccati equation.

$$SA + A^T S - SBR^{-1}B^T S - C^T QC = 0 \tag{14}$$

The closed loop dynamics equation is then defined as

$$X' = (A+BK) X \tag{15}$$

For the multivariable optimal control, the choice of a performance index, rather than feedback gains, to obtain the desired response is the central feature of the method. The solution of the optimal regulator problem is well defined, if the equations for a complex multi-input, multi-output plant is in hand. The principal difficulty lies not in the solution but in the choice of a suitable performance index. The solution is optimal in the sense that the chosen performance index is minimized, but different optimal solutions can be obtained by altering the Q and R matrices. The performance index may be interpreted as a quantitative measure of the system performance. The R matrix penalizes the control input required. The Q matrix penalizes the error in maintaining a desired trajectory.

A system model which includes only flapping dynamics is obtained from the system model developed in Chapter 3 by simply letting the perturbation variables associated with lag degrees of freedom be zero. This kind model has been used for controller design of helicopters by many previous investigators. The feedback controller then was designed by using the MacFarlane-Potter concept of eigenvector decomposition instead of integrating matrix Riccati equations.

5.3.1 Standard Performance Index

The quadratic performance index used here is of the form

$$J = \int_0^{\infty} q(Y^T I \; Y) + r(U^T I \; U) \, dt \tag{16}$$

In the present study the output scaling matrix C is chosen so that the output vector y only corresponds the three fuselage rotation attitudes, i.e. the system velocities, the translational displacements, and the blade dynamic variables are not included in the cost function. The weighting matrixes Q and R are assumed to be diagonal, a production of a number and a unit matrix, qI and rI. Some investigaters consider that q/r=1 gives a good choice in terms of balancing control effort, system stablity, and system response[37]. For the design of tighter controllers, which tend to hold fuselage pitch, roll and yaw angles to smaller deviations, weighting factor q/r on the fuselage rotation angles is increased from 1 to 5, and then to 25. These tighter controllers are then evaluated on the complete system model including the lag dynamics.

The main feedback gains obtained by applying the linear optimal regulator theory on the model which does not include the lag degrees of freedom, and the dampings of the advancing lag and coning lag modes obtained by applying the same feedback on the complete model including the lag degrees of freedom are presented in Tables 5-7, 5-8, and 5-9 for the cases of hover, 60KTS and 100KTS level flight respectively.

The resulting eigenvalues obtained from the complete system model by applying the feedback law obtained from the model without the lag degrees of freedom show that increasing the weighting factor q/r results in an instability in the lag degrees of freedom. The dampings of the advancing lag mode and the coning lag mode vary with the same trend obtained for the simple roll rate feedback. The correspond-

The Primary Feedback Gains:

q/r	1	5	25
Als / Roll Attitude	0.65	1.736	4.143
Bls / Pitch Attitude	0.966	2.087	4.529
Tot / Yaw Attitude	0.989	2.198	4.869
Als / Roll Rate	0.1225	0.285	0.5635
Bls / Pitch Rate	0.4487	0.7718	1.3
Tot / Yaw Rate	0.6965	1.076	1.633

The Damping of Lag Modes:

Advancing Lag	-0.2635	1.143	2.784
Coning Lag	-1.354	-1.039	-0.2897

Table 5-7 The Primary Feedback Gains and The Damping of Lag Modes For Standard Optimal Feedback at Hover

The Primary Feedback Gains:

q/r	1	5	25
Als / Roll Attitude	0.89	1.792	4.195
Bls / Pitch Attitude	0.857	1.972	4.439
Tot / Yaw Attitude	0.7575	1.905	4.434
Als / Roll Rate	0.13	0.290	0.5685
Bls / Pitch Rate	0.3996	0.744	1.316
Tot / Yaw Rate	0.4037	0.6848	1.079

The Damping of Lag Modes:

Advancing Lag	-0.9548	-0.0147	1.197
Coning Lag	-0.9901	-0.5625	0.1967

Table 5-8 The Primary Feedback Gains and The Damping of Lag Modes For Standard Optimal Feedback at 60KTS

The Primary Feedback Gains:

q/r	1	5	25
A1s / Roll Attitude	0.6716	1.775	4.189
B1s / Pitch Attitude	0.7678	1.82	4.194
Tot / Yaw Attitude	0.6661	1.799	4.333
A1s / Roll Rate	0.1248	0.2797	0.5506
B1s / Pitch Rate	0.3418	0.6623	1.217
Tot / Yaw Rate	0.3678	0.6597	1.067

The Damping of Lag Modes:

Advancing Lag	-1.352	-0.6556	0.3157
Coning Lag	-0.8667	-0.3597	0.4177

Table 5-9 The Primary Feedback Gains and The Damping of Lag Modes For Standard Optimal Feedback at 100KTS

ing feedback boundary is also the same as the boundary for the simple roll rate feedback. In fact, when the weighting ratio q/r increases, the primary feedback gains increase together by about the same factor. The attitude feedback gains increase beyond the limiting value, which produce instability for the simple attitude feedback, at q/r=5 without resulting the flapping instability because the rate feedback gains increase as well, which stabilizes the coupled fuselage/regressing flap mode as shown in the last section. However, when the roll rate gain is beyond the limiting value, there is no significant stabilizing effect from other feedback loops. Hence the instability that occurs in these cases has the same trend as roll rate feedback alone studied in the last section.

It is worthwhile to mention that at hover the limiting q/r ratio for the instability due to unmodeled lag dynamics is less than 5. This number is much smaller than a similar limiting boundary due to unmodeled flapping dynamics given in Ref.6. This suggests that as far as stability is concerned, the inclusion of the lagging dynamics in the system modelling for the controller design has more practical significance than the inclusion of the flapping dynamics, although the latter may be more important in terms such as control and response.

5.3.2 Frequency-Shaped Performance Index

The poles associated with the suppressed lag degrees of freedom have low open-loop damping and are relative high frequency. They lie very close to the imaginary axis in the s-plane. Therefore any misplaced control energy (spillover) will push them quickly into instability. Readjusting Q and R to prevent this (the only means available for the standard performance index design) can cause a drastic loss of closed-loop damping in the design mode poles, in some cases to the point where almost no closed-loop improvement in damping is possible. The problem arises from the fact that penalty matrices Q and R penalize the states and controls by the same amount at all frequencies.

One way to avoid constant penalties is the use of frequency-shaped cost functionals, an extention of standard linear optimal regulator design[38]. In this method, the performance index to be minimized is assumed to be a function of frequency as follows:

$$J = \int_{-\infty}^{\infty} Y^T(j\omega)Q(j\omega)Y(j\omega) + U^T(j\omega)R(j\omega)U(j\omega) \quad d\omega \qquad (17)$$

Note that here the weighting matrices Q and R are functions of frequency, rather than constant matrices. The detailed discussion of this method is given in Refs.39 and 40. The physical concept of the frequency-shaped cost functionals is that the performance index is defined such that the low frequency error in maintaining a desired trajectory and the high frequency inputs are more heavily penalized such that the feedback energy is mainly placed on the low frequency fuselage dynamics. The cost function can be defined in three ways: (1) frequency-shaped response penalty with constant control penalty, (2) frequency-shaped control penalty with constant response penalty, and (3) frequency-shaped both response and control penalties. It should be noticed that the frequency-shaped response penalty leads to increasing degrees of freedom of the system to be augmented, and the frequency-shaped control penalty leads to feed forward of the derivatives of the control inputs. The numerical study shows that introducing new degrees of freedom of the system, whose order is quite high already, not only results in difficulties for system analysis but also requires extremely high feedback gains which are physically unrealistic. Therefore, only a frequency-shaped control penalty is used in this study.

The performance index then is defined as:

$$J = \int_{-\infty}^{\infty} q\ Y^T Y + r \left(\frac{\omega^2 + b^2}{b^2} \right) U^T U \ d\omega \tag{18}$$

The frequency-shaped control penalty used here is equivalent to inclusion of a shaping filter in the forward path of a standard optimal control problem. The corresponding shaping filter has a transfer function of the form:

$$U = b/(jw+b)\ Uc \tag{19}$$

The low pass characteristics of the filter will reduce the high frequency component in the feedback so as to penalize the high frequency control. This is physically convenient for the implementation because actuator dynamics can be thought of as having the form of shaping filters. Since the frequencies of the coning and advancing lag modes are about 38 and 16 rad/sec, the corner frequency of the low pass filter used in the study is chosen to be 10 rad/sec.

The ratio q/r here can not be directly compared with the ratio in the eq.(16) because the frequency-shaped control penalty has changed the spectrum distribution of r in frequency domain. Thus the ratio q/r is decided independently here and the chosen ratios for the frequency-shaped cost functions are 10, 100, 1000, and 10000.

The main feedback gains obtained by applying the linear optimal regulator theory with frequency-shaped cost control penalty on the model which not includes the lag degrees of freedom and the dampings of the advancing lag and coning lag modes obtained by applying the same feedback on the complete model which includes the lag degrees of freedom are presented in Tables 5-10, 5-11, and 5-12 for the cases of hover, 60KTS and 100KTS level flight respectively.

The resulting eigenvalues obtained from the complete system model show the same trend for an instablity in lag modes as standard optimal control. However corresponding feedback gains for the instablity are much higher than the standard cost function. The frequency shaped-optimal feedback has introduced new poles into the overall system, the Butterworth configuration of the system has been changed so that

The Primary Feedback Gains:

q/r	10	100	1000	10000
A1s ------------- Roll Attitude	0.94	5.3	22.2	78.0
B1s ------------- Pitch Attitude	3.07	9.44	29.0	88.77
Tot ------------- Yaw Attitude	3.13	9.84	30.9	96.37
A1s ------------- Roll Rate	0.2	1.16	4.22	12.1
B1s ------------- Pitch Rate	1.71	4.28	10.37	24.37
Tot ------------- Yaw Rate	2.53	5.64	12.4	26.86

The Damping of Lag Modes:

Advancing Lag	-2.00	-2.01	-1.63	0.6
Coning Lag	-1.40	-1.78	-2.36	-1.11

Table 5-10 The Primary Feedback Gains and The Damping of Lag Modes For Frequency Shaped Optimal Feedback at Hover

The Primary Feedback Gains:

q/r	10	100	1000	10000
$\dfrac{\text{A1s}}{\text{Roll Attitude}}$	1.00	5.6	22.8	78.3
$\dfrac{\text{B1s}}{\text{Pitch Attitude}}$	2.58	8.56	27.7	87.59
$\dfrac{\text{Tot}}{\text{Yaw Attitude}}$	1.96	7.76	26.8	86.98
$\dfrac{\text{A1s}}{\text{Roll Rate}}$	0.27	1.27	4.3	12.16
$\dfrac{\text{B1s}}{\text{Pitch Rate}}$	1.44	3.94	10.09	24.75
$\dfrac{\text{Tot}}{\text{Yaw Rate}}$	1.55	3.85	8.88	19.6

The Damping of Lag Modes:

Advancing Lag	-2.04	-2.09	-2.03	-1.07
Coning Lag	-1.26	-1.48	-1.56	-0.44

Table 5-11 The Primary Feedback Gains and The Damping of Lag Modes For Frequency Shaped Optimal Feedback at 60KTS

The Primary Feedback Gains:

q/r	10	100	1000	10000
Als ------------- Roll Attitude	0.83	5.24	22.27	77.88
Bls ------------- Pitch Attitude	2.23	7.68	25.63	82.85
Tot ------------- Yaw Attitude	1.49	6.92	25.57	85.43
Als ------------- Roll Rate	0.25	1.21	4.14	11.83
Bls ------------- Pitch Rate	1.20	3.45	9.22	23.54
Tot ------------- Yaw Rate	1.38	3.66	8.70	19.5

The Damping of Lag Modes:

Advancing Lag	-2.10	-2.13	-2.08	-1.07
Coning Lag	-1.23	-1.37	-1.10	0.046

Table 5-12 The Primary Feedback Gains and The Damping of Lag Modes For Frequency Shaped Optimal Feedback at 100KTS

q/r	1		5	
	Damping	Frequency	Damping	Frequency
Hover	-0.99	1.243	-1.46	1.862
	-1.29	1.971	-1.76	2.737
	-2.93	4.227	-3.63	5.495
	-2.22	7.504	-2.33	7.414
	-5.80	0.000	-7.46	0.000
	-6.68	0.000	-9.30	0.000
60 KTS	-1.03	1.807	-1.40	2.454
	-1.50	2.025	-2.16	2.897
	-3.15	4.255	-4.24	6.123
	-2.34	7.335	-2.23	6.920
	-4.94	0.000	-5.78	0.000
	-9.33	0.000	-16.2	2.228
100 KTS	-1.08	1.829	-1.56	2.568
	-1.62	2.443	-2.26	3.228
	-4.09	4.708	-5.15	6.729
	-2.52	7.420	-2.30	7.039
	-6.12	0.000	-7.19	0.000
	-9.61	0.000	-15.6	0.000

q/r	25	
	Damping	Frequency
Hover	-2.10	2.808
	-2.45	3.716
	-5.29	6.687
	-2.44	7.261
	-8.82	0.000
	-11.5	0.000
60 KTS	-1.96	3.370
	-3.12	4.264
	-2.11	6.768
	-6.19	7.457
	-6.72	0.000
	-17.5	5.903
100 KTS	-2.20	3.700
	-3.31	4.531
	-2.33	6.729
	-6.82	8.212
	-8.69	0.000
	-23.2	0.000

Table 5-13 The Poles Assceiated With The Short Period Flight Dynamic Characteristics of The Helicopter Under Standard Optimal Feedback

q/r	10		100	
	Damping	Frequency	Damping	Frequency
Hover	-0.79	1.545	-1.14	2.208
	-0.89	1.891	-1.34	2.638
	-1.85	1.745	-2.49	3.224
	-4.45	2.338	-5.29	3.702
	-4.43	5.137	-6.92	6.951
	-2.07	7.672	-2.15	7.768
60 KTS	-1.80	1.130	-2.12	2.791
	-0.81	1.844	-1.10	2.387
	-1.29	2.496	-2.14	3.683
	-3.78	2.101	-4.72	3.032
	-5.27	5.312	-7.32	7.800
	-2.24	7.747	-2.48	7.773
100 KTS	-1.98	0.687	-1.20	2.593
	-0.89	1.954	-2.95	3.075
	-1.32	2.654	-2.02	3.516
	-4.25	1.944	-5.13	3.255
	-5.56	6.063	-2.76	7.969
	-2.47	7.972	-7.61	8.690

q/r	1000		10000	
	Damping	Frequency	Damping	Frequency
Hover	-1.61	3.101	-2.26	4.297
	-1.96	3.625	-2.47	5.087
	-3.40	4.539	-4.51	5.268
	-6.68	5.618	-9.48	8.727
	-2.41	7.962	-3.35	8.358
	-12.4	11.19	-15.4	0.000
60 KTS	-1.57	3.192	-2.40	4.398
	-2.62	4.166	-4.27	5.313
	-2.79	5.226	-1.84	5.757
	-6.29	4.302	-10.0	6.375
	-3.21	7.921	-5.00	9.365
	-10.9	11.63	-18.2	11.49
100 KTS	-1.67	3.571	-2.99	4.888
	-2.51	4.563	-1.57	5.491
	-3.79	5.204	-5.14	5.745
	-6.31	5.047	-5.42	9.550
	-3.64	8.092	-8.72	8.234
	-11.5	13.06	-17.9	17.57

Table 5-14 The Poles Associated With The Short Period Flight Dynamical Characteristics of The Helicopter Under Frequency Shaped Optimal Feedback

damping ratio can not be used as a measurement of the system augmentation. The dampings and frequencies of the short period modes associated closely with the fuselage dynamics are presented in Table 5-13 and Table 5-14 for both standard and frequency-shaped cost functions. If the lowest damping of these modes is used as a measurement for the system's augmentation, the case q/r=1000 with the frequency-shaped cost function will be more stabilized by the feedback than the case q/r=5 with the standard cost function, and the case q/r=10000 with the frequency-shaped cost function will be more stabilized by the feedback than the case q/r=25 with the standard cost function. The feedback limitations for the frequency-shaped optimal control due to the unmodelled lag degrees of freedom therefore are not only numerically much larger but also offering much stronger system augmentation in stability and control characteristics. In addition, the feedback gains required by the q/r=10000 case are far higher than those that are physically practical. This suggests that by applying the frequency-shaped cost function on the helicopter automatic control system design, the unstable effect due to the unmodelled lag degrees of freedom can be removed.

To illustrate the advantages of the optimal feedback control, the frequency responses of helicopter roll attitude to lateral cyclic input are shown in Figs. 5-23, 5-24, and 5-25 for the standard optimal feedback control and in Figs. 5-26,

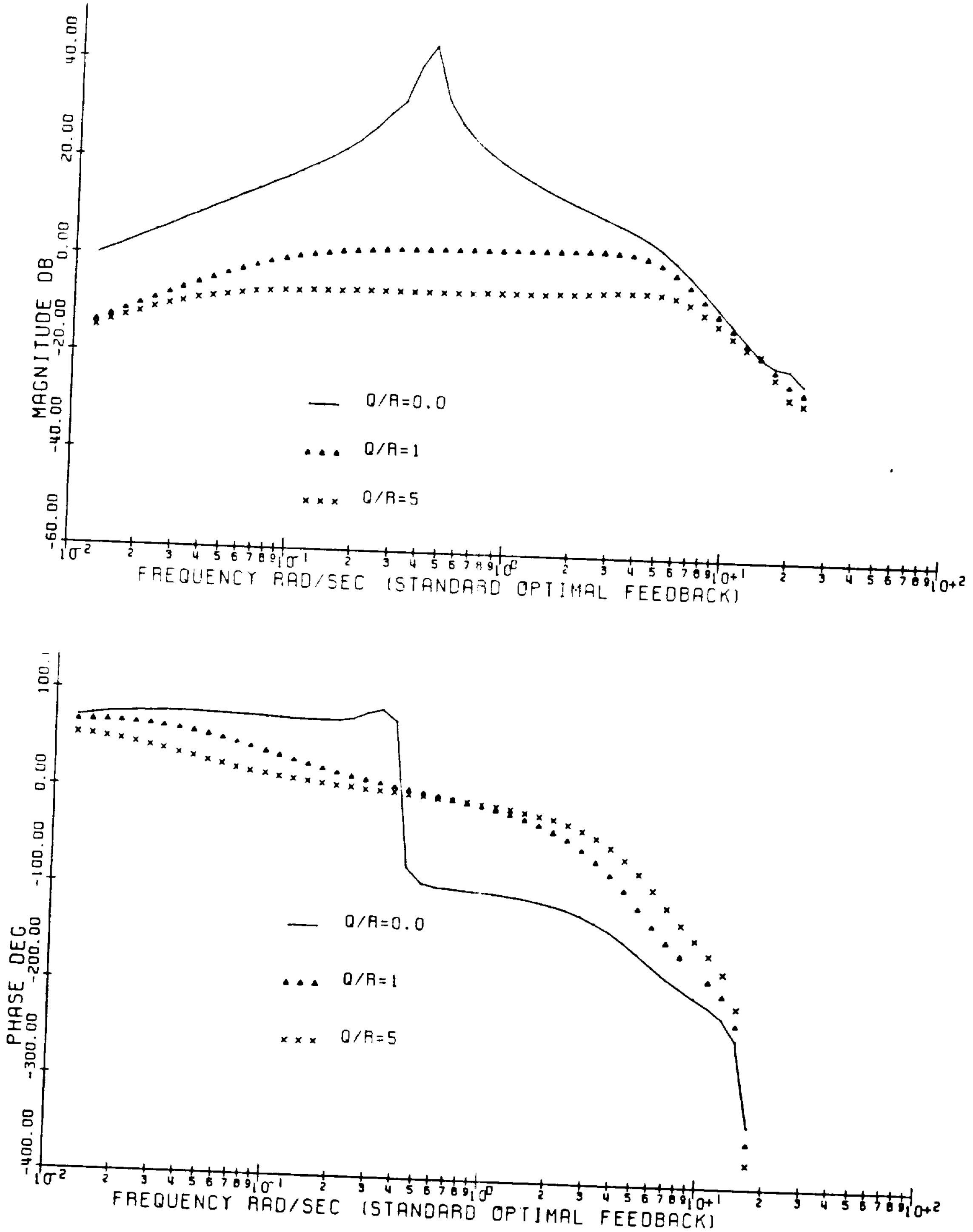

Fig. 5-23 Frequency Response of ϕ/A_{1s} With Standard Optimal Feedback at Hover

ORIGINAL PAGE IS
OF POOR QUALITY

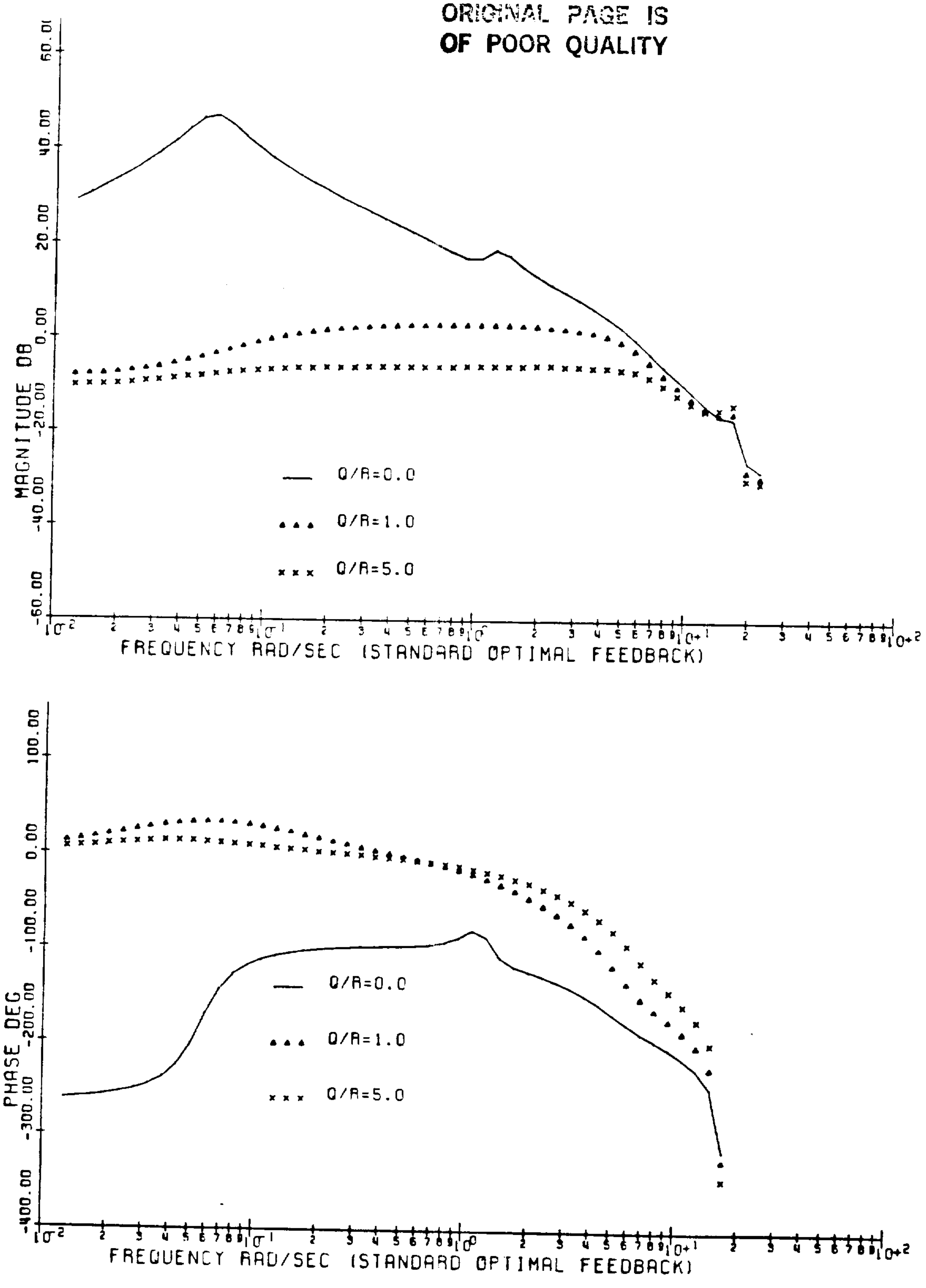

Fig. 5-24 Frequency Response of ϕ/A_{1s} With Standard Optimal Feedback at 60 KTS

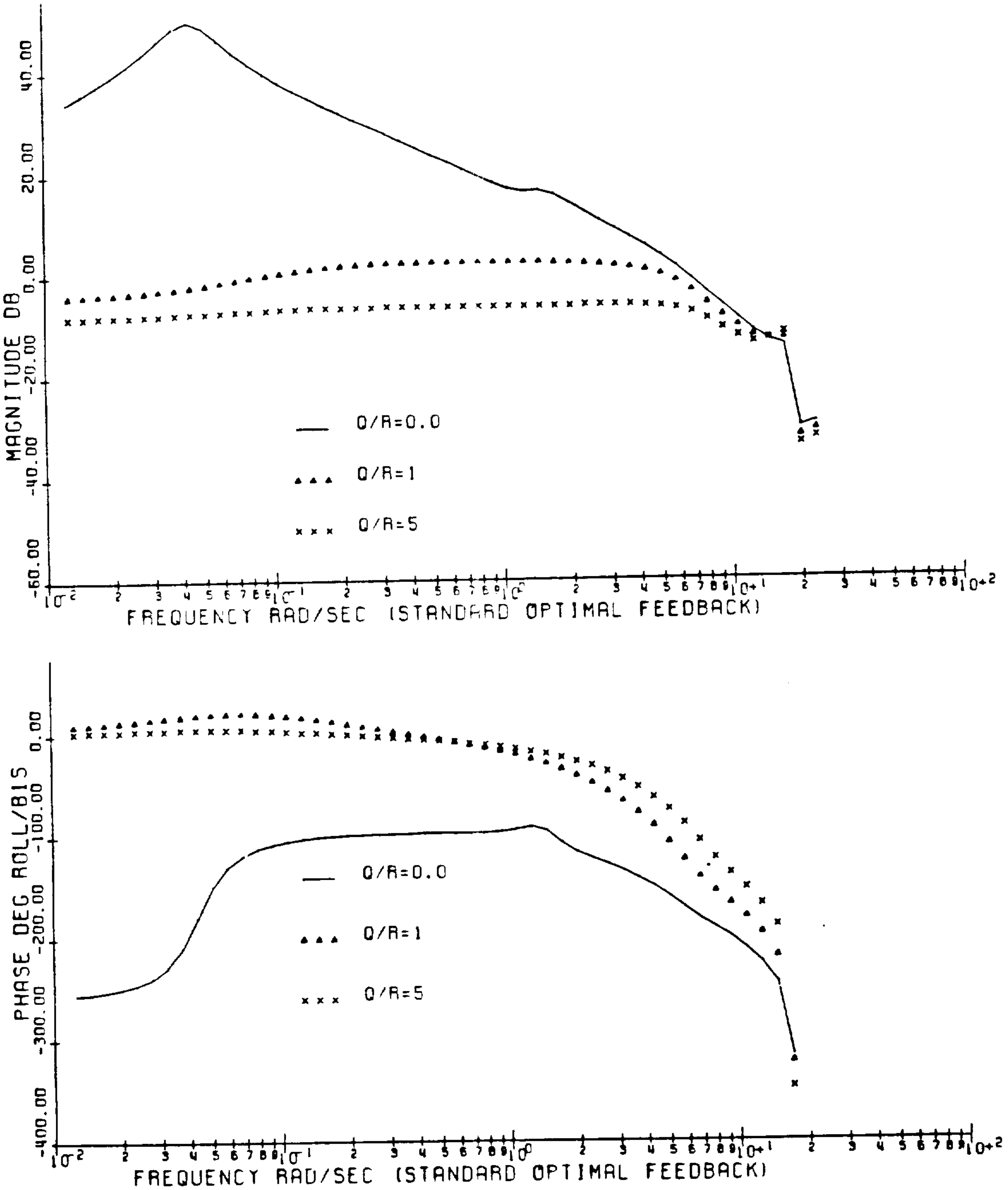

Fig. 5-25 Frequency Response of ϕ/A_{1s} With Standard Optimal Feedback at 100 KTS

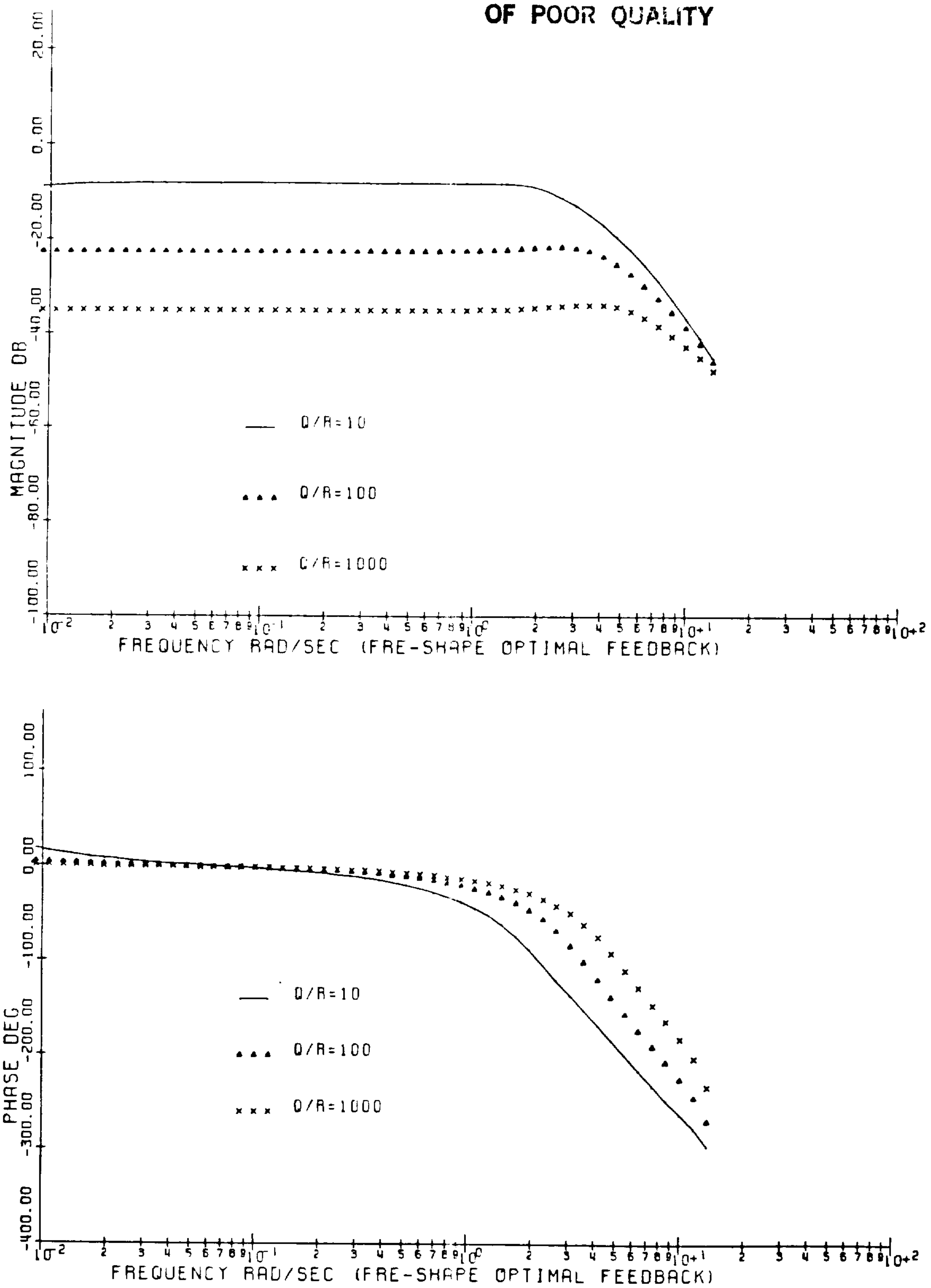

Fig. 5-26 Frequency Response of ϕ/A_{1s} With Frequency Shaped Optimal Feedback at Hover

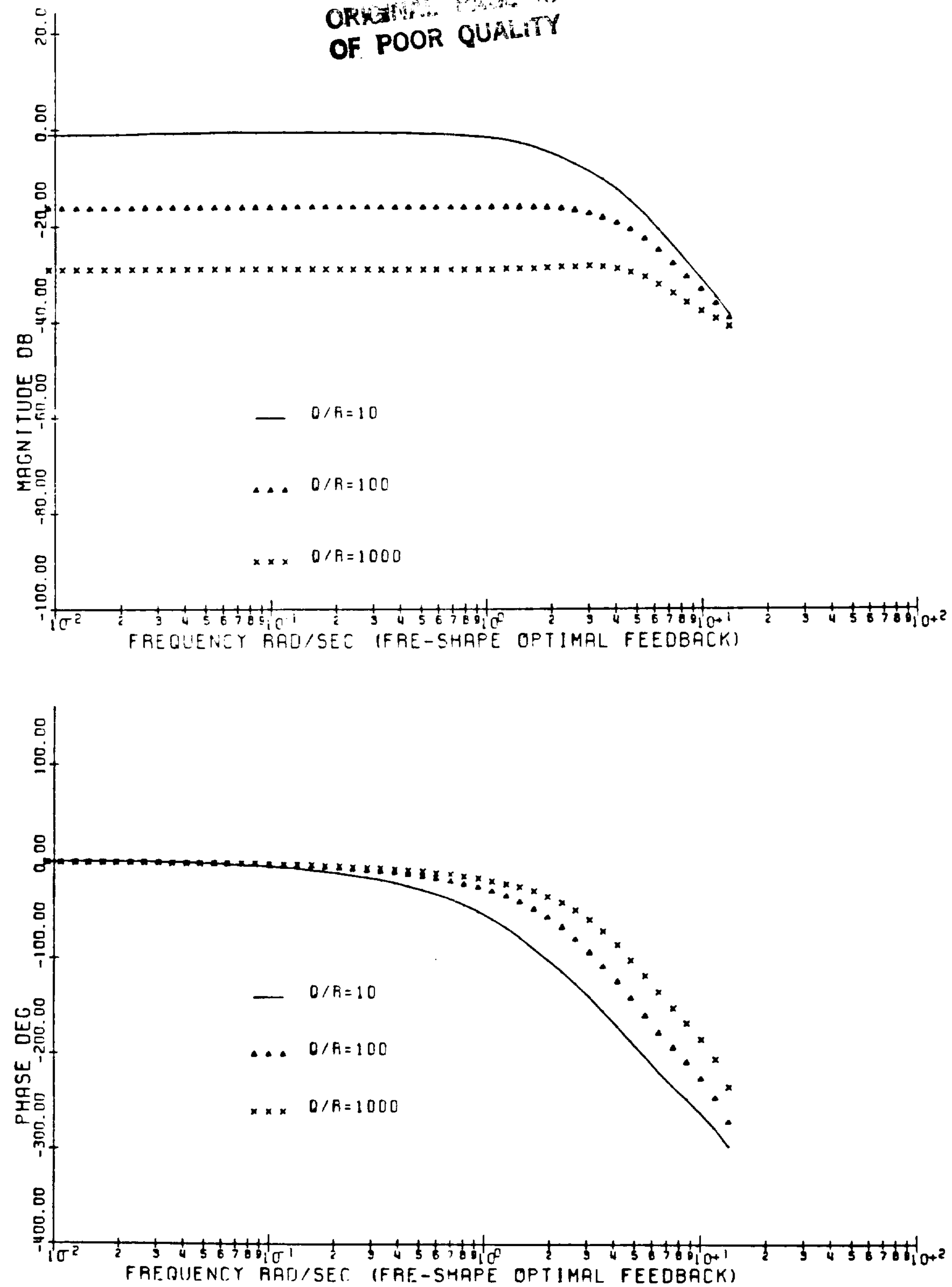

Fig. 5-27 Frequency Response of ϕ/A_{1s} With Frequency Shaped Optimal Feedback at 60 KTS

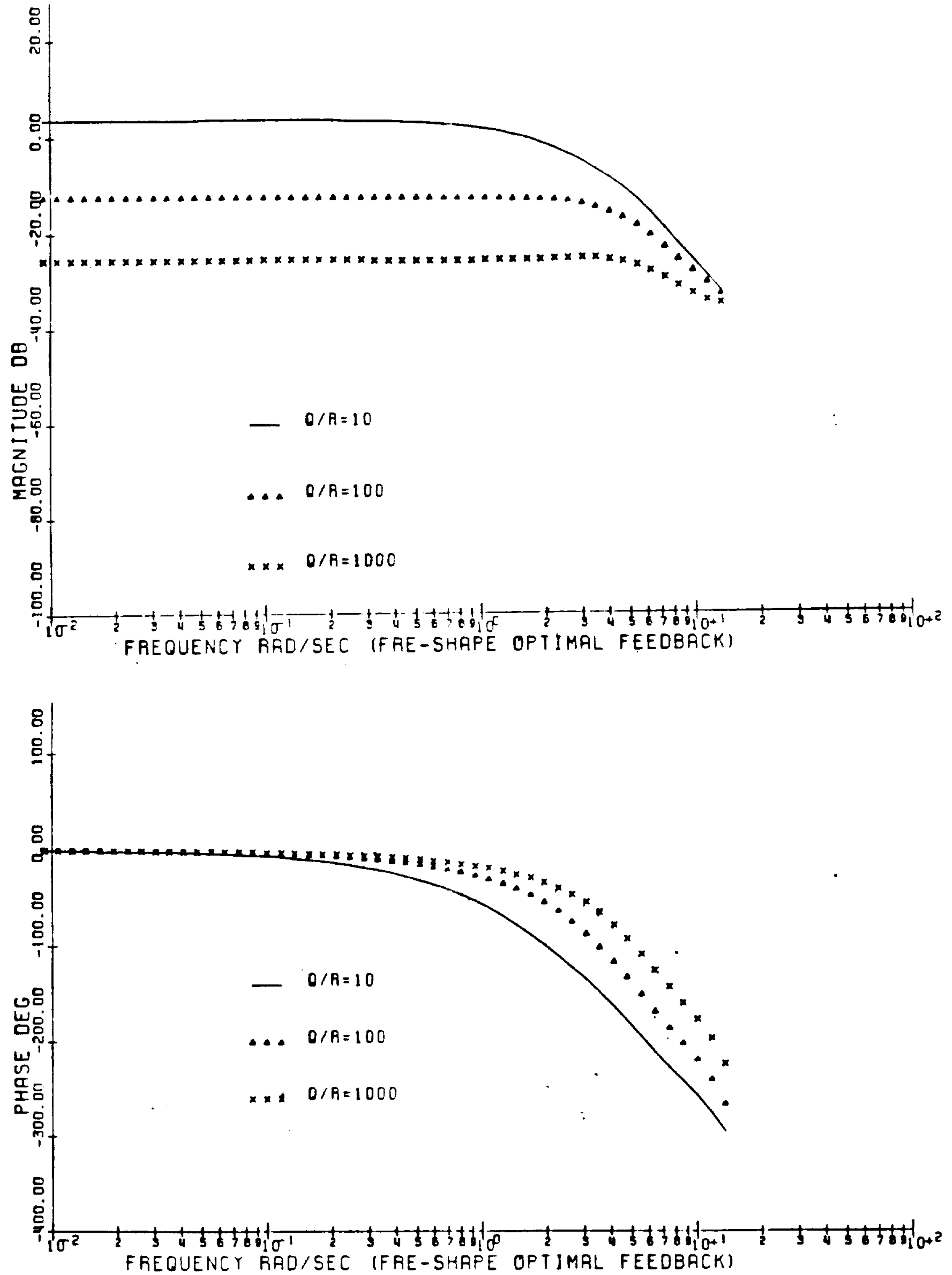

Fig. 5-28 Frequency Response of ϕ/A_{1s} With Frequency Shaped Optimal Feedback at 100 KTS

5-27, and 5-28 for the frequency-shaped optimal feedback control.

By comparing with the corresponding frequency responses obtained by the simple attitude feedback, it can be seen that the main improvements obtained by the standard optimal feedback control are limited in phase characteristics. The Bode amplitude characteristics by the standard optimal feedback is only improved a little by smoothing the peak at high frequency end in the bandwidth obtained by the strong attitude feedback. The phase characteristics, in contrast, have a significant improvement by reducing the phase shift at high frequency range 5-15 rad/sec. At these high frequencies, the simple attitude feedback cannot offer any reduction. As for the very low frequencies, the standard optimal feedback gives the same trend in both amplitude and phase characteristics as the simple attitude feedback.

The frequency-shaped optimal feedback control, however, has improved the frequency responses in both amplitude and phase characteristics. The frequency responses obtained by the frequency-shaped optimal feedback have perfect low frequency characteristics. The amplitude characteristics at low frequencies up to 2 rad/sec is a straight line for any q/r ratio. For phase characteristics, the frequency-shaped optimal control has totally removed the phase lead resulting from the nonminimum phase characteristics; this is especially obvious in the hover case. In addition, at a quite wide range of frequency, the phase shift is very small and is significant reduced along with the increasing of the q/r ratio. For the high frequency part, in spite of the fact that the frequency-shaped optimal control is designed to reduce the high frequency augmentation, the obtained improvements seem still better for the high gain simple attitude feedback. The amplitude characteristics obtained by the frequency-shaped optimal feedback are not only better than the simple attitude feedback by removing the high frequency peak but also better than the standard optimal feedback in term of the maximum achievable bandwidth. Take hover case as a example, the q/r=5 standard optimal feedback case has almost the same bandwidth with the q/r=1000 frequency-shaped optimal feedback case. However for standard optimal feedback, the advancing lag mode has became unstable far below the q/r=5, in contrast, for the frequency-shaped optimal feedback, the system will be stable until q/r=10000. For the high frequency phase characteristics, the reductions of phase shift obtained by the frequency-shaped optimal feedback are smaller than those obtained by the standard optimal feedback but still offer improvements which can not be obtained by the simple attitude feedback because for the simple attitude feedback, there is no phase shift reduction at frequencies higher than 6 rad/sec. Therefore, it is clearly suggested that the improvements obtained by the frequency-shaped optimal feedback are much more practical.

5.3.3 Simplified Optimal Control

The design of linear controllers in this section results in a feedback structure which requires the measurement and feedback of all state variables except translational positions. The obvious impracticality of this requirement has led to several research efforts directed toward the synthesis of simplified controllers which are more easily implemented than would be the optimal control. As a result, a series of simplified controllers are developed through successive reduction in the number of feedback loops while using the feedback gain factors obtained for the optimal control. The sequence of the loop reduction is determined by both the difficulties for measurement and the importance of the feedback requirement of the loop;the latter is naturally measured by the amplitude of the corresponding gain for the optimal control. In addition, particular emphasis is placed on eliminating the feedback of rotor degrees of freedom. The gain constants for these reduced state feedback controller are chosen as the values obtained for the corresponding states in the optimal controller.

The first loop reduction is eliminating the feedback of dynamic inflow because these state variables can not be measured. and removing the feedback of translational fuselage velocities because the corresponding gains for this group state variables are far smaller than others, consequently they are considered the least important for the feedback control. The number of remaining feedback loops for this simplified controller, called controller A, is 12. For the controller B, flapping velocities of the blade are also eliminated from the feedback. This is due to both the difficulties in measurement and the importance consideration. The number of remained feedback loops for this simplified controller is 9. The controller C is formed by eliminating flapping attitudes from the system feedback loops. The required gains for these attitude feedback loops are in the same order as those for fuselage attitudes, but the measurements are more difficult and more expensive than the corresponding fuselage attitudes because the resolution of the measurements from rotating to nonrotating axes is required. The number of remained feedback loops for this simplified controller C is 6. The final loop reduction is eliminating the feedback of three fuselage angular velocities simply because for standard optimal control, removing these feedback loops result in a favourable increasing of the dampings of the lag modes, which are the very modes resulting stablity limitations for the feedback control. The number of remained feedback loops for this simplified controller D is 3.

The poles associated with the short period flight dynamical characteristics obtained by various reduced loop controllers are shown in the Table 5-15 for the simple standard optimal feedback control with q/r=1 and in the Table 5-16

Number of feedback loops	12		9	
	Damping	Frequency	Damping	Frequency
Hover	-1.01	1.239	-1.01	1.239
	-1.30	1.979	-1.30	1.963
	-2.99	4.578	-2.96	4.563
	-2.22	7.502	-2.22	7.501
	-1.35	17.13	-12.7	17.20
	-0.28	39.42	-0.33	40.01
60 KTS	-1.06	1.833	-1.06	1.828
	-1.54	2.056	-1.56	2.049
	-3.07	4.302	-3.06	4.212
	-2.35	7.333	-2.35	7.328
	-0.99	17.16	-0.94	17.21
	-0.94	39.13	-0.84	39.54
100 KTS	-1.09	1.847	-1.09	1.845
	-1.64	2.553	-1.66	2.541
	-4.01	4.683	-3.94	4.578
	-2.51	7.423	-2.52	7.419
	-0.87	16.88	-0.83	16.92
	-1.36	38.73	-1.33	38.99

Number of feedback loops	6		3	
	Damping	Frequency	Damping	Frequency
Hover	-1.02	1.239	-1.02	1.589
	-1.89	2.871	-0.03	2.521
	-3.01	7.061	-0.66	5.825
	-2.23	7.460	-2.02	7.643
	-1.60	16.79	-1.53	17.98
	-0.07	39.11	-2.03	39.51
60 KTS	-1.20	1.834	-1.79	2.042
	-1.75	2.674	-0.32	2.583
	-1.96	7.005	-5.88	5.453
	-3.52	7.601	-2.12	7.881
	-1.15	16.96	-1.37	17.75
	-0.91	38.93	-2.09	39.43
100 KTS	-1.14	1.917	-0.23	2.048
	-2.00	3.168	-0.44	2.826
	-1.97	7.371	-0.63	5.980
	-4.27	9.031	-2.28	8.249
	-1.04	16.52	-1.39	17.36
	-1.33	38.60	-2.13	38.89

Table 5-15 The Poles Associated With The Short Period Flight Dynamic Characteristics of The Helicopter Under Simplified Standard Optimal Feedback

Number of feedback loops	12		9	
	Damping	Frequency	Damping	Frequency
Hover	-1.61	3.127	-1.64	3.133
	-1.90	3.628	-2.00	3.532
	-3.44	5.186	-3.13	5.177
	-8.10	3.895	-7.33	4.355
	-2.43	7.960	-2.44	7.956
	-10.3	0.000	-11.0	0.000
60 KTS	-1.43	3.194	-1.49	3.192
	-2.74	4.104	-2.92	3.971
	-2.33	5.336	-2.17	5.272
	-6.59	3.712	-9.98	5.907
	-3.23	7.932	-3.27	7.943
	-11.6	10.55	-16.2	8.544
100 KTS	-1.49	3.540	-1.55	3.537
	-2.59	4.872	-2.45	5.204
	-3.30	5.058	-3.29	4.458
	-8.32	3.304	-8.14	4.703
	-3.60	8.088	-3.67	8.151
	-10.9	13.26	-12.7	13.53

Number of feedback loops	6		3	
	Damping	Frequency	Damping	Frequency
Hover	-1.62	3.398	0.326	2.814
	-0.74	5.392	0.770	3.561
	-3.13	0.000	-6.87	1.022
	-13.6	9.951	0.695	6.575
	-2.33	7.999	-1.92	7.661
	-11.5	0.000	-11.8	0.000
60 KTS	-1.22	4.297	0.453	3.103
	-1.19	5.453	0.545	3.705
	-1.55	7.849	0.619	6.324
	-3.04	0.000	-1.87	8.001
	-3.15	9.618	-11.5	2.551
	-19.5	7.610	-24.9	7.190
100 KTS	-1.28	4.307	0.405	3.154
	-0.97	5.978	0.538	3.891
	-1.92	8.438	0.623	6.665
	-3.18	0.000	-11.6	0.000
	-2.25	10.99	-1.95	8.359
	-24.2	11.13	-15.6	11.96

Table 5-16 The Poles Associated With The Short Period Flight Dynamical Characteristics of The Helicopter Under Simplified Frequency Shaped Optimal Feedback

for the frequency-shaped optimal feedback control with q/r=1000. Both of them can offer stabilized system dynamics at all of three chosen flight conditions if all of state variables are available for measurement. Since the standard optimal control with high q/r ratio usually results in lag dynamical instability, the poles associated with the lag degrees of freedom are also given in the Table 5-15.

The elimination of the feedback of the dynamic inflow, the translational velocities and the flapping velocities together has little effect on the system dynamics. Compared with the baseline optimal controller, the variation of the short period fuselage dampings and frequencies is quite small, less than 5% for the standard optimal control and 10% for the frequency-shaped optimal control. These results suggest that at least half of the feedback loops theoretically required by the optimal control method, dynamic inflow, fuselage translational velocities and blade flapping velocities, are not necessary for practical implementation. The 18 loop feedback control system studied here can be replaced with 9 loop implementation without any significant impact on the system dynamics. The state variables involved in these 9 unnecessary loops are difficult to measure and to reconstruct. Therefore the difficulties in implementing the optimal control methodology is greatly reduced by simply eliminating these feedback loops. In the remaining feedback loops, the only blade state variables left are the flapping angles. Although without feedback these state variables, the overall system is still stable, the dynamic characteristics are almost the same as the original system without any augmentation of the damping ratio. It seems, therefore, that the flapping angle feedback has to be part of the optimal control implementation. Fortunately these state variables need not be measured because it has been found they can be estimated sufficiently accurately from fuselage state measurements[6].

5.3.4 Summary

Results in this section show that the multivariable optimal control theory is a powerful tool to design high gain augmentation control systems. The frequency-shaped optimal control design can offer much better flight dynamic characteristics than either the simple feedback control or the standard optimal feedback control. The feedback gains computed from the optimal control theories can be used to develop reduced state feedback systems. The feedback loops required can be significantly reduced to the half of the original optimal control designs without any noticable effect on the overall system dynamics.

Results in this section also show that the lagging dynamics has a more significant impact on the automatic controller design than the flapping dynamics. If a standard design method is used, the lag degrees of freedom must be included in the system modelling. Otherwise a high gain control system design can lead to unstable close-loop responses due to the unmodelled lag dynamics. Using a frequency-shaped control penalty in the system performance index is an effective way to obtain a stable margin for the feedback system design without need to model the lagging dynamics.

This margin is essential for any real implementation of a control system because the actual structure has an infinite number of modes, and any finite description of the actual system, though very high order, still has modeling errors. These are errors which cannot be modeled generally due to limited knowledge of the structural behavior at high frequencies. Thus if a system controller is important to the stability and performance, a very robust control system is required. This is especially true for the helicopter systems because the difficulties for modeling the high harmonic blade dynamics and aerodynamics. Therefore the frequency-shaped cost penalty seems to be a very good methodology for the helicopter controller design.

Chapter VI

CONCLUSIONS AND RECOMMENDATIONS

This thesis has had four fundamental objectives:

(1) By applying the matrix displacement method and with the help of a symbolic computer processor, to develop a linear description of helicopter system including blade dynamics.

(2) To take the rotor/empennage interaction into account without destruction of the linearity of the system model.

(3) To investigate the effects of blade dynamics on the automatic control system design with the model developed.

(4) By using the modern optimal control technology, to find a control methodology capable of removing the limitations due to the unmodelled high frequency blade lag dynamics on the flight control system design of the helicopter.

As indicated in the correlation results with flight test data shown in Chapter 4, the first and second objectives of the study have been largely achieved. The excellent correlations for all kinds of small control inputs at hover and for lateral and directional control inputs at various forward flight speeds are evidence of the success of the linearized model and the simple but effective description of the effects of the main rotor wake on the tail rotor and fixed tails. It is the first linear model of the helicopter including blade dynamics for forward flight, that makes the analysis of flight stability and control by the convenient eigenvalue and eigenvector analysis and the feedback control design by modern linear control theory possible. The validation of the model reveals many new ideas.

(1) A linearized model of the helicopter is quite satisfactory for predicting the stability and control characteristics. The proper linear model produces a good representation of helicopter control responses for forward flight as well as hover.

(2) For forward flight the sidewash variation at tail rotor and vertical tail and the nonuniform downwash at horizontal tail are more important for flight dynamic analysis than the most inertia, mechanical, and aerodynamic nonlinearities. Therefore, better understanding of the influence of rotor wake on the tail surfaces and tail rotor is one of the most important factors needed to improve the representation of helicopter motions. Consequently the proper simple method to treat the influence will be a key breakthrough for development of helicopter simulation.

(3) The simple flat wake model employed in this paper although crude appears to be a good approximation when sideslip angle remains relatively small.

(4) The influence of the dynamic inflow is most significant in hover and somewhat less significant in translational

flight. Its effect can be estimated by methods given in the literature.

The disadvantages of the model mainly result from the assumption of constant rotating speed of the main rotor, which have not been shown to be the case for longitudinal control inputs at forward flight. It seems that the inclusion of the engine and drive train will be the logical next step for better modeling. Changes of rotor speed are a result of an imbalance of the main rotor torque required and the engine torque available. Therefore the rotor speed degree of freedom must involve the engine dynamics and fuel control system. As for enlarging the range in which the model is validated for lateral and directional control, the first thing to do should be improving the modeling of the influences of the main rotor wake on the tail rotor and fixed tail surfaces. It seems that for small perturbation assumption there is still room left for increasing control inputs.

The third and fourth objectives also have been largely achieved by the classical and optimal control studies of Chapter 5. The results obtained by simple feedback control methodology have very good agreements with the results obtained by previous works for hover flight condition and have physically consistent results for translational flight conditions. The results obtained by the optimal control methodology has successfully introduced a new feedback control concept originally developed for space structure stabilization into the helicopter control system design. The following conclusions may be drawn.

(1) The control feedback gain limitations due to unmodeled lagging dynamics are much closer to those currently used in the helicopter industry than those due to unmodeled flapping dynamics. Therefore much attention has to be given to the lag degrees of freedom.

(2) Most of the feedback gain limitations are quite high except the roll rate, which has the same order as those currently used in the helicopter industry.

(3) The application of frequency-shaped optimal control methodology gives us a practical robust control design method for high gain tighter controller design without need to worry about the effects of spillover by the unmodeled high frequency modes.

REFERENCES

[1] C.W.Ellis, "Effects of Rotor Dynamics on Helicopter Automatic Control System Requirements" Aeronautical Engineering Review, July 1953

[2] R.E.Donham,S.V.Cardinale and I.B.Sachs, "Airborne and Ground Resonance Characteristics of a Soft In-Plane Rigid-Rotor System" J. Am. Helicopter Soc. 14 (1969)

[3] R.S.Hansen, "Towards a Better Understanding of Helicopter Stability Derivatives" J. Am. Helicopter Soc. 29 (1984)

[4] K.Miyajima, "Analytical Design of a High Performance Stability and Control Augmentation System for a Hingeless Rotor Helicopter" J. Am. Helicopter Soc. 24 (1979)

[5] H.C.Curtiss Jr., "Stability and Control Modelling" Paper No. 41 in Twelfth European Rotorcraft Forum Sept. 1986

[6] W.E.Hall Jr. and A.E.Bryson Jr., "Inclusion of Rotor Dynamics in Controller Design for Helicopters" J. Aircraft Vol.10. No.4 April 1974

[7] S.J.Briczinski and D.E.Cooper "Flight Investigation of Rotor/Vehicle State Feedback" NASA CR-132546

[8] K.H.Hohenemser and Sheng-Kuang Yin, "The Role of Rotor Impedance in the Vibration Analysis of Rotorcraft" Vertica Vol 3. No. 3/4 1979

[9],R.A.Ormiston, "Aeromechanical Stability of Soft Inplane Hingeless Rotor Helicopters" Third European Rotorcraft and Powered Lift Aircraft Forum, Paper No 25 (1977).

[10] J.J.Howlett "UH-60A black Hawk Engineering Simulation Program: Volume I - Mathematical Model" NASA CR-166309 1981

[11] W.Warmbrodt and P.Friedmann, "Formulation of Coupled Rotor /Fuselage Equations of Motion." Vertica 3, 254-271 (1979).

[12] W.Johnson, "A Comprehensive Analytical Model of Rotorcraft Aerodynamics and Dynamics." NASA TM 81182 (1980).

[13] D.H.Hodges, "Aeromechanical Stability of Helicopter With a Bearingless Rotor--Part I: equations of motion" NASA TM-78459 (1978).

[14] J.Levin, "Formulation of Helicopter Air Resonance Problem in Hover With Active Controls" M.Sc. Thesis, Univ.of California,Los Angeles (1981).

[15] R.T.Lytwyn,W.Miao and W.Woitsh, "Airborne and Ground Resonance of Hingeless Rotors." J. Am. Helicopter Soc. 16 (1971)

[16] F.K.Straub and W.Warmbrodt, "The Use of Active Controls to Augment Rotor/Fuselage Stability" J. Am. Helicopter Soc. 30 (1985)

[17] Gopal H. Gaonkar and David A. Peters "Flap-Lag Stability With Dynamic Inflow by the method of Multiblade Coordinates" J. Aircraft 17 pp112-119 (1980)

[18] Mark.G.Ballin "Validation of a Real-Time Engineering Simulation of the UH-60A Helicopter" NASA TM-88360 1987

[19] B.Etkin, "Dynamics of Atmospheric Flight" John Wiley & Sons,Inc. New York 1972

[16] M.P.Gibbons and G.T.S.Done, "Automatic Generation of Helicopter Rotor Aeroelastic Equations of Motion" Vertica Vol 8. No 3.1984

[17] G.H.Gaonkar and D.A.Peters, "Effectiveness of Current Dynamic-Inflow Models in Hover and Forward Flight" J. Am. Helicopter Soc. Vol 31 No 2 (1986)

[18] Wayne Weisner and Gary Kohler, "Tail Rotor Performance in Presence of Main Rotor , Ground, and Winds" J. Am. Helicopter Soc. 19 (1974)

[19] Dean E. Cooper, "YUH-60A Stability and Control" J. Am. Helicopter Soc. 23 (1978)

[20] V.K.Baskin, "Theory of The Lifting Airscrew" NASA TT F-823 1976

[21] Vil'dgrube, L. S. "Theory of Lifting Airscrew With a Flat Vortex System" All-Union Meeting on Theoretical and Applied Mechanics. Proceedings of Lectures USSR, 1960

[26] R.T.N.Chen and W.S.Hindson "Analytical and Flight Investigation of the Influence of Rotor and Other High-order Dynamics on Helicopter Flight Control System Bandwidth" Paper presented at International Conference on Rotorcraft Basic Research, Research Triangle Park, NC, February 1985

[27] David R. Downing and Wayne H. Bryant "Flight Test of a Digital Controller Used in a Helicopter Autoland System" Automatica, Vol. 23, No. 3, May 1987

[28] R. F. Stengel, J. R. Broussard and P. W. Berry "Digital Controllers for VTOL aircraft" Proceedings of the 1976 IEEE Conference on Decision and Control, Dec. 1976

[29] K.B.Hilbert and G.Bouwer "The design of a Model-Following Control System For Helicopters" AIAA Paper 84-1941, 1984

[30] D.L.Key and R.H.Hoh "New Handling Qualities Requirement and How They can be Met" Proceedings of the Annual Forum of American Helicopter Society, 43rd, 2, 1987

[31] W.L.Garrard and B.S.Liebst "Design of a Multivariable Flight Control System for Handling Qualities Enhancement" Proceedings of the Annual Forum of American Helicopter Society, 43rd, 2, 1987

[32] Dale,Enns "Multivariable Flight Control for an Attack Helicopter" Proceedings of the 1986 Automatic Control Conference, Williamsburg VA. June, 1986

[33] M.I.Young, D.J.Bailey, and M.S.Hirschbein, "Open and Closed Loop Stability of Hingeless Rotor Helicopter Air and Ground Resonance" Paper No.20. NASA SP-352, pp 205-218.

[34] W.Johnson, Helicopter Theory. Princeton University Press, Princeton, New Jersey (1980)

[35] A.E.Bryson, and Y.C.Ho "Applied Optimal Control" Hemisphere Publishing, Washington D.C. 1975

[36] T.Kailath "Linear Systems" Prentice-Hall, Englewood Cliffs, N.J. 1980

[37] F.K.Straub, "Optimal Control of Helicopter Aeromechanical Stability" Vertica Vol 11. No 3.1987

[38] B.D.O.Anderson and J.B.Moore "Linear Optimal Control" Prentice Hall, Englewood Cliffs, N.J. 1971

[39] N.K.Gupta, "Frequency-Shaped Cost Functionals: Extensions of Linear Quadratic Gaussian Design Methods" AIAA J. Guidance and Control, Nov./Dec. 1980

[40] Lt.D.B.Ridgely, Siva S.Banda, and C.D.V.Palmer, "Reduced Order Control Design, Benefits and Cost of Frequency-shaped LQG Methodology" AIAA Guidance and Control Conference, Gatlinburg, TN, Aug. 1983

APPENDIX A

Derivation of System Equations of Motion

1) The Transformations between frames

The notations for transformation matrices are

$$\Phi x(\phi) = \begin{bmatrix} 1 & 0 & 0 \\ 0 & \cos\phi & -\sin\phi \\ 0 & \sin\phi & \cos\phi \end{bmatrix} \quad \Phi y(\theta) = \begin{bmatrix} \cos\theta & 0 & \sin\theta \\ 0 & 1 & 0 \\ -\sin\theta & 0 & \cos\theta \end{bmatrix}$$

$$\Phi z(\psi) = \begin{bmatrix} \cos\psi & -\sin\psi & 0 \\ \sin\psi & \cos\psi & 0 \\ 0 & 0 & 1 \end{bmatrix} \quad \Phi y(\beta) = \begin{bmatrix} \cos\beta & 0 & \sin\beta \\ 0 & 1 & 0 \\ -\sin\beta & 0 & \cos\beta \end{bmatrix}$$

$$\Phi z(\zeta) = \begin{bmatrix} \cos\zeta & -\sin\zeta & 0 \\ \sin\zeta & \cos\zeta & 0 \\ 0 & 0 & 1 \end{bmatrix} \quad \Phi z(\psi_k) = \begin{bmatrix} \cos\psi_k & -\sin\psi_k & 0 \\ \sin\psi_k & \cos\psi_k & 0 \\ 0 & 0 & 1 \end{bmatrix}$$

The fig. 2-1 shows the relationship between the F_1 frame and the inertial frame:

$$\begin{Bmatrix} x \\ y \\ z \end{Bmatrix}_e = \begin{Bmatrix} x \\ y \\ z \end{Bmatrix}_{f1} + \begin{Bmatrix} -\ Vt\ \cos(\alpha) \\ 0 \\ -\ Vt\ \sin(\alpha) \end{Bmatrix} \qquad (1)$$

Fig. 2-2 shows the relationship between the F_1 frame and the F_2 frame. Beside the translational perturbations, which carry the frame origin from the trim hub center to the perturbated hub center, the perturbated rotations have following sequence:

(1) A rotation $-\psi$ about Z_{f1}, carrying axes to OX'Y'Z'.

(2) A rotation θ about Y', carrying axes to OX"Y"Z".

(3) A rotation $-\phi$ about X", carrying axes to the F_2 frame.

Therefore, the transformation relationship for a vector is

$$\{X\}_{f1} = \{\Delta X_{hub}\} + \Phi z(-\psi)\Phi y(\theta)\Phi x(-\phi)\ \{X\}_{f2} \qquad (2)$$

where $\langle \Delta X_{hub} \rangle$ is the translational perturbation at hub.

Fig. 2-3 shows the relationship between the F_z frame and the H frame, it is easy to obtain

$$\langle X \rangle_{f2} = \Phi z(\Psi_k)\ \langle X \rangle_h \tag{3}$$

Fig. 2-4 shows the relationship between the H frame and the B frame. Beside the hinge offset displacement, the rotations have following sequence:

(1) A rotation $-\zeta$ about Z_h, carrying axes to $O_h{}'X_h{}'Y_h{}'Z_h{}'$.

(2) A rotation $-\beta$ about $Y_h{}'$, carrying axes to the B frame.

The tranformation relationship for a vector is

$$\langle X \rangle_h = \begin{Bmatrix} e \\ 0 \\ 0 \end{Bmatrix} + \Psi z(-\zeta)\ \Psi y(-\beta)\ \langle X \rangle_b \tag{4}$$

2) Kinetic Energy

The position of a fuselage element is given by

$$\langle Xm \rangle_e = \langle Xcg \rangle_e + \Phi z(-\psi)\Phi y(\theta)\Phi x(-\phi)\ \langle Xm \rangle_f \tag{5}$$

$\langle Xm \rangle_f$ contains the body axis coordinates of the point, $\langle Xcg \rangle_e$ and $\langle Xm \rangle_e$ are the locations of the center of gravity and the point in the inertial axis system.

The position of an element of a blade in the B frame is given as:

$$\langle Xm \rangle_b = [\ r,\ 0,\ 0\ ]^T \tag{6}$$

Then the position of an element of the blade in the inertial axis system is given by:

$$\{Xm\}_{\bullet} = \Phi z(-\psi)\ \Phi y(\theta)\ \Phi x(-\phi) \left[\Phi z(\psi_k) \left[\Phi z(-\zeta)\ \Phi y(-\beta) \begin{bmatrix} r \\ 0 \\ 0 \end{bmatrix} + \begin{bmatrix} e \\ 0 \\ 0 \end{bmatrix} \right] \right] + \{Xh\}_{\bullet} \qquad (7)$$

$\{Xh\}_{\bullet}$ is the location of the rotor hub center in the inertial axis system.

The kinetic energy can be written as:

$$T = \frac{1}{2} \int_{f+b} [(\frac{dx_m}{dt})^2 + (\frac{dy_m}{dt})^2 + (\frac{dz_m}{dt})^2]\ dm \qquad (8)$$

3) Potential Energy

The potential energy is given by

$$V = M\ g\ (z_{cg})_{\bullet} + (\sum_k K_\beta\ \beta_k^2 + \sum_k K_\zeta\ \zeta_k^2)/2 \qquad (9)$$

4) Generalized Force:

Using the position vector given in Eq.(6), it is straight forward to get the velocity of an element of a blade in the inertial axis $\{Vb(r)\}_{\bullet}$. The expression for the velocity components in the B frame is

$$\{Vb(r)\}_b = \Phi y(\beta)\ \Phi z(\zeta)\ \Phi z(-\psi_k)\ \Phi x(\phi)\ \Phi y(-\theta)\ \Phi z(\psi)\ \{Vb(r)\}_{\bullet} \qquad (10)$$

$\{Vb(r)\}_{\bullet}$ is the velocity components of the rotor element relative to the inertial axis in the inertial frame. $\{Vb(r)\}_b$ is the velocity components in the B frame.

Then we get the normal and tangential airfoil velocities of the element of the blade in the B frame from the relationship:

$$\begin{bmatrix} V_{\iota} \\ V_{\iota} \\ V_{p} \end{bmatrix} = \{Vb(r)\}_{b} \tag{11}$$

From quasisteady strip theory we have:

$$dD_{k} = \frac{\rho}{2} c_{b} V_{\iota_k}^{2}(r)\ Cd_{o}\ dr \tag{12}$$

$$dL_{k} = \frac{\rho}{2} C_{l}^{\alpha} c_{b} V_{\iota_k}^{2}(r)\ \left(\theta_{k}(r) - \frac{Vp_{k}(r) + Vn_{k}(r)}{V_{\iota_k}(r)} \right) dr \tag{13}$$

where $\theta_{k}(r)$ is the local pitch angle of the blade:

$$\theta(r)_{k} = \theta_{o} - \theta_{1} r - A_{1s} \cos\psi_{k} - B_{1s} \sin\psi_{k} \tag{14}$$

where $Vn_{k}(r)$ is the total local downwash of the blade:

$$\begin{aligned} Vn_{k}(r) &= Vno_{k}(r) + Vnd_{k}(r,t) \\ &= Vnot + V_{v1}\, r \cos\psi_{k} \qquad (\text{ Steady Inflow }) \\ &\quad + V_{o}(t) + V_{c}(t)\, r \cos\psi_{k} + V_{c}(t)\, r \sin\psi_{k} \qquad (15) \\ &\qquad\qquad (\text{ Dynamic Inflow }) \end{aligned}$$

The aerodynamic moments and forces of the kth blade are obtained by:

$$Fn_{k} = \int_{0}^{R-e} dFn_{k}(r) = \int_{0}^{R-e} dL_{k}(r)$$

$$F_{\iota_k} = \int_{0}^{R-e} dF_{\iota_k}(r) = \int_{0}^{R-e} dD_{k}(r) + \left(\frac{Vp_{k}(r) + Vn_{k}(r)}{V_{\iota_k}(r)} \right) dL_{k}$$

$$M_{f_k} = \int_{0}^{R-e} r\ dFn_{k}(r) \qquad M_{\iota_k} = \int_{0}^{R-e} r\ dF_{\iota_k}(r) \tag{16}$$

Where M_f and M_{ι} are the blade flap and lag aerodynamic moments and Fn and Fi are the blade normal and inplane aerodynamical shear forces. The expressions for these forces and moments in the H frame are:

$$\begin{bmatrix} -F_{p_h} \\ -F_{i_h} \\ F_{n_h} \end{bmatrix}_k = \Phi y(\beta)\ \Phi z(\zeta) \begin{bmatrix} 0 \\ -F_i \\ F_n \end{bmatrix}_k$$

$$\begin{bmatrix} M_{x_h} \\ -M_{f_h} \\ -M_{l_h} \end{bmatrix}_k = \Phi y(\beta)\ \Phi z(\zeta) \begin{bmatrix} 0 \\ -M_f \\ -M_l \end{bmatrix}_k \qquad (17)$$

Then the virtual work terms due to the aerodynamic forces acting on the rotor blades can be obtained by

$$\begin{aligned} \delta W_r = \sum_k [\ & M_{f_k}\ \delta\beta_k + M_{l_k}\ \delta\zeta_k + (\ M_{l_{hk}} + F_{i_{hk}} e)(\ \delta\psi\ ) \\ & + (\ M_{f_{hk}} + F_{n_{hk}} e\ )(\ -\delta\phi \sin\psi_k - \delta\theta \cos\psi_k\ ) \\ & + M_{x_{hk}}\ (\ \delta\phi \cos\psi_k - \delta\theta \sin\psi_k\ ) \\ & + F_{p_{hk}}\ (\ -\ \delta x_{he} \cos\psi_k - \delta y_{he} \sin\psi_k\ ) + F_{n_{hk}}\ \delta z_{he} \\ & + F_{i_{hk}}\ (\ +\ \delta x_{he} \sin\psi_k - \delta y_{he} \cos\psi_k)\ ] \qquad (18) \end{aligned}$$

Following the same procedure, the virtual work terms due to the tail rotor, the fixed tail surfaces, and the fuselage can be obtained.

5) The Lag Damper Modelling

The lag damper is modeled by a dissipation function:

$$D = \sum_k C_\zeta \left(\frac{d\zeta}{dt}\right)^2 / 2 \qquad (19)$$

6) The equations of motion

Then, the final system equations are

$$\frac{d}{dt}\left(\frac{\partial(T-V)}{\frac{dQ_i}{dt}}\right) - \frac{\partial(T-V)}{\partial Q_i} + \frac{\partial D}{\partial\left(\frac{dQ_i}{dt}\right)} = \frac{\delta W}{\delta Q_i} \qquad (20)$$

7) The Multiblade Coordinates

The multiblade coordinates are defined as follow:

$$\beta_k = \beta_o - \beta_1 \cos\psi_k - \beta_2 \sin\psi_k \qquad (21)$$

$$\zeta_k = \zeta_o - \zeta_1 \cos\psi_k - \zeta_2 \sin\psi_k \qquad (22)$$

Then, one obtains the multiblade coordinates in terms of blade flapping and lagging angle.

Collective flapping and lagging (coning):

$$\beta_o = \frac{1}{N} \sum_k \beta_k \qquad \zeta_o = \frac{1}{N} \sum_k \zeta_k \qquad (25)$$

First order cyclic flapping and lagging (tilting):

$$\beta_1 = \frac{1}{N} \sum_k -\beta_k \cos\psi_k \qquad \beta_2 = \frac{1}{N} \sum_k -\beta_k \sin\psi_k \qquad (26)$$

$$\zeta_1 = \frac{1}{N} \sum_k -\zeta_k \cos\psi_k \qquad \zeta_2 = \frac{1}{N} \sum_k -\zeta_k \sin\psi_k \qquad (27)$$

APPENDIX B

Pitt's Model of Dynamic Inflow

The static coupling matrix, the air mass inertial matrix and the dimensional adjustor matrix are given below:

$$[M] = \begin{bmatrix} \dfrac{128R}{72\pi} & 0 & 0 \\ 0 & \dfrac{-16R}{45\pi} & 0 \\ 0 & 0 & \dfrac{-16R}{45\pi} \end{bmatrix}$$

$$[L] = \frac{1}{Vso} \begin{bmatrix} \dfrac{1}{2} & \dfrac{15\pi}{64}\sqrt{\dfrac{1-\sin\alpha\alpha}{1+\sin\alpha\alpha}} & 0 \\ \dfrac{15\pi}{64}\sqrt{\dfrac{1-\sin\alpha\alpha}{1+\sin\alpha\alpha}} & \dfrac{-4\sin\alpha\alpha}{1+\sin\alpha\alpha} & 0 \\ 0 & 0 & \dfrac{-4}{1+\sin\alpha\alpha} \end{bmatrix}$$

$$[D] = \begin{bmatrix} \dfrac{1}{\rho\pi R^2} & 0 & 0 \\ 0 & \dfrac{1}{\rho\pi R^4} & 0 \\ 0 & & \dfrac{1}{\rho\pi R^4} \end{bmatrix}$$

$$Vso = \frac{(Vnot - V\sin\alpha)(2Vnot - V\sin\alpha) + V^2\cos\alpha}{\sqrt{V^2\cos^2\alpha + (Vnot - V\sin\alpha)^2}}$$

$$\alpha\alpha = \mathrm{Tan}^{-1}\left(\frac{Vnot - V\sin\alpha}{V\cos\alpha}\right)$$

APPENDIX C

The Flat Vortex Theory For Nonuniform Inflow

1) Flat vortex model

Under assumptios mentioned in Chapter 3, it will be more convenient to use air-trajectory reference frame for the derivation of the flat vortex theory. Thisreference frame has an origin fixed to the hub center of the helicopter, and the OX axis is directed along the velocity vector but backward. The OZ axis is directed up. As a result, the vortex layer will move in the plane z=0 in this frame. Therefore, all position components in this appendix are in this air-trajectory frame.

Circulation of a free vortex layer of width Δr which springs from one blade is

$$\Delta\Gamma(r) = - \frac{d\Gamma(r)}{dr} \Delta r \qquad (1)$$

The equation defining the shape of a single free vortex is given under the following form:

$$x = \mu R (\psi_o - \psi) + r \cos\psi \qquad y = r \sin\psi \qquad (2)$$

where ψ_o is the azimuth angle at which the free vortex left the blade.

Let us single out an elemental vortex layer associated with two azimuth positions being different by an angle $\Delta\psi_o$. Circulation per unit length in this vorticity layer will be

$$\Delta\Psi = \frac{\Delta\Gamma(r)}{2\pi} \frac{\Delta\psi_o}{\Delta s} \qquad (3)$$

where Δs is the distance between the cycloids.

$$\Delta s = \Delta x \sin\gamma \qquad tg\gamma = \frac{r \cos\psi}{\mu R + r \sin\psi} \tag{4}$$

From (2) we have:

$$\Delta x = \mu R \Delta\psi_o \tag{5}$$

Then:

$$\frac{\Delta\psi_o}{\Delta s} = \frac{1}{\mu R \sin\gamma} \quad \text{and} \quad \Delta\Psi = \frac{\Delta\Gamma(r)}{2\pi \mu R \sin\gamma} \tag{6}$$

Let us replace the free cycloidal vortex layer with two systems of vortex layers: one system of free longitudinal vortices and one system of free lateral vortices. Circulation per unit length of the lateral vortex layer is:

$$\Delta\Psi y = \Delta\Psi \sin\gamma = \frac{\Delta\Gamma(r)}{2\pi \mu R} \tag{7}$$

and the longitudinal one:

$$\Delta\Psi x = \Delta\Psi \cos\gamma = \frac{\Delta\Gamma(r)}{2\pi \mu R} \frac{\mu R + r \sin\psi}{r \cos\psi} \tag{8}$$

Free lateral rectilinear vortices will exist only within a circle of radius r. Outside of this circle, the lateral votices will disappear as a result of geometric summation of the incremental circulation, and only longitudinal ones will remain with doubled value of the circulation per unit length.

2) Nonuniform induced velocity at tail surfaces

As mentioned in the Chapter 3, the nonuniform induced velocity contribution of the longitudinal vortices is the only one being considered.

It is assumed that in the trim condition the velocity field experienced by the tail rotor and tail surfaces is that on the wake. The induced velocity field of the longitudinal vortices can be determined by replacing the actual system of longitudinal vortices by rectilinear vortices extending from $x = -\infty$ to $x = +\infty$.

Then by applying the Biot-Savart Law, the vertical component of the induced velocity at a point $(x_T, y_T, 0)$ on the wake by a free vortex layer of width Δr is given as

$$\Delta Vz(r) = \frac{\Delta\Gamma(r)}{2\pi\ \mu\ \pi R}\int_{-r}^{+r}\frac{\mu\ R + r\ \sin\psi}{(y - y_T)\ r\ \cos\psi}\,dy \qquad (9)$$

Let: $y = r\ \sin\psi$; $dy = r\ \cos\psi\ d\psi$, Then we have:

$$\Delta Vz(r) = \frac{-\Delta\Gamma(r)}{2\pi\ \mu\ \pi R}\int_{\pi/2}^{3\pi/2}\frac{\mu\ R + r\ \sin\psi}{r\ \sin\psi - y_T}\,dy$$

$$= \frac{-\Delta\Gamma(r)}{2\pi\ \mu\ R}\left[-1 - \left(\frac{\mu R}{r} + \frac{y_T}{r}\right)\frac{1}{\pi}\int_{\pi/2}^{3\pi/2}\frac{d\psi}{\sin\psi - y_T/r}\right. \qquad (10)$$

Since:

$$\int_{\pi/2}^{3\pi/2}\frac{d\psi}{\sin\psi - (y_T/r)} = \begin{cases} 0 & -r \le y_T \le r \\ \dfrac{-\pi}{\sqrt{y_T^2 + r^2}} & y_T > r \\ \dfrac{-\pi}{\sqrt{y_T^2 + r^2}} & y_T < -r \end{cases} \qquad (11)$$

Then we obtain:

$$\Delta Vz(r) = \begin{cases} \dfrac{\Delta\Gamma(r)}{2\pi\ \mu\ R}\left(-1 - \dfrac{\mu\ R + y_T}{\sqrt{y_T^2 + r^2}}\right) & y_T < -r \\ -\dfrac{\Delta\Gamma(r)}{2\pi\ \mu\ R} & -r \le y_T \le r \end{cases} \qquad (12)$$

$$\left| \; \frac{\Delta\Gamma(r)}{2\pi\,\mu\,R}\left(-1+\frac{\mu\,R+y_T}{\sqrt{y_T^{2}+r^{2}}}\right) \qquad y_T > r \right.$$

The vertical induced velocity due to all free vortices springing from the blade will be

$$Vz(y) = \int_{0}^{R} \Delta Vz(r)\,\frac{d\Gamma(r)}{dr}\,dr$$

$$= \left\{ \begin{array}{l} \dfrac{-\mu\,R - y}{2\pi\,\mu\,R}\displaystyle\int_{o}^{y}\frac{d\Gamma(r)}{dr}\,\frac{dr}{\sqrt{y^{2}+r^{2}}} \\[2ex] \dfrac{\mu\,R + y}{2\pi\,\mu\,R}\displaystyle\int_{o}^{y}\frac{d\Gamma(r)}{dr}\,\frac{dr}{\sqrt{y^{2}+r^{2}}} \end{array} \right. \qquad (13)$$

The distribution of circulation along the rotor radius is assumed to be parabolic:

$$\Gamma(r) = a\,r^{2}\,(\,R - r\,) \qquad (14)$$

$$\frac{d\Gamma(r)}{dr} = a\,r\,(\,2R - 3r\,) \qquad (15)$$

Then we have:

$$Vz(y) = \left\{ \begin{array}{ll} -\dfrac{\mu\,R + y}{2\pi\,\mu\,R}\,a\left(2R - \dfrac{3\pi\,y}{4}\right) y & (R>y>0) \\[2ex] -\dfrac{\mu\,R + y}{2\pi\,\mu\,R}\,a\left(2R + \dfrac{3\pi\,y}{4}\right) y & (0>y>-R) \end{array} \right. \qquad (16)$$

The parameter a is determined by setting lift = weight:

$$T = \rho\int_{o}^{R}\Gamma(r)\;V_T(r)\;dr$$

$$= \rho\int_{o}^{R} a\,r^{2}\,(\,R - r\,)\,\Omega\,r\,dr = W \qquad (17)$$

$$a = \frac{20\;W}{\rho\,\Omega\,R^{5}} = (20\pi)\,\frac{\Omega}{R}\,C_T \qquad (18)$$

The normalized nonuniform downwash is defined as:

$$Cz = \frac{Vz(y)}{\left(\frac{a\ R^2}{2\pi\ \mu}\right)} = -\left(\mu + \frac{y}{R}\right)\frac{y}{R}\left(2 \mp \frac{3\pi y}{4\ R}\right)$$

$$= \frac{Vz(y)}{20(C_T\Omega R)/(2\mu)} \cong \frac{1}{10}\ \frac{Vz(y)}{2\ Vnot} \qquad (19)$$

2 Vnot is the uniform downwash at tail surfaces from the momentum theory. The lateral distribution of nondimensional downwash of eq.(19) for μ=0.22 is shown in Fig.3-1.

Following the same procedure, we obtain:

$$\Delta Vy(r) = \frac{\Delta\Gamma(r)}{2\pi\ \mu\ R}\ \frac{1}{\pi} \int_{-r}^{r} \frac{z_T\ (\ \mu\ R + r\ \sin\psi\ )\ dy}{(\ z_T^2 + y^2)\ r\ \cos\psi}$$

$$= \frac{\Delta\Gamma(r)}{2\pi\ \mu\ R}\ \frac{1}{\pi} \int_{\pi/2}^{3\pi/2} \frac{z_T\ (\ \mu\ R + r\ \sin\psi\ )\ d\psi}{z_T^2 + r^2\sin^2\psi}$$

$$= \frac{\Delta\Gamma(r)}{2\pi}\ \frac{1}{\sqrt{r^2 + z_T^2}} \qquad (20)$$

Then we have:

$$Vy(z) = \frac{1}{2\pi} \int_{0}^{R} \frac{a\ r\ (\ 2R - 3r\ )}{\sqrt{r^2 + z^2}}\ dr$$

$$= \frac{a\ R^2}{2\pi}\left(\sqrt{1 + \left(\frac{z}{R}\right)} - \frac{4z}{R}\right.$$

$$\left. + 3\left(\frac{z}{R}\right)^2 \ln\left(\frac{R + \sqrt{R^2 + z^2}}{z}\right)\right) \quad (z>0) \quad (21)$$

The normalized nonuniform sidewash is defined as:

$$Cy = \frac{Vy(z)}{\left(\frac{a\ R^2}{2\pi\ \mu}\right)} = \mu\left(\sqrt{1 + \left(\frac{z}{R}\right)} - \frac{4z}{R}\right.$$

$$\left. + 3\left(\frac{z}{R}\right)^2 \ln\left(\frac{R + \sqrt{R^2 + z^2}}{z}\right)\right)$$

$$= \frac{1}{10}\ \frac{Vy(z)}{2\ Vnot} \qquad (z>0) \qquad (22)$$

For $Z<0$, we have $Vy(-z) = -\ Vy(z)$.

The longitudinal distribution of the sidewash given by eq.(22) for $\mu=0.22$ is shown in Fig.3-2.

For $|z| < 0.2\ R$, we use:

$$Vy(z) \cong \pm \frac{a\ R^2}{2\pi}\left(1 - \frac{4y}{R}\right) \qquad (z \gtrless 0) \qquad (23)$$

3) Effects on Tail Surfaces

When there is sideslip, the position of a spanwise section of the horizontal tail relative to the center line of the wake at the wake layer will be:

$$y = (\ y_h + T_{hx}\ \beta_f\ ) \qquad (24)$$

Then we have the roll moment contribution of the horizontal tail:

$$Mxh = \frac{\rho}{2} V_h\ H_c\ C_\alpha^l \int_{-Rh}^{Rh} Vz(y_h + T_{hx}\beta_f) y_h dy_h$$

$$= \left(\frac{\rho\ V_h\ H_c\ a}{960\pi\ \mu\ R}\right)\left(\ 45\pi\ R\ \mu\ (Rh)^4 - 160\ \mu\ R^2 (Rh)^3\right.$$

$$\left. + (\ 135\pi\ T_{hx}(Rh)^4 - 320\ R\ T_{hx}\ (Rh)^3\ )\ \beta\right.$$

$$+ 90\pi \; \mu \; R \; (Rh)^2 \; T_{hx}^2 \; \beta^2 + 90\pi \; (Rh)^2 \; T_{hx}^3 \; \beta^3$$

$$- 15\pi \; R \; T_{hx}^4 \; \beta^4 - 9\pi \; T_{hx}^5 \; \beta^5 \;) \qquad (25)$$

The terms for forming the linearized approximation are given below:

$$Mxh \Big|_{\beta_h = 0} = \frac{\rho \; V_h \; H_c \; C_\alpha^l \; a \; Rh^3}{192 \; \pi} (9\pi \; Rh - 32 \; R \;) \qquad (26)$$

$$\frac{\partial Mxh}{\partial \beta_f} \Big|_{\beta_f = 0} = \frac{\rho \; V_h \; H_c \; C_\alpha^l \; a \; T_{hx} Rh^3}{192\pi \; \mu \; R} (27\pi \; Rh - 64 \; R \;)$$

Similarly, the pitch moment contribution:

$$Myh = \frac{\rho}{2} V_h \; H_c \; C_\alpha^l \; T_{hx} \int_{-rh}^{rh} Vz(y_h + T_{hx}\beta_f) dy_h$$

$$= (\frac{\rho \; V_h \; H_c \; a \; T_{hx}}{192\pi \; \mu \; R}) (\; 32 \; R \; (Rh)^3 - 9\pi \; (Rh)^4$$

$$+ (96\mu \; T_{hx} Rh \; R^2 - 36\pi \; \mu \; R \; T_{hx} (Rh)^2) \; \beta$$

$$+ (96 \; R \; T_{hx}^2 Rh - 54\pi \; T_{hx}^2 (Rh)^2) \; \beta^2$$

$$- 12\pi \; \mu \; R \; T_{hx}^3 \; \beta^3 - 9\pi \; T_{hx}^4 \; \beta^4 \;) \qquad (27)$$

and the required terms:

$$Myh \Big|_{\beta_f = 0} = (\frac{\rho \; V_h \; H_c \; T_{hx} \; C_\alpha^l \; a \; R \; (Rh)^3}{192\pi \; \mu \; R}) (32 \; R - 9\pi \; Rh \;) \qquad (28)$$

$$\frac{\partial Myh}{\partial \beta_f} \Big|_{\beta_f = 0} = \frac{\rho \; V_h \; H_c \; T_{hx}^2 \; C_\alpha^l \; a \; R \; Rh}{16\pi} (8R - 3\pi \; Rh)$$

For the tail rotor thrust contribution, we begin from the local angle of attack of the tail rotor:

$$\alpha_T = \frac{Vy(z)}{V_T} \cong \pm \frac{a\ R^2}{2\pi\ V_T}\left(1 - \frac{4z}{R}\right) \qquad (z \gtrless 0) \qquad (29)$$

Thrust contributions of the tail rotor due to nonuniform sidewash at zero sideslip angle and zero angle of attack can be given as:

$$T_T = \iint_S \frac{\partial T_T}{\partial \alpha_T} \Delta\alpha_T(z)\ ds(z) = 0 \qquad (30)$$

When there is an angle of attack variation, the tail rotor thrust will vary as:

$$\Delta T_T = K \oint_l \frac{\partial T_T}{\partial \alpha_T}\bigg|_l \alpha_T(z)\bigg|_l\ ds\bigg|_l \qquad (31)$$

K is a parameter decided by the correlation with flight test.

The vertical position of a point of the tail rotor relative to the wake is

$$z = z_T + \alpha\ T_{Tx} \qquad (32)$$

Then:

$$\Delta z = T_{Tx}\ \Delta\alpha \qquad ds\bigg|_l = dx\bigg|_l \Delta z \qquad (33)$$

From experimental data[21], the effect of viscosity will be significant at $z < 0.1R$. Therefore, let $\Delta\alpha_T = 0$ for $|z| < 0.1R$. The thrust variation of the tail rotor due to the angle of attack variation can be obtained by integrating Eq.(31) with the relation Eq.(33). The same procedure also applies to the vertical tail.